Ti and Co-Cr-Mo Matrix Syntactic Foams for Bio-Applications

Thesis submitted in accordance with the requirements of the University of Liverpool for the Degree of Doctor in Philosophy

by

Xiaobing Xue

October 2010

Abstract

The demands for joint replacements have been increasing and metallic implant materials are particularly welcome for joint implant applications. However, compared with the human bone, the elastic moduli of metals are significantly high. This causes stress shielding, which results in bone resorption and thus leads to various degrees of bone loss. A material with a low elastic modulus can transfer more physiological load to the femur. Therefore, the bone resorption in the femur and the failure of the cement mantle can be prevented.

The main objective of this study is to develop novel materials by embedding hollow or porous ceramic microspheres (CMs) into metal matrices by powder metallurgy or casting for implant applications. The metal matrix syntactic foams, Ti and Co-Cr-Mo alloy based, are designed to increase the mechanical strength without increasing the elastic modulus.

Ti matrix syntactic foam was manufactured using a powder metallurgy process. Increasing Ti volume percentage and compaction pressure increased the density and decreased the porosity of the Ti matrix. Both volume measurement and water absorption methods were used to estimate the volume percentage of the crushed CMs. For a given Ti volume percentage, the volume percentage of crushed CMs was increased by increasing the compaction pressure; for a given compaction pressure, increasing Ti volume percentage decreased the volume percentage of the crushed CMs.

The Ti matrix syntactic foam was brittle. Increasing either Ti volume percentage or compaction pressure resulted in an increase in the compressive and flexural strength. When the compaction pressure was lower than 100 MPa, the elastic modulus increased with increasing Ti volume percentage and compaction pressure. Above 100 MPa, further increases in Ti volume percentage and compaction pressure decreased the elastic modulus. The Rockwell hardness of the Ti matrix syntactic foam increased linearly with the Ti volume percentage and the compaction pressure. The impact toughness of the Ti matrix syntactic foam increased significantly with increasing the Ti volume percentage.

Ti matrix syntactic foam showed excellent biological performance. The toxicity test showed that the Ti matrix syntactic foam had sufficient chemical inertness in the cell culture medium. The direct contact tests exhibited an excellent cell spreading on the Ti matrix syntactic foam surface. The examination of the calcifications of cells on the surface of Ti matrix syntactic foam by von Kossa stain method showed that the calcifications of osteoblasts were affected by the surface condition of the Ti matrix syntactic foam. The specimens fabricated with higher compaction pressures had much smoother surfaces, and thus less calcification of osteoblast.

A feasibility study on the manufacturing of Co-Cr-Mo alloy matrix syntactic foam with pressure and centrifugal casting processes was carried out. The main defects were non-uniform distribution of CMs, porosity, partial filling of melt in mould and deformed CMs. These defects were mainly caused by the raw material used and the manufacturing process.

Acknowledgments

The author would first like to sincerely thank Dr Y.Y. Zhao and Dr R.L. Williams for their supervision and guidance throughout the PhD programme. Their help, knowledge, and insight are invaluable.

The author would also like express gratitude to Dr L.P. Zhang, Dr V. Kearns and Dr D. Jones for their kind help in the experimental work during the time of the PhD programme.

Many thanks go to those who contributed to the experimental aspects of this research. They are: Mr D. Atkinson for preparation of the samples, Mr S. Pennington for the mechanical testing, and Mr J. Mathew for the preparation of the steel tubes.

I would last like to thank all my friends and family for their support and encouragement throughout the PhD.

Statement of Originality

This thesis is submitted for the degree of Doctor in Philosophy in the faculty of Engineering at the University of Liverpool. The research project reported herein was carried out, unless otherwise stated, by the author, in the Department of Engineering at the University of Liverpool between October 2006 and October 2010.

No part of this thesis has been submitted in support of an application for a degree or qualification of this or any other University or educational establishment. However, some parts of this thesis have been published in co-authorship with Dr Y.Y. Zhao in the following papers:

Zhao, Y.Y., Tao, X.F. & Xue, X.B., (2008). Manufacture and Mechanical Properties of Metal Matrix Syntactic Foams. In: Proceedings of Materials Science and Technology (MS&T) 2008. Pittsburgh, Pennsylvania, USA, 2008, pp. 2607-2615.

Xue, X.B., Zhao, Y.Y., Kearns, V., Williams, R.L. & Jones, D., (2010). Mechanical and Biological Properties of Titanium Syntactic Foams. In: Supplemental Proceedings of 2010 TMS Annual Meeting & Exhibition, Vol. 2. The Minerals, Metals & Materials Society (TMS), Warrendale, Pennsylvania, USA, 2010, pp. 129-135.

X.B. Xue

October 2010

List of Symbols

b:	(mm)	Width of the specimen used in three-point bending test
d:	(mm)	Depth of the specimen used in three-point bending test
E:	(GPa)	Elastic modulus of the specimen
F:	(N)	Maximum load applied to the specimen during three-point bending test
L:	(mm)	Span length used in three-point bending test
N_c:		Counted cell number density
P:		Porosity of sample
p:		Gradient of the linear part of the load-displacement curve
W_c:	(g)	Weight of the CM in the sample
W_I:	(g)	Weight of injected molten Co-Cr-Mo alloy
W_L:	(wt%)	Weight percentage of lost CMs during casting
W_s:	(g)	Weight of Co-Cr-Mo matrix syntactic foam sample
W_{Ti}:	(g)	Weight of Ti in the sample
V_a:	(mm^3)	Total air pores volume in the CMs
V_c:	(mm^3)	Volume of the CMs before compaction
V_{ca}:	(mm^3)	Volume of the connected pores
V_{cc}:	(mm^3)	Volume of the crushed CMs
V_{uc}:	(mm^3)	Volume of the un-crushed CMs

V_n:	(mm^3)	Volume needed to culture cells with a cell number density of 5 x 10^4 μml
V_s:	(mm^3)	Volume of the sample
V_{sc}:	(mm^3)	Volume of the solid ceramic in the sample
V_{Ti}:	(mm^3)	Volume of Ti powder in the sample
V_{TM}:	(mm^3)	Volume of the Ti matrix in the sample
V_1:	(mm^3)	Ideal volume of the preform without crushed CMs
V_2:	(mm^3)	Actual volume of the preform with crushed CMs
f_{Ti} :		Actual volume fraction of Ti
ρ_{Ti}:	(g/cm^3)	Density of Ti
ρ_{sc}:	(g/cm^3)	Density of solid ceramic
ρ_c:	(g/cm^3)	Density of the CMs
σ:	(MPa)	Flexural strength
φ_v:		Volume percentage of crushed CMs calculated by volume measurement method
φ_w:		Volume percentage of crushed CMs calculated by water absorption method

Contents

Chapter 1 Introduction

1.1 Implant Materials

Implant materials are objects manufactured from non-living materials and inserted into the human body, intended to remain in the body for a period of time in order to perform a specific function. Depending on the applied position, the implant materials can be classified as knee, hip, eye, ear, heart, kidney, brain or breast implants. Joint implants are one of the main markets continuing to grow rapidly. The demands for joint replacements have increased steadily in the last decade, as shown in Fig. 1.1 (Park & Lakes 2007).

The implant materials can be categorized according to the base materials as: (a) metallic implant materials, such as stainless steel, Co-based alloys, Ti and its alloys; (b) ceramic implant materials, such as aluminium oxide, zirconium oxide, calcium phosphate and glass ceramic; and (c) polymeric implant materials. In joint implant applications, an implant material needs to possess good corrosion resistance, biocompatibility, bioadhesion, biofunctionality, processability and availability. Metallic implant materials are particularly important for joint implant applications due to a combination of high fracture strength, good corrosion resistance and good biocompatibility.

Compared with human bone, the elastic moduli of current implant materials are significantly high, as shown in Fig. 1.2 (Perren *et al.* 2001). The most noticeable implant failure with growing implant period is loosening of the implant device, as shown in Fig.

1.3 (Park & Lakes 2007). The loosening of the implant device is caused by the stress shielding effect, which results in bone resorption, and thus leads to various degrees of bone loss. The subsequent bone remodelling may increase the pain of patient, decrease the function of the femur and femoral components, or loosen the implant devices.

Currently there are two methods to avoid stress shielding: improving the fixation of the device and using low elastic modulus materials to match the human bone. The fixation can be improved by modifying the surface of the implant, e.g. coating a porous layer to increase the adhesion of the implant device. A material with a low elastic modulus can transfer more physiological load to the femur. Therefore, the bone resorption in the femur and the failure of the cement mantle can be reduced.

Porous materials have recently attracted a lot of interest as biological materials, because they can have a low elastic modulus. However, they have a low mechanical strength compared with solid materials. There is a need to develop porous materials with high strength and low elastic modulus for biological applications.

1.2 Objectives

The main objective of this study is to develop novel materials, by embedding hollow or porous ceramic microspheres into metal matrices by powder metallurgy or casting, for

implant applications. The aim is to design the metal matrix syntactic foams, Ti and Co-Cr-Mo alloy based, to have a high mechanical strength without increasing the elastic modulus. The relationships between the mechanical and biological properties and the manufacturing conditions will be studied.

1.3 Structure of Thesis

There are five chapters in this thesis. Chapter 2 reviews the literature on the structure of human bone, the property requirements for implant materials, the development and manufacturing of implant materials, and the properties of the current implant materials. The stress shielding effect and the solutions used to solve it are discussed. The manufacturing processes, properties, advantages and disadvantages of metal foams, especially Ti foam and metal matrix syntactic foams, are reviewed. Powder metallurgy, a technique relevant to this study, is also reviewed.

Chapter 3 gives a detailed description of the manufacturing method, mechanical tests and biological tests of the Ti matrix syntactic foam. The relationships between density and porosity and the manufacturing conditions, e.g. Ti volume percentage and compaction pressure, are presented and discussed. The percentage of crushed ceramic microspheres as a function of manufacturing condition is estimated. The effects of the manufacturing conditions on the mechanical properties, including compressive strength, flexural strength,

elastic modulus and hardness, are presented and discussed. The performance of the Ti matrix syntactic foam in *in vitro* biological tests is also studied.

Chapter 4 presents a feasibility study on the fabrication of a Co-Cr-Mo alloy matrix syntactic foam by casting. The manufacturing process, structure and characteristics of the Co-Cr-Mo alloy matrix syntactic foam are described and discussed.

Chapter 5 summarises the conclusions obtained from this study and makes a few suggestions for future work.

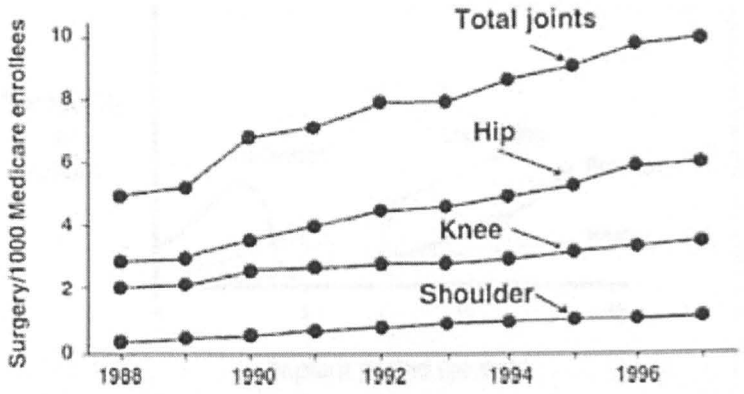

Fig. 1.1 Statistics of joint replacements in the 1990s (Park & Lakes 2007).

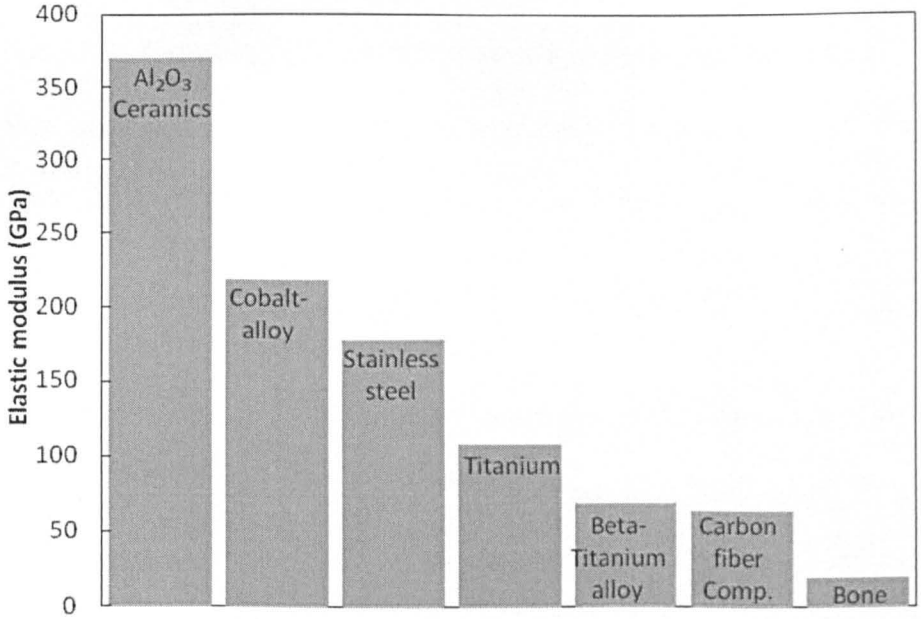

Fig. 1.2 Elastic moduli of different types of implant materials in comparison with that of bone (Perren *et al.* 2001).

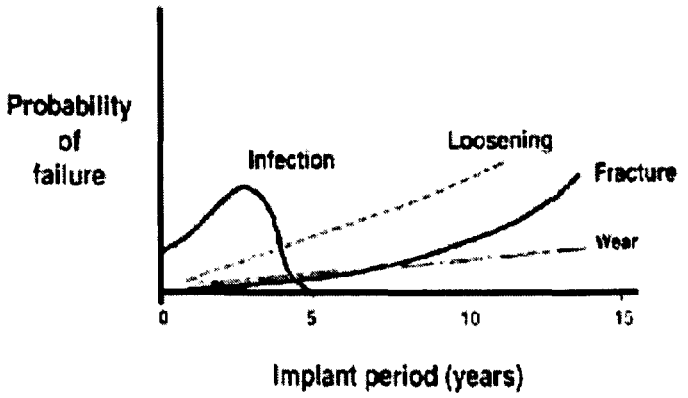

Fig. 1.3 Schematic illustration of probability of failure with the implant period growth (Park & Lakes 2007).

Chapter 2 Literature Review

2.1 Structure and Properties of Human Bone

Fig. 2.1 shows a schematic image of the cortical and trabecular bone (SEER 2005). There are two main types of bone: compact (dense) and cancellous (spongy). The compact bone, also known as cortical bone, forms the surface layers or cortex of mature bone; the cancellous bone, synonymous with trabecular or spongy bone, forms the interior of the bone (Gunn 2002). The compact bone, containing less porosity, is found mainly in the shafts of long bones where a strong, tubular structure is required. It gives bones the smooth, white and solid appearance. The cancellous bone, containing large porosity, is found in the parts of bones where lightness, strength and area are required. Bone marrow is found between the trabecules which form the internal support structure of the bone.

Recent research showed that the compositions and true tissue densities of normal trabecular and compact bone are similar. Further research suggested that the microscopic material properties of trabecular bone are similar to those of compact bone (Martin 1972; McElhaney *et al.* 1970; Pugh *et al.* 1973a; Pugh *et al.* 1973b; Townsend *et al.* 1975). Therefore, whole bones can be modelled as composite structures consisting of both a solid and a fluid phase. The solid phase is the mineralized bone tissue, and the fluid phase is composed of blood vessels, blood, red and yellow marrow, nerve tissue, miscellaneous cells, and interstitial fluid (McElhaney *et al.* 1970). The compressive behaviour of human bone as a two-phase porous structure has been examined with and without marrow (Carter *et al.* 1977). The stress-strain curves, as shown in Fig. 2.2, show a roughly linear region,

followed by obvious yielding. After the yielding, a large region of nearly constant stress is shown. This region is named as post-yield region, which indicates the progression of trabecular bone failure and pore collapse. Normally, this post-yield region develops until the specimens are compressed by more than half their original thickness.

The mechanical behaviour of compact bone and cancellous bone has been examined many times. However, the mechanical behaviours of the bones vary with human age, gender and position in the human body. The mechanical properties of compact and cancellous bone are listed in Table 2.1

Table 2.1 The mechanical properties of compact and cancellous bone.

	Compact bone	Cancellous bone
Denstiy (g/cm^3)	1.30±0.03 (1)	0.34-0.35 (4)
Elastic Modulus (GPa)	3.88-11.7 (2)	0.43 in axial, 0.127 in transverse (4)
Compressive strength (MPa)	88.3-163.8 (2)	4.5 in axial, 1.6 in transverse (4)
Flexural strength (MPa)	88.9-113.8(3)	

(1) Orvieto *et al.* 1992; (2) Ascenzi & Bonucci 1967; (3) Ascenzi & Bonucci 1968; (4) Giesen *et al.* 2001.

2.2. Bone Implant Materials

2.2.1 Requirements

Implant materials have been widely applied in clinical science. Every year, there are more than 300 000 hip and knee implants and between 100 000 and 300 000 dental implants used in the United States to replace or restore function to diseased and damaged tissues (Puleo & Nanci 1999).

For bone implants, the general criteria for material selection are (Katti 2004):

a. They are highly biocompatible and do not cause an inflammatory or toxic response beyond an acceptable tolerable level.

b. They have appropriate mechanical properties, closest to bone.

c. Manufacturing and processing methods are economically viable.

More requirements about the mechanical properties of the implant materials used for osteosynthesis are summarized as follows (Williams 1973b):

a. Elasticity. Some implant devices have to be flexible, and some have to be rigid, depending on the application, position and function. The two elastic moduli, elastic modulus and shear modulus, of the implant materials need to be variable so that the material can be tailored.

b. Yield or proof stress. In some applications, a permanent deformation of implant material is extremely undesirable due to the possibly fatal consequence. However,

in some applications, the implant material needs to deform to the required shape either at operation or during healing.

c. Ductility. Ductility is sometimes desirable for the fabrication and *in vivo* deformation, but sometimes extensive ductility is not desirable.

d. Toughness. It is important that the implant material should have adequate toughness.

e. Time-dependent deformation. The material should not creep under the applied loads, as creep may lead to damage to the function.

f. Ultimate strength. This property is required so that the material can produce adequate strength when the nature and magnitude of the applied stress is considered.

g. Fatigue strength. The implant material should have good resistance to the influence of the repeated stress.

h. Hardness. This property is particularly important in soft tissue reconstruction.

i. Wear resistance. This property is very important. Low wear resistance can result in generation of wear particulates, corrosion debris and the subsequent biologic response. They can cause major problems that may limit the durability of the joint reconstruction and the success of the procedure (Jacobs *et al.* 2006).

2.2.2 Development of metallic materials

2.2.2.1 Stainless steel

The development of stainless steel as an implant material has mainly been focused on the improvement of the corrosion resistance. The first stainless steel used for implants was 18-8, which is stronger than plain carbon steel and more resistant to corrosion (Park & Lakes 2007). Later molybdenum was introduced to 18-8 to improve the corrosion resistance. This alloy became known as type 316 stainless steel. In the 1950s, the carbon content of the 316 stainless steel was reduced, and thus a better corrosion resistance was achieved. This steel is known as 316L. 316 and 316L steels are the most widely used implant stainless steels nowadays. Some properties of annealed stainless steels are given in Table 2.2 (Williams 1973b).

Table 2.2 The mechanical properties of some stainless steels

	18Cr-8Ni softened	Extra-low carbon 18Cr-10Ni softened	316 softened	316 cold worked
Yield strength (MPa)	200-230	200-250	240-300	700-800
Tensile strength (MPa)	540-700	540-620	600-700	1000
Elongation (%)	50-65	55-60	35-55	7-10
Young's modulus (GPa)	200	200	200	200
Hardness (V.P.N.)	175-200	170-200	170-200	300-350

It is shown in table 2.2 that stainless steel has sufficient strength to meet the requirements described in Chapter 2.2.1 for implant applications. However, stainless steel has an elastic modulus approximately 10 times as that of the human bone. A significant stress shielding effect would occur, especially after a total femur replacement.

During manufacturing, 316 and 316L steels work-harden very rapidly, so heat treatment is necessary. However, the chromium carbide, formed during heat treatment can deplete Cr and C in the grains and thus cause corrosion. Therefore, the heat treatment needs to be controlled to avoid production of chromium carbide in grain boundaries. Moreover, using heat treatment can result in another undesirable effect, surface oxide scales. The surface oxide scale needs to be removed by polishing. Afterwards, the surface needs to be cleaned, degreased, passivated in nitric acid, washed and sterilized (Park & Lakes 2007).

2.2.2.2 Co-Cr based alloys

There are two major types of Co-Cr based alloy: Co-Cr-Mo and Co-Ni-Cr-Mo alloys. Co-Cr-Mo alloy is commonly used in dentistry and in making artificial joints. Co-Ni-Cr-Mo alloy is used for making the stems of prostheses for heavily loaded joints, for example knee and hip. The mechanical properties of Co-Cr based alloy are shown in Table 2.3 (Williams 1973b).

Table 2.3 The mechanical properties of Co-Cr based alloy

	Cast alloy	Wrought alloy (solution annealed)	Wrought alloy (cold worked)
Yield strength (MPa)	490	450	1050
Tensile strength (MPa)	690	950	1540
Elongation (%)	8	60	9
Young's modulus (GPa)	200	230	230
Hardness (V.P.N.)	300	240	450

The properties of Co-Cr alloy, as shown in table 2.3, are very similar to those of the stainless steel. It can satisfy the strength requirements of implant applications, but its elastic modulus is too high compared with that of the human bone. Therefore, the stress shielding effect is still a problem which prevents the Co-Cr alloy from wide applications in implants.

The normal cold-working fabrication procedure used for other metals is not suitable for Co-Cr. This is because its strength can be increased rapidly by plastic deformation. The common manufacturing method for Co-Cr based alloy is lost wax or investment casting. The procedure can be described as follows (Park & Lakes 2007):

a. A wax pattern of the desired component is made.

b. The pattern is coated with a refractory material, first by a thin coating with a slurry (suspension of silica in ethyl silicate solution) followed by complete investing after drying.

c. The wax is melted out in a furnace (100-150°C).

d. The mould is heated to a high temperature, burning out any traces of wax or gas-forming materials.

e. Molten alloy is poured with gravitational or centrifugal force.

2.2.2.3 Ti and Ti based alloys

Ti and its alloys have good biocompatibility, high strength-to-weight ratio, relatively low elastic modulus, high fatigue strength and excellent corrosion resistance as compared with widely used biomedical cobalt alloys and stainless steels, and therefore have been widely used in orthopaedic implants (Long & Rack 1998).

The earliest applications of Ti as a material for medical, surgical and dental devices were based on the post-World War II advances in Ti manufacturing processes for aerospace and military requirements. The four commercially pure (CP) Ti grades (ASTM 67), Ti-6Al-4V ELI (ASTM F 136), and standard Ti-6Al-4V (ASTM F 1472) were the first Ti biomaterials introduced in implantable components and devices. Its applications include

medical, surgical and dental devices (Steinemann & Perren 1984); hip and knee prostheses (Windler & Klabunde 2001); human joint replacements (McKellop *et al.* 2001); osteosynthesis applications (Perren *et al.* 2001); dental applications (Buser 2001; Esposito 2001); cardiac and cardiovascular applications (Olin 2001); audiology applications (Holgers & Hakansson 2001).

The mechanical properties of Ti depend strongly on the impurity content. The higher impurity content, the stronger but less ductile the metal is. The mechanical properties of four grades of CP Ti and Ti6Al4V are shown in Table 2.4 (Williams 1973b).

Table 2.4 The mechanical properties of CP Ti and Ti-6Al-4V

	CP Ti				Ti-6Al-4V	
	Grade 1	Grade 2	Grade 3	Grade 4	Wrought	Casting
Tensile strength (MPa)	240	345	450	550	860	860
Yield strength (MPa)	170	275	380	485	795	758
Elongation (%)	24	20	18	15	10	8
Young's modulus (GPa)	116					

The strength of Ti, as shown in table 2.4, is slightly lower than those of the stainless steel and Co-Cr alloy, but can still satisfy the requirements of implant applications. Ti has a

much lower Young's modulus than those of the stainless steel and Co-Cr alloy, but it is still higher than that of the human bone. It can still results in the stress shielding effect after implant surgery.

Ti has a very high reactivity at high temperature. Oxygen can defuse in Ti very rapidly and embrittle the Ti. Therefore, an inert atmosphere or vacuum is required for manufacturing. The common manufacturing processes for Ti products are casting and powder metallurgy.

Ti casting products are produced by the investment casting process. Ceramic moulds and special coatings are used to minimize the surface contamination. The molten metal is poured directly into the mould of the final part shape. The casting is hot isostatically pressed (HIP) to heal internal shrinkage porosity, followed by stress relief annealing and pickling to remove any possible surface contamination.

Ti powder metallurgy products are produced by cold pressing Ti powder into the desired final shape, and hot sintered in vacuum to consolidate and bond the particles. A post-sintering HIP process may be employed to further densify the part made from powder.

2.3 Implant Loosening

2.3.1 Causes

The surveys conducted by Havelin *et al.* (1993) and Malchau *et al.* (1993) showed that more than two thirds of all revisions of femural implants were caused by implant loosening, i.e., disruption of the implant/bone or cement interface (Postiglione & Domenico 2003). A major factor in implant loosening is caused by stress-shielding. Stress shielding in clinical definition refers to a phenomenon in which the physiological load applied to the bone is reduced due to the presence of an implant with stiffness greater than that of bone. With stress shielding, the bone becomes less dense and weaker. Periprosthetic bone remodeling secondary to stress-shielding may contribute to increased pain or decreased function, fracture of the femur or the femoral component, loss of fixation of the implant, increased prevalence or severity of osteolysis, and difficulty in performing a revision (Huiskes 1993; McCarthy *et al.* 1991). The solutions to implant loosening mostly focus on the improvement of the fixation and decreasing the elastic modulus of implants.

2.3.2 Improvement of fixation

2.3.2.1 Cement fixation

There are two clinically-proven principles currently applied for the fixation of prosthesis components: with cement and without cement.

In cement fixation, the prosthesis component is fixed in the bony implant bed with bone cement based material. In order to do this, the femur is machined with rasps and the cup with reamers, so that a 1 to 5 mm thick cement mantle can subsequently be applied. After removing any blood and medullary fat, the cement, which is prepared at the time of surgery, is applied with syringes inside the bony implant bed.

In cement fixation, the bone screw occupies an important position and they have been well studied in the clinical literature (Evans *et al.* 2006; Hyldahl *et al.* 1991; Lowery & McDonough 1998; Panagiotopoulos *et al.* 1994; Skinner & Powles 1986; Wimmer & Gluch 1998). New designs were proposed to avoid the stiffer screws "shielding" the bone from carrying the normal mechanical stress. One of these designs was a graded-stiffness composite screw intergrating two different material components: one was a low-stiffness –titanium core with an elastic modulus of 40 GPa, and the other was a polymeric external layer/threads with an elastic modulus of 10 GPa. This dynamic fixation design provided good clinical results and was considered as a standard treatment of femoral fractures (Adams *et al.* 2001). The other design was an active-compression hollow screw containing a rigid metal sphere.

2.3.2.2 Cementless fixation

Fixation without cement, also known as cementless fixation, requires a direct contact between the prosthesis and the bone. It requires an outstanding biocompatibility and

positive effect on osseointegration of the implant material. This fixation is particularly suitable for Ti and its alloys. This fixation is achieved by press fitting the prosthesis in the bone to form a stable primary mechanical anchoring. Generally, this press fitting needs a few weeks, or a few months to form the fixation.

A porous surface, coating onto the implants is a popular process to improve the cementless fixation. The bone tissue can penetrate into the pores, crevices or meshing of the porous implant surface, and thus achieves an intimate bond between the metal and the bone. Therefore, a porous surface coating on the implant material is an efficient method to increase the fixation of cementless fixation (Windler & Klabunde 2001). Several coatings are used to produce specific surface properties on components that cannot be provided by the base materials. Coatings can expand their areas of application by increasing the resistance of the surface against wear and corrosion (Lausmaa 2001).

In the Ti surface coating process, pure Ti powder is sprayed onto the substrate by a plasma gas, Ar + H_2, with a spraying pressure of approximately 10 KPa. The substrate was pre-heated to 400-500°C before the spraying process. The thickness of the coating layer was regulated with spraying time (Yang *et al.* 2000). The growth of bone cells onto and into this rough and porous surface improves the force transmission between bone and implant and avoids stress concentration. Therefore, this surface fulfils one of several prerequisites for a durable secondary anchoring of the implant.

More recently, another alternatve surgical technique designed for cementless fixation was proposed. It tried to reduce the stress shielding by employing a direct bone-prosthesis contact. In this method, a general geometry for the natural load-transfer mechanism through the proximal femur was developed as much as possible in the first stage. Next, a proximal plate was added to distribute the contact load over the entire cross section of the femur and to reduce stress shielding in the cortical bone, as shown in Fig. 2.3 (Joshi *et al.* 2000). This plate was designed using proximal fixation (Munting & Verhelpen 1995). This device had a cabling system to help fix the prosthesis to the bone and produce a more natural bending load over the cross section of the femur by fixing the trochanter to the implant. This method is more suitable for the short stem than the long stem because the combination of a shortened stem and a proximal plate results in a major reduction in both stress shielding and interfacial shear stress. Because the plate is designed as a separate component, the prosthesis can be more easily customized to fit different sized femurs. This prosthesis provides contact with the entire cross section of the proximal femur resulting in much lower stress shielding when compared with a conventional intramedullary design.

2.3.3 Matching the elastic moduli of bones

Stress shielding can result in bone resorption and the subsequent implant loosening (Lenthe *et al.* 1997). To avoid implant loosening, the bone needs to carry its normal load after implant surgery. For metallic implant materials, their elastic moduli need to be

decreased; for composite implant materials, their elastic moduli need to be improved. The function of the femur can therefore be maintained.

For metals, ceramics and most materials which do not exhibit viscoelasticity, the strain is proportional to the applied stress in the elastic region (Williams 1973a). The slope of this linear curve is defined as the elastic modulus of the material. The higher value of the elastic modulus, the stiffer the material. To decrease the elastic modulus of metallic implant materials, air voids are introduced into the metal matrix to form a porous structure. The porous structure can result in a larger strain for a given stress than the solid structure. Therefore, the elastic modulus is decreased.

2.4 Ti Metal Foam

2.4.1 Introduction

There is a vast amount of literature in metal foams (Banhart *et al.* 1999; Banhart *et al.* 2003; Degischer & Kriszt 2002; Gibson & Ashby 1988). Metal foam is a cellular structure consisting of a solid metal and gas filled pores. The pores can be sealed (closed-cell) or interconnected (open-cell). The porosity in metal foam can give the material good energy and sound absorption properties, and make possible their use in filters, catalysts, and several other applications. Because of the porosity, metal foam strains more than the base material when a stress is applied. Therefore, the stiffness of metal foam is much lower than the base material.

2.4.2 Manufacturing methods

The most common manufacturing processes for metal foams are melt based for metals and alloys with low melting point and low reactivity with atmospheric gases (i.e., oxygen and nitrogen), such as aluminium. For metals with high melting points, such as Ti and Co-Cr based alloys, melting them cannot be achieved easily. Particularly for Ti, it has extreme chemical affinity with atmospheric gases. Oxygen and nitrogen can dissolve rapidly in liquid or solid Ti above 400°C. These dissolved gases result in a loss of ductility of Ti. Moreover, liquid Ti is highly reactive with most mould materials, further increasing the difficulty of melt processing. Using casting process to fabricate bulk Ti also requires high vacuum, high temperature processing equipment.

Powder metallurgy can produce bulk Ti at much lower temperatures and under less stringent chemical reactivity constraints. The process has avoided the liquid route. This is especially important for metal Ti foams since foams have high surface areas which can increase the possibility of contamination. The powder metallurgy process for Ti metal foam can be described as Fig. 2.4. First, the Ti metal powder is blended with the space holder, or foaming agent. The space holder can be spherical or angular small particles. The particle size of the space holder represents the desired pore size. After mixing, the mixture is compacted with a uniaxial or isostatic compaction pressure. After the compaction, the space holder is removed with a low temperature heat treatment. The preform is subjected to the sintering process. In this manufacturing process, the pore size, shape and amount are determined by the space holder used. A large number of studies

have used this manufacturing process to produce Ti foams. For example, Wen *et al.* (2001) used ammonium hydrogen carbonate as space holder, which can be decomposed at 200°C, and sintered Ti at 1200°C for 2 hours; Rausch & Banhart (2002) used polymer granules as the space holder, which can be removed chemically at 130°C, and sintered Ti at 1100-1250°C; Wheeler *et al.* (1983) used Mg powder as the space holder, which can be removed by evaporation at 1400°C when the Ti powder is sintered.

Alternatively, the space holder can be removed after sintering. The sintering and dissolution process (SDP) (Zhao & Monaghan 2008) is a novel manufacturing method for Ti foam. In this method, sodium chloride (NaCl) powder was selected as the space holder. At first, Ti powder was blended with NaCl powder and compacted into a green sample in a steel tube under a pressure of 250 MPa using a hydraulic press (Zhao *et al.* 2004). Iron powder was used to seal the tube end to protect the green samples from excessive oxidation in atmospheric conditions during sintering. Additional NaCl powder was used to separate the green samples from the iron powder seals to prevent interference with the Ti/NaCl compact. The green samples together with the steel tubes were sintered in a standard electric furnace under normal atmospheric conditions, at temperatures ranging from 750-950°C for 2, 4 and 6 hours. After sintering, the samples were air cooled to room temperature and removed from the steel tube. In terms of the melting of NaCl during high temperature sintering, the NaCl formed a layer at the sample surface. This layer was removed using grinding paper. Further residual NaCl was removed using an ultrasonic dissolution process in heated water for three hours.

Using NaCl powder as space holder can help to decrease the oxidation of Ti during sintering. The NaCl powder used was melted around 785°C. During the sintering at 800° C, the molten NaCl experienced less flow and effectively sealed and protected the Ti foam from exposure to the air (Zhao & Monaghan 2008). When the sintering temperature was increased to above 900°C, a highly oxidised sample was produced, because the fully molten NaCl resulted in movement of gas around the sample.

2.4.3 Properties

2.4.3.1 Biocompatibility

Porous implant components based on biocompatible metallic materials can promote interactions between bone and the surrounding tissue (Inoue *et al.* 1987). A lot of research was conducted on Ti metal foam. The pores facilitate the bone tissue formation by allowing the migration and proliferation of osteoblasts and mesenchymal cells. In addition, a porous surface provides mechanical interlocking between the implant and the surrounding bone, enhancing mechanical stability at the interface (Dizlek *et al.* 2009).

Ti metal foam can also provide a good pore size for implant applications. The requirements for the pore size in these materials have been identified for the implant applications, such as the minimum pore size for bone replacement needing to be larger than 100 μm (Hulbert *et al.* 1970), and the pores needing to be interconnected to maintain

the vascular system required for continuing bone development (Dizlek *et al.* 2009). In Ti metal foam, the pore size and distribution are determined by the space holder. By controlling the space holder parameters, such as size and position in the preform, it is easy to fabricate a product with desirable pore structure.

2.4.3.2 Mechanical behaviour

While maintaining excellent biocompatibility, Ti metal foam has quite different mechanical properties from bulk Ti because of the existence of pores. The mechanical properties of Ti metal foam are strongly affected by the porosity. The compressive and bending behaviours with different porosities are shown in Figs. 2.5 and 2.6, respectively (Thomas 2007).

In the compressive tests, the specimens were cylinders with a diameter of 16 mm, and a height of 16 mm. The porosities ranged from 50% to 80%. The specimens could be deformed by 50% without appearance of any macroscopic cracks. Generally, a higher porosity resulted in a lower compressive strength. In each stress-strain curve, there was a region with a stable stress and a large strain. The higher the porosity, the larger this region was.

In the three point bending tests, the specimens had a cross section of 4.2 mm X 8.2 mm and a span length of 30 mm. The porosities ranged from 50% to 80%. The displacements corresponding to the maximum bending stress were nearly the same for the specimens with different porosities. The bending stress strongly depended on the porosity of the specimen.

Fig. 2.7 shows the relationship between the stiffness and yield strength for Ti metal foams with porosities between 50 and 80%. It is shown that the mechanical properties of Ti metal foam can be close to those of human bones. By changing the porosity of Ti metal foam, the compressive strength and bending strength can be changed. Oh *et al.* (2002a) sintered spherical unalloyed Ti particles with and without applied pressure and achieved a porosity between 19 and 35%. The stiffness of the porous titanium was close to that of human bone.

2.4.4 Advantages and disadvantages

The porous structure, particularly open-cell structure, of Ti foam extends the applications of implant materials in implant surgery. The porous surface of metal foam can enhance the fixation of implants by the bone tissue penetration into the pores. The interconnection with the pores can maintain the vascular system required for the bone development. The porous structure decreases the elastic modulus of the implant material and makes it more

comparable to the human bone. By varying the porosity, the stiffness of Ti metal foam can be distributed between the cancellous bone and cortical bone, as shown in Fig. 2.7.

However, the requirements for the implant materials from the surgery are complex. The most important properties of implant materials are considered to be elastic modulus, yield strength, ductility and good toughness (Williams 1973b). Recent research showed that although the modulus values of sintered Ti compacts and Ti foams of varying porosities were comparable with those of bone, the compressive strength values were lower than those of cortical bone due to the relatively low yield strength of the Ti powder used (Oh *et al.* 2002a; Wen *et al.* 2002). Therefore, to increase the mechanical strength of implant materials while maintaining a comparable elastic modulus to human bone is a new challenge.

2.5 Metal Matrix Syntactic Foams

2.5.1 Introduction

Metal matrix syntactic foams are a class of composite materials consisting of a continuous metal matrix embedded with hollow or porous ceramic particles. In comparison with metal foams, they have higher compressive yield strength and more homogeneous mechanical properties, although they usually have higher densities (Zhao *et al.* 2008). The metal matrix is normally formed by either casting or powder metallurgy. The casting method is suitable for low-melting-point metals, and the powder metallurgy method is

mainly used for high-melting-point metals. The metal matrix produced by casting is much denser than that produced by powder metallurgy and has a uniform ceramic microsphere (CM) distribution. However, in the casting process, the volume ratio between the metal matrix and the CMs cannot be varied, and thus the mechanical properties cannot be varied in a wide range. Moreover, for metals with high melting points, applying a casting process is difficult and costly. It needs high temperature with inert gas protection or high vacuum to decrease oxidation. In contrast, powder metallurgy can be easily applied to metals with high melting points, such as Ti. The mechanical properties of the metal matrix syntactic foams can be controlled to a certain extent by varying the volume ratio between the metal matrix and CM particles.

2.5.2 Manufacturing processes

Metal matrix syntactic foams can be manufactured either by the casting process or by the sintering process. For metals or alloys with low-melting points, such as aluminum and magnesium, using the casting process can achieve a higher quality metal matrix. For metals or alloys with high-melting points, such as Ti and steel, it is more appropriate to use the sintering process.

2.5.2.1 Casting processes

The casting processes are well documented and have been used to fabricate metal syntactic foams in many cases (Orbulov *et al.* 2009; Stobener & Rausch 2009; Tao *et al.*

2009). The most common material used for the metal matrix is aluminium. This is because aluminium and its alloys have low density, relatively low melting point and good castability (Orbulov *et al.* 2009). The common processes used for the fabrication of Al matrix syntactic foam are infiltration casting, stir casting and liquid sintering (Zhao & Tao 2009).

Infiltration casting, also known as pressure infiltration or melt infiltration, can produce a continuous metal matrix easily. In this method, the molten metal is pressed into loosely packed ceramic particles and solidifies to produce the alminium matrix. The pressure used is roughly about 10 MPa (Orbulov *et al.* 2009). The advantages of this method are good controllability and reproducibility, uniform distribution of ceramic particles and good interfacial bonding between the metal matrix and the ceramic particles. However, because the ceramic particles have already packed before the molten metal infiltration, the amount of space between the ceramic particles is nearly fixed. As a consequence, the volume ratio between the metal matrix and ceramic particles is nearly fixed too.

Stir casting, also known as blending casting, is widely used to manufacture metal matrix syntactic foams. In this method, the metal ingot is melted in a furnace. Flux or inert gas is normally used to prevent the oxidation of the molten metal. Ceramic particles are preheated to a temperature close to the temperature of the molten metal, and then added to the molten metal and stirred continuously using a mechanical stirrer. During the stirring, the temperature is still maintained at the temperature of the molten metal. The stirring

time and stirring speed depend on the viscosity of the molten metal. For example, for Al-12%Si alloy, the stirring time is 5-8 minutes and stirring speed is 550 rpm (Ramachandra & Radhakrishna 2005). Finally, the molten metal, together with the ceramic particles, is poured into the mould and solidified in the mould. By using this method, variable volume fractions of the ceramic particles in the syntactic foam can be obtained. However, it has a few shortcomings. Because of the lower density of the ceramic particles compared with the molten metal, they tend to float to the top of the molten metal. As a consequence, the distribution of the ceramic particles is not uniform. The ceramic particles are normally not wetted by the molten metal, and thus tend to cluster together. These two reasons result in an inhomogeneous structure in the syntactic foam. One solution to increase the wettability of the ceramic particles is adding magnesium in the melt (Ramachandra & Radhakrishna 2005). A vortex method is also used to improve the distribution of ceramic particles in the molten metal (Ramachandra & Radhakrishna 2005; Surappa & Rohatgi 1981).

The liquid sintering method, also known as liquid phase sintering, is an old technique in the ceramic industry. It is a sintering process involving coexisting liquid and particulate solid during some part of the thermal cycle (German 1985). In the liquid sintering method, to fabricate a metal syntactic foam, the metal particles and ceramic particles are blended uniformly, and then heated to above the melting point of the metal. Pressure is applied to remove the air voids included in the mixture and to disrupt the oxide shell of the molten particles (Tao *et al.* 2008). This manufacturing process can produce a homogeneous structure with uniform distribution of ceramic particles. The volume fraction of ceramic particles can also be varied easily. However, this process has a few shortcomings which

can result in a poor structure and consequently low mechanical properties, such as the oxidation of Al particles and the entrapment of oxides in the matrix, poor blending quality of the metal and ceramic particles. (Zhao & Tao 2009).

2.5.2.2 Sintering process

The sintering process to manufacture metal matrix syntactic foams is very similar to that used to fabricate metal foams. The difference is that the space holder is replaced by the ceramic particles and after sintering the ceramic particles are not removed. During the sintering, a solid metal matrix is formed and the ceramic particles are thus embedded into the metal matrix. Depending on the properties of metal matrix, the sintering conditions, such as sintering temperature, time and environment, can be different. Taking Fe matrix syntactic foam as an example, the Fe powder is blended with ceramic particles uniformly, compacted to 150 MPa and subjected to the sintering process with a sintering temperature of 850°C and a sintering time of 4 hours (Zhao *et al.* 2008).

2.5.3 Compressive behaviour

Compared with metal foams, metal matrix syntactic foams have a higher compressive yield strength and more consistent mechanical properties but usually higher densities and lower plasticity. Compared with metal matrix composites, they have lower strength but offer some compressibility (Zhao & Tao 2009). The mechanical properties of metal

matrix syntactic foams are mainly determined by the matrices. The metal matrix can be formed either by casting or by sintering. Depending on the manufacturing method of the metal matrix, the mechanical behaviour is different.

For metal matrix syntactic foams fabricated by the melt infiltration process, the metal matrix is continuous and homogenous. However, the volume percentage of metal matrix in the syntactic foam cannot be varied. In the manufacturing process, the molten metal is pressed into the gaps between the ceramic microspheres. The volume of the metal matrix is determined by the volume of the gaps between the ceramic microspheres, which cannot be changed easily. As the volume percentage of the metal matrix is approximately fixed, the mechanical behaviour is mainly determined by the properties and structure of the constituents, i.e. the matrix and the ceramic particles (Zhao & Tao 2009). A study was conducted to change the volume percentage of the metal matrix by mixing two different sized ceramic microspheres with a range of volume ratios. The results showed that the volume percentage of the metal matrix in the syntactic foam was between 60%-75% (Tao *et al.* 2009).

For metal matrix syntactic foams fabricated by the sintering process, the metal matrix cannot have the same continuous and homogenous structure as that fabricated by the casting process. However, the volume percentage of the metal matrix can be varied in a large range. By changing the weight ratio between the metal powder and the ceramic microspheres, a wide range of volume percentages of metal matrix in the syntactic foam

can be obtained. The compressive behaviour of steel matrix syntactic foam fabricated by the sintering process was examined (Zhao *et al.* 2008). With the volume percentage of the steel matrix in the syntactic foam increased from 40% to 70%, obvious variation in compressive behaviour among different samples was observed. A higher volume percentage of the steel matrix resulted in a higher compressive strength and a larger corresponding strain. The collapse strength initially increased with volume percentage of steel, and then decreased above a volume percentage of 60%.

2.5.4 Effects of manufacturing conditions

The compressive strength of metal matrix syntactic foam can be affected by the mechanical properties of the metal matrix and ceramic particles, the volume percentage, structure and distribution of the ceramic particles, and the interfacial bonding between the metal matrix and ceramic particles (Zhao & Tao 2009). The effects of the metal matrix and the ceramic particles are discussed as follows.

2.5.4.1 Effect of metal matrix

The properties of the metal matrix contribute to the properties of metal matrix syntactic foam to a large extent. Different metal matrices have different properties. Even for the same type of metal matrix, the mechanical properties of the metal matrix can be different due to different impurities and manufacturing conditions, such as heat treatment. For example, there is a large difference between the compressive strengths of Al matrix

syntactic foams with an Al 7075 matrix and a commercially pure Al matrix (Palmer *et al.* 2007). The compressive strength of A201 matrix syntactic foam by peak-aging is much higher than that by annealing (Kiser *et al.* 1999).

2.5.4.2 Effect of ceramic particles

The compressive strength of metal matrix syntactic foam is dependent on the strength, volume percentage, inner structure and porosity of ceramic particles (Zhao & Tao 2009). Usually, the ceramic particles used to fabricate metal matrix syntactic foam have hollow or porous structure to achieve higher specific strength. The ceramic particles with hollow structure have much higher strength than the porous ones. The metal matrix syntactic foam fabricated with porous ceramic particles has lower compressive strength than those fabricated with hollow ceramic particles (Tao *et al.* 2009).

The volume percentage of ceramic particles can significantly affect the compressive strength of metal matrix syntactic foam. Therefore, the volume percentage of ceramic particles is usually determined by the requirement of the application. However, the volume percentage of ceramic particles cannot be changed easily for some manufacturing process, such as the infiltration process, which has been discussed in section 2.5.2.1. The other manufacturing processes, such as stir casting and liquid sintering, can achieve a wider range of volume percentages of ceramic particles (Daoud 2008; Tao & Zhao 2009). Generally, decreasing the volume percentage of ceramic particles in the metal matrix

syntactic foam, or increasing the volume percentage of metal matrix, can increase the compressive strength of the metal matrix syntactic foam. However, when the volume percentage of metal matrix was increased over a limit, the compressive strength was nearly unchanged (Tao & Zhao 2009). If the volume percentage of the metal matrix was increased further, the compressive strength of the metal matrix syntactic foam was decreased (Daoud 2008).

Increasing the wall thickness of the ceramic microspheres can significantly increase the compressive strength (Kiser *et al.* 1999; Wu *et al.* 2007). The particle size of ceramic microspheres can also affect the compressive strength, but this effect is arguable (Palmer *et al.* 2007; Surappa & Rohatgi 1981; Wu *et al.* 2007).

2.6 Powder Metallurgy

2.6.1 Introduction

There are five basic manufacturing processes that utilize metal powders. They are conventional powder metallurgy (P/M), which is the dominant process in industry, metal injection moulding (MIM), powder forging (P/F), hot isostatic pressing (HIP) and cold isostatic pressing (CIP) (Metal Powder Industries Federation 1998). P/M is a forming and fabrication technique consisting of three major processing stages. First, the primary material is physically powdered, divided into many small individual particles. Next, the powder is injected into a mould or passed through a die to produce a weakly cohesive

structure very near the dimensions of the object ultimately to be manufactured. Finally, the end part is formed by applying pressure, high temperature, and long sintering time. The P/M process can be used for a variety of alloys, giving the designer a wide range of material properties.

The mechanical properties of Ti-6Al-4V produced using different production methods are shown in Table 2.5 (Buser 2001).

Table 2.5 Comparison of mechanical properties of Ti-6Al-4V fabricated with different processes.

Process	Porosity (%)	Yield Strength (MPa)	Tensile Strength (MPa)	Elongation (%)
ASTM B265 Grade 5	0	830	895	10
Cast	0	840	930	7
Cast + forge	0	875	965	14
Elemental sinter	2	786	875	8
Elemental HIP	<1	805	875	9
Prealloy HIP	0	880	975	14

Ti P/M products are produced by two different processes, depending on the production quantity and mechanical property requirements.

a. Prealloyed, gas atomized powder is hot isostatically pressed. This process provides product properties comparable to those fabricated by the cast and forged process.

b. Elemental powders are die compacted and vacuum sintered. This process is

mainly applicable to those applications with high volume, less demanding requirements. The products fabricated by this process can be subsequently HIP processed to further improve properties.

2.6.2 Powder die compaction

Powders are compacted in dies to produce coherent and durable porous preforms. The preform may have an immediate use, such as a pharmaceutical tablet, or be a precursor for the production of a more dense body by subsequent sintering as in the case of ceramics or metal. Powder compaction has been well studied and the stress distribution is examined by many researchers (Aydin *et al.* 1996; Briscoe & Rough 1998; Coube & Riebel 2000; Zahlan *et al.* 2001). Understanding the stress distribution is important for the improvement of the powder compaction.

When a material is subjected to a force, two types of deformation can take place: elastic and plastic deformation. Elastic deformation can be recovered by removing the force. However, plastic deformation is permanent. When the powder is subjected to compaction, both elastic and plastic deformations occur. In the first stage, the powder is initially loose. When the hydrostatic pressure is increased to beyond a certain level, the powder volume is reduced by compaction. When the pressure is increased beyond a critical point, the material will shear at constant volume (Zahlan *et al.* 2001).

During die compaction, if the lower punch is fixed, the force applied to the upper, moveable punch is named applied force. The reaction force applied to the lower punch is named transmitted force. The applied stress and transmitted stress are shown in Fig. 2.8 (Briscoe & Rough 1998). During the upper punch movement, the difference between the applied stress and the transmitted stress becomes larger and larger. When the applied force reaches a critical point, the movement of the upper punch is nearly stopped, and the stress increases rapidly. At this time, the difference between the applied stress and transmitted stress is nearly constant.

Another obvious exhibition in powder compaction is the density variation within the preform. A variety of experimental methods have been used to determine the density distributions developed within a green powder compact formed by single acting uniaxial die pressing (Kandeil *et al.* 1977; Macleod & Marshall 1977). The general agreement can be summarized as: in the outer circumference of the top and bottom of the compact, the density distribution decreases from surface to centre; in the central axis, the density increases from top to bottom. A typical density distribution is shown in Fig. 2.9.

2.6.3 Sintering

The term sintering is commonly used to refer to the heat treatment by which powders are consolidated into coherent and/or dense polycrystalline aggregates. It is one of the most important and versatile methods of integration of materials in metallurgy and ceramics.

Understanding of the process involved in sintering is vital to understand the central problem of powder technology.

During sintering, an obvious volume change can be observed. This phenomenon is brought by the unbalanced forces acting between particles in the interior of the compacts. These unbalanced forces are due to the capillary force, which is trying to reduce the total surface, and the energy of the system. This capillary force comes from the surface pressure difference of the separation plane. It is usually assumed that at equilibrium the pressures of two phases in contact should be equal. This is true if surface effects are not taken into consideration. However, if the surface of separation is not plane, then any displacement producing volume change will change its area and energy. In other words, the existence of a curved surface of separation between two phases results in the appearance of an additional force. As a result, the pressures in the two phases are not equal; the difference is called surface or interface pressure.

The capillary force is strongly dependent on the surface geometry. However, in most sintering, the distribution of powder particle shape and dimension is unknown. The general physical description and prediction of the changes taking place during sintering is hard to predict, at least before the problems involving the systems of simplified geometry are solved (Kuczynski 1972). Under the capillary force, a mass flow phenomenon which can bring about the changes of volume and shape will occur during the sintering. The

mass flow consists of viscous or plastic flow, volume diffusion, surface or grain-boundary diffusion, and evaporation and condensation (Kuczynski 1972).

In the compacts, the contacts between the powder particles can be either interpenetration or tangency. In the case of interpenetration, the distance between the particles decreases with the sintering time; the space between the particles is filled by the mass flow from the inside of the particles. In the case of tangency, there is no appreciable shrinkage, and the space between the particles is filled by the mass flow from the particle surfaces. This mass flow forms a bridge between the particles. By building the bridges between adjacent particles, the mechanical strength of the material is increased.

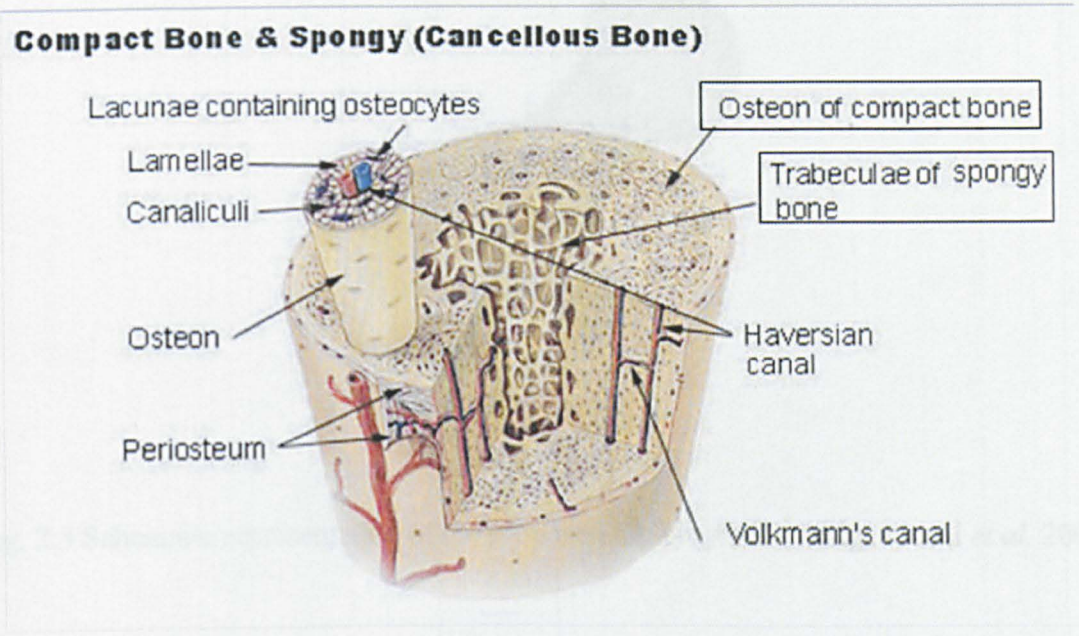

Fig. 2.1 A schematic image of the cortical and trabecular bone (SEER 2005).

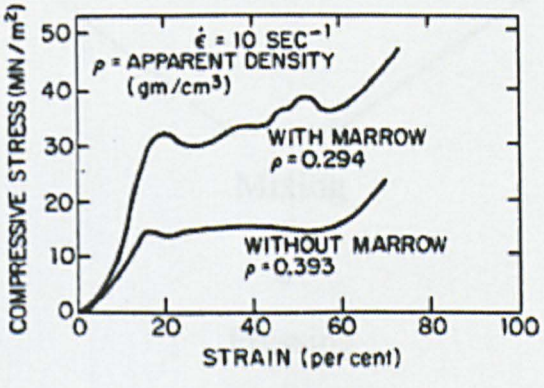

Fig. 2.2 The stress-strain curves of human bone examined with and without marrow as a two-phase porous structure (Carter *et al.* 1977).

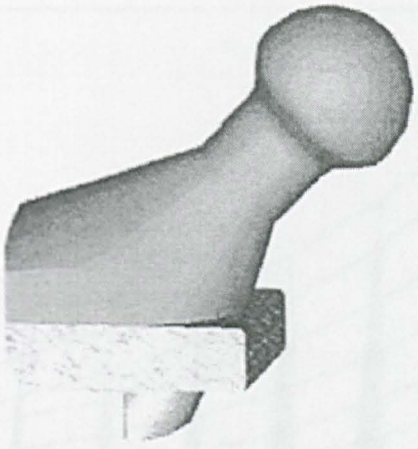

Fig. 2.3 Schematic representation of the proposed hip prosthesis design (Joshi *et al.* 2000).

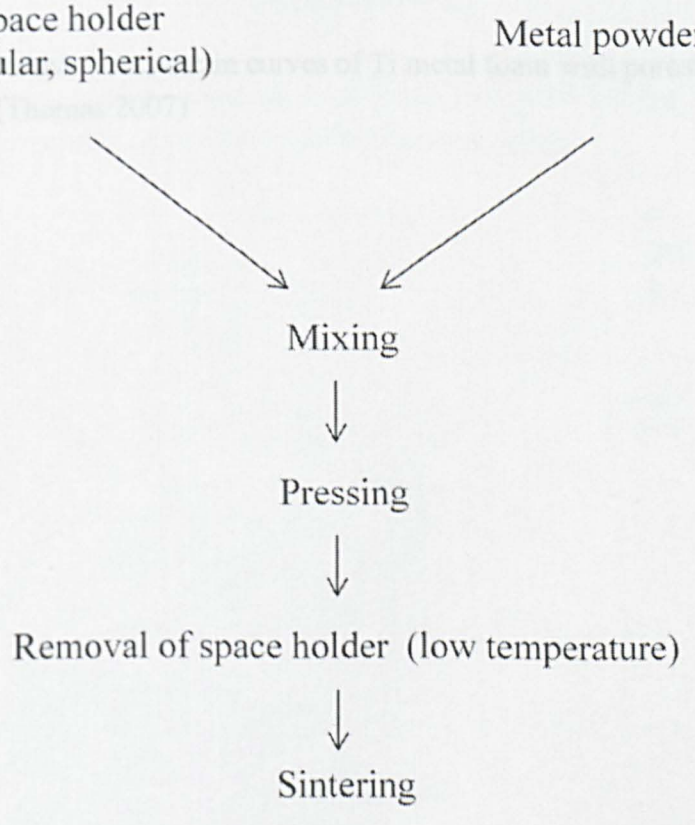

Fig. 2.4 Schematic of powder metallurgy process for metal foams.

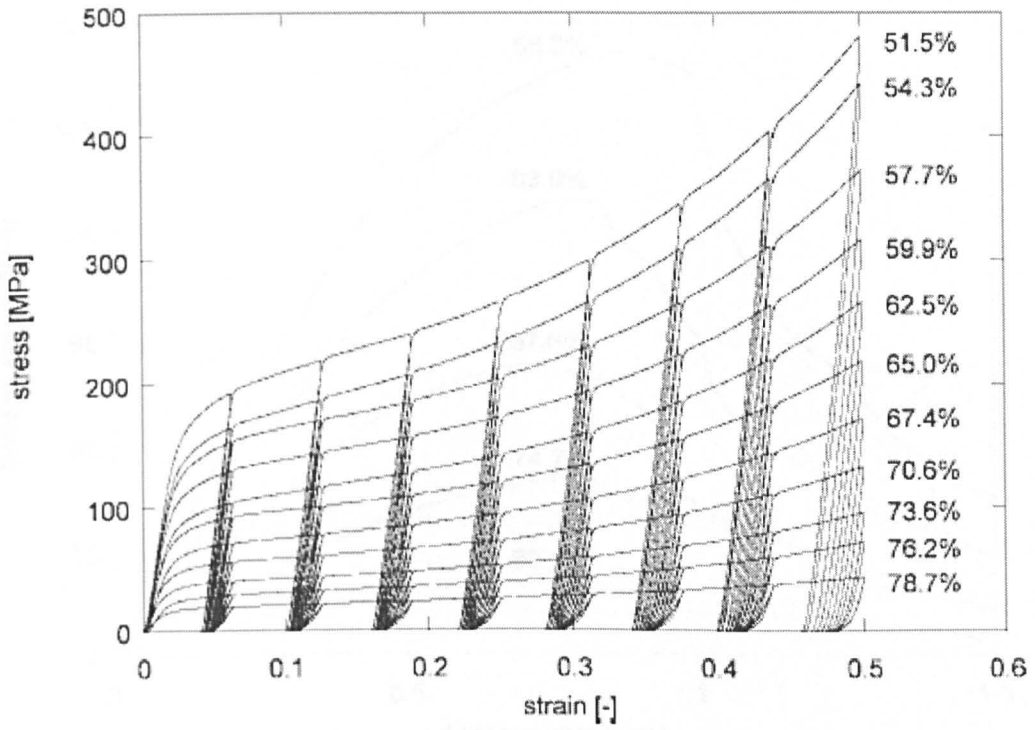

Fig. 2.5 The compressive stress-strain curves of Ti metal foam with porosities ranging from 50% to 80% (Thomas 2007)

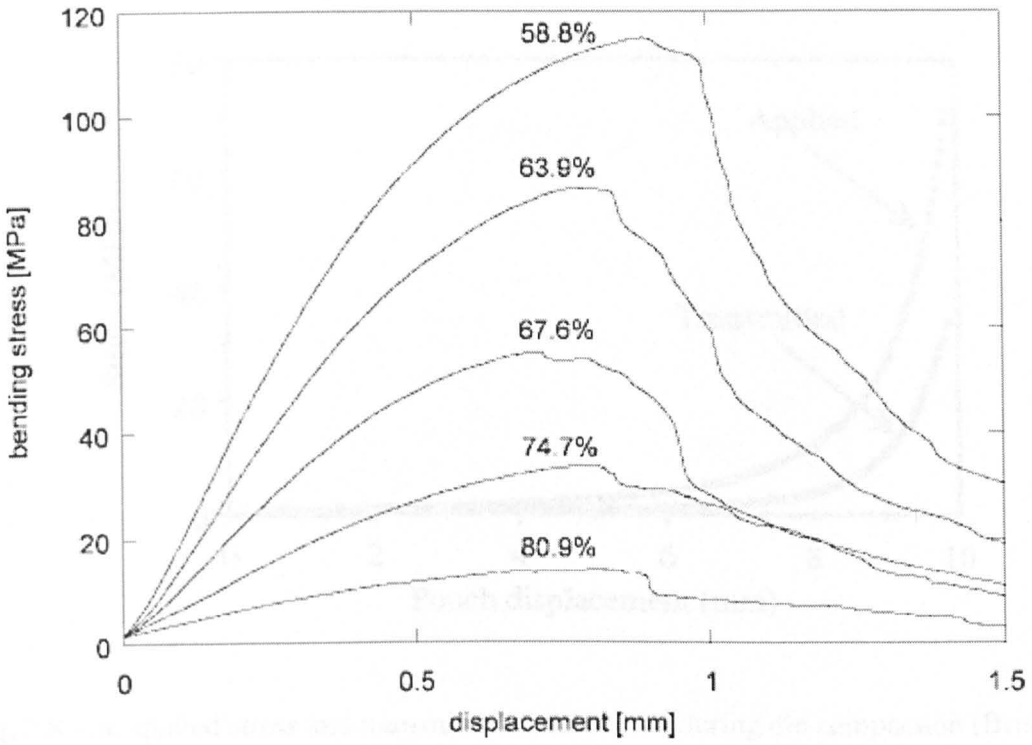

Fig. 2.6 The load-displacement curves obtained from three point bending test of Ti metal foam with porosities ranging from 50% to 80% (Thomas 2007).

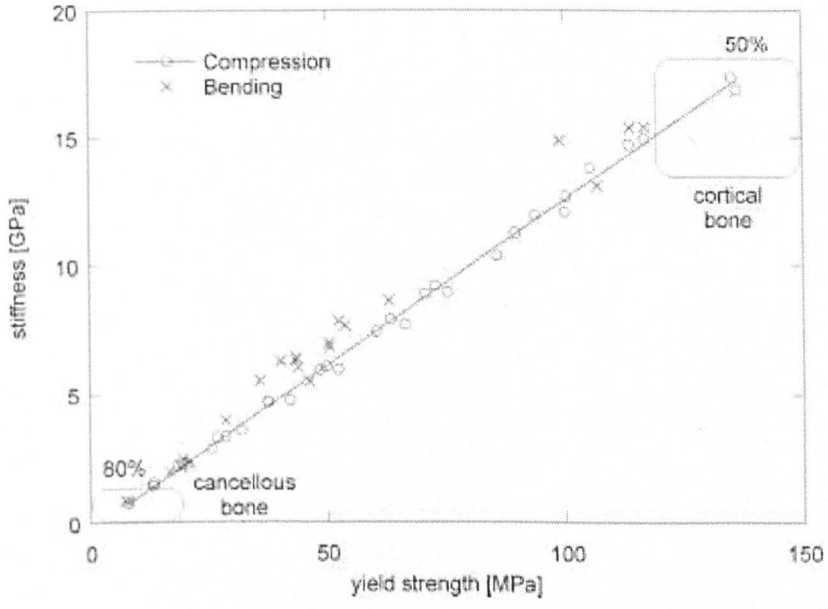

Fig. 2.7 Relationship between stiffness and yield strength for Ti metal foams with porosities between 50 and 80%. The data for cancellous and cortical bone are shown for comparison (Thomas 2007).

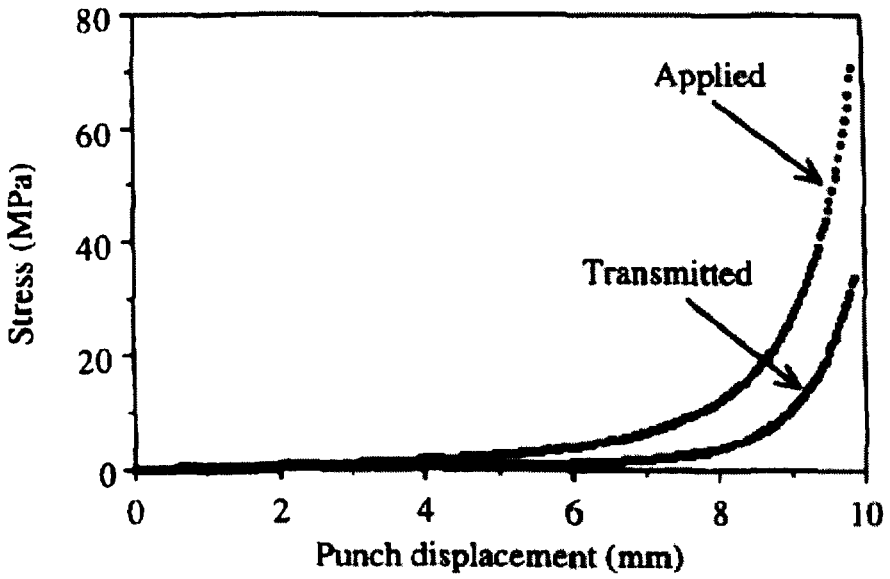

Fig. 2.8 The applied stress and transmitted stress curves during die compaction (Briscoe & Rough 1998).

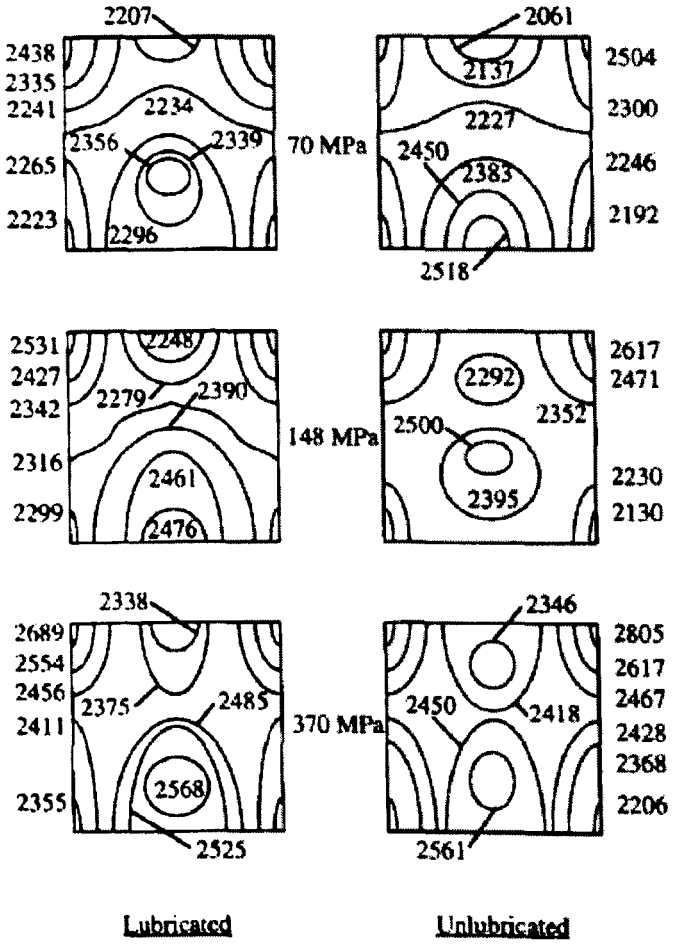

Fig. 2.9 The density distribution at different compaction stresses in lubricated and unlubricated dies (Briscoe & Rough 1998). The unit of the number shown in the figure is kg/m^3.

Chapter 3 Ti Matrix Syntactic Foam

3.1 Introduction

Ti is an excellent biomaterial for orthopedic and dental applications because of its good biocompatibility and corrosion resistance. Previous research has shown that Ti surfaces can support cell growth and differentiation (Ratner 2001), and many papers have shown that many proteins can be absorbed, such as albumin (Klinger *et al.* 1997; Serro *et al.* 1997), laminin V (Tamura *et al.* 1997), glycosaminoglycans (Collis & Embery 1992), collagenase (Kane *et al.* 1994), fibronectin (Steinemann 1998), complement proteins (Elwing *et al.* 1987) and fibrinogen (Sundgren *et al.* 1986). However, the surveys conducted by Havelin *et al.* (1993) and Malchau *et al.* (1993) showed that more than two thirds of all revisions of femoral implants were caused by implant loosening, i.e., disruption of the implant/bone or cement interface (Ridzwan *et al.* 2006). A major factor causing implant loosening is stress-shielding, a phenomenon in which the physiological load applied to the bone is reduced due to the presence of an implant with a stiffness greater than that of bone (Huiskes *et al.* 1992; Soininvaara *et al.* 2002). With stress shielding, the bone becomes less dense and weaker. Implant materials with an elastic modulus similar to that of human bone are thus desirable in implant applications, so that the distribution of loads in the bone is not altered. Bone is an anisotropic material and varies in its mechanical properties throughout the body. Therefore, a material that can be designed to have a variable elastic modulus would be an attractive candidate for implants.

A novel material, Ti matrix syntactic foam, was developed for implant applications and studied in this chapter. It was manufactured by mixing pure Ti powder and ceramic microspheres (CMs) followed by sintering in a vacuum furnace at high temperature. The structures of the natural fracture and cross-sectional surfaces of the samples were analyzed using optical microscope and scanning electron microscope. The densities and porosities of the samples were measured using Archimedes' method. The survival percentages of CMs in the samples were estimated. Compression and three-point bending tests were conducted. The compressive strength, flexural strength and elastic modulus were determined and compared with those of human bones. The hardness and impact toughness were also measured.

3.2 Experimental

3.2.1 Fabrication of samples

3.2.1.1 Raw materials

The raw materials used in fabricating the Ti matrix syntactic foam samples are a 99.4% pure Ti powder supplied by Active Metals Ltd U.K., and the Ceramic Microspheres (CMs), supplied by Pty Ltd Australia. The Ti powder particles have an irregular shape and are smaller than 45μm, with a nominal average particle size of 30μm (supplied by the company), as shown in Fig. 3.1. The EDX spectrum of the Ti powder is shown in Fig. 3.2. The major peaks are Ti kα and Ti kβ. There are small amounts of Al and N in the powder. However, the compositions of Al and N are too low to be detected and shown in spectrum.

The fine particles of the Ti powder can ensure that a homogeneous Ti matrix is formed and the CMs are surrounded by sufficient Ti powder particles during manufacturing.

The CMs have an approximately spherical shape, a composition of ~60% SiO_2, ~40% Al_2O_3 and 0.4-0.5% Fe_2O_3 by weight, and an average density of 0.8g/cm^3 (data supplied by company). Fig. 3.3 shows a SEM micrograph of the CM powder particles. The CMs have two typical structures, which are either hollow (Fig. 3.4a) or porous (Fig. 3.4b). The CM powder was sieved by a series of sieves on a vibration siever for 30 min. The CMs in the particle size range of 125 – 250 μm were used in this study. Although the majority of the CMs in this range were between 125-250μm, a small proportion of the CMs were smaller than 125 μm. A recent study was conducted to analyze the CM structure between 125 -250 μm (Tao & Zhao 2009). The CMs in the range of 125 – 250 μm had approximately 65% porous CMs and 35% hollow CMs. The CM particles have a compressive strength roughly of 45 MPa (Zhang & Zhao 2007). The compressive behaviour of CMs is shown in Fig. 3.5. Static compression tests were conducted on four different types of CMs. Type A are mainly hollow spheres with thick shells; type B, C, and D have relatively thin shells and contain irregular pores with thick wall. The CMs used in this study are type A.

3.2.1.2 Preparation of the preforms

A powder metallurgy process was used to manufacture the Ti matrix syntactic foam samples. It consisted of two stages: preparation of preform and sintering.

The preforms of the Ti and CM powder mixtures had a cylindrical shape with a height of 10 mm. The samples intended for mechanical and biological tests had diameters of 50 mm and 22 mm, respectively. Before mixing, the weights of the Ti powder and CMs for the preforms were determined by the volume percentage of Ti in the syntactic foam.

The required weights of Ti, W_{Ti}, and CMs, W_c, for each sample were calculated by:

$$W_{Ti} = V_s \times V_{Ti} \times \rho_{Ti} \tag{3.1}$$

$$W_c = V_s \times (1 - V_{Ti}) \times \rho_c \tag{3.2}$$

where V_s is the target volume of the sample, V_{Ti} is the intended volume percentage of Ti, and ρ_{Ti} and ρ_c are the densities of Ti and CM particle, respectively. V_D was 19.6 cm^3 for mechanical test samples and 3.5 cm^3 for biological test samples, corresponding to sample diameters of 50 and 22 mm, respectively. V_{Ti} was 40%, 50%, 60%, 70% or 80%.

The Ti powder and CMs were firstly dehydrated in a furnace at 200°C for 3 hours. This was to remove the moisture, which could prevent Ti particles from flowing smoothly

between CMs. After dehydration, the Ti powder was blended with CMs uniformly. Because Ti has a much higher density than that of the CMs, the blending process was carried out carefully until the CMs had a uniform distribution in the mixture. The powder mixture was ready for subsequent compaction.

Fig. 3.6 is a schematic diagram showing the process of the preparation of a preform. A cylindrical stainless steel tube was used to contain the Ti-CM mixture. The internal diameter of the tube was chosen according to the final sample dimensions required. The wall thickness of the tube was chosen to be sufficient to withstand the compaction force to prevent the tube from distortion and twisting during the compaction process. The internal surface of the tube was smoothed using 1200 grit paper and cleaned to avoid contamination. Once cleaned, the tube was placed on a machined stainless steel plug. An amount of iron powder, with an irregular particle shape and an average particle size of 100 μm, was poured into the tube through a funnel and compacted to seal one end of the tube using a hydraulic press. The pressure used for this iron powder layer was 200 MPa. The amount of the iron powder was chosen to create roughly a 10 mm layer after compaction. This iron powder layer was used to prevent the Ti/CM preform from contamination from the carbon released from the heating components of the furnace during the subsequent sintering. Afterwards, the Ti/CM powder mixture was poured into the tube and compacted to a pressure of 45, 70, 100, 150 or 200 MPa. Finally, another amount of iron powder was added and pressed to form a 10 mm iron layer to seal the other end of the tube. The pressure used for this iron powder layer was slightly lower than that used for the Ti/CM powder mixture.

3.2.1.3 Sintering

The preform, together with the stainless steel tube, was sintered in a vacuum furnace (Vacua-Therm Sales Ltd., U.K.) following the heating program shown in Fig. 3.7. The heating rate in the whole process was set to 10°C/min. The preforms were first preheated to 200°C and maintained at this temperature for 30 min to remove moisture and the adsorbed gases in the furnace chamber, so that a higher vacuum could be achieved. The furnace was pumped down to $1 \times 10^{-2} - 1 \times 10^{-3}$ mbar in about 30 minutes. The temperature was then increased to 1200°C for the sintering. The sintering time was 1.5 hours. The vacuum was kept at $1 \times 10^{-3} \sim 1 \times 10^{-4}$ mbar during the sintering process. After the completion of the sintering, the furnace chamber was naturally cooled to 500°C, and then was injected with Ar to accelerate the cooling of the samples.

The sintering temperature and time were selected according to the recommendations for industrial manufacturing processes (Freese et al., 2001). Natural cooling in the high temperature range can relieve the internal stress in the samples, which prevents dimentional distortions. Forced cooling in the low temperature range can accelerate the cooling process and thus decrease the extent of oxidation of the samples.

3.2.1.4 Summary of sample conditions

The manufacturing conditions used to fabricate the samples are summarized in Table 3.1. The sample identification number is characterized by the target or nominal Ti volume percentage and compaction pressure.

Table 3.1 Summary of the manufacturing conditions

Sample NO.	F_{Ti} (%)	Weight of Ti (g)		Weight of CM (g)		Compaction Pressure (MPa)
		ϕ22 mm	ϕ50 mm	ϕ22 mm	ϕ50 mm	
40-45	40	6.8	35.3	1.8	9.4	45
50-45	50	8.5	44.2	1.5	7.9	
60-45	60	10.3	53	1.2	6.3	
70-45	70	11.9	61.8	0.9	4.7	
80-45	80	13.6	70.6	0.6	3.1	
40-70	40	6.8	35.3	1.8	9.4	70
50-70	50	8.5	44.2	1.5	7.9	
60-70	60	10.2	53	1.2	6.3	
70-70	70	11.9	61.8	0.9	4.7	
80-70	80	13.6	70.6	0.6	3.1	
40-100	40	6.8	35.3	1.8	9.4	100
50-100	50	8.5	44.2	1.5	7.9	
60-100	60	10.2	53	1.2	6.3	
70-100	70	11.9	61.8	0.9	4.7	
80-100	80	13.6	70.6	0.6	3.1	
40-150	40	6.8	35.3	1.8	9.4	150
50-150	50	8.5	44.2	1.5	7.9	
60-150	60	10.2	53	1.2	6.3	
70-150	70	11.9	61.8	0.9	4.7	
80-150	80	13.6	70.6	0.6	3.1	
40-200	40	6.8	35.3	1.8	9.4	200
50-200	50	8.5	44.2	1.5	7.9	
60-200	60	10.2	53	1.2	6.3	
70-200	70	11.9	61.8	0.9	4.7	
80-200	80	13.6	70.6	0.6	3.1	

3.2.2 Structural analysis

3.2.2.1 Optical microscopy and SEM analysis

The microstructure and macrostructure of the Ti matrix syntactic foam samples were observed by optical microscopy and scanning electron microscopy (SEM) (Hitachi S-2460N). To analyze the internal structure by optical microscopy, the sample was first cut by a high speed cutting machine. The cross section was ground carefully using 1200 grit paper, and then cleaned in an ultra sonic bath for 20 minutes to remove any loose particles from the surface. The sample was subsequently dehydrated by 90% ethanol for 5 minutes and then dried by hot air. The cross-sectional surface was observed using a stereo optical microscope.

For SEM observation, a natural internal surface was created by breaking the sample into two parts. The surface was cleaned by high pressure air. Since the CM particles are insulative, they cannot be observed by SEM directly. The surfaces were gold coated for 20 minutes before SEM observations. There are two different detection modes were used in this study: secondary electron (SEI) image and back-scattered electron (BSE) image. Using SEI can produce a high resolution image of the sample surface, and BSE can provide the information of the distribution of CMs by detecting the elements of Si and Al.

The cross-sectional surface of a Ti matrix syntactic foam created by natural breaking was not ideal for revealing the distribution of CMs in Ti matrix. This is because the cross-

sectional surface was not flat, some CMs were damaged during the breaking and fell out, and the holes were not clearly visible. For the observation of CM distribution, the cross-sectional surfaces of the Ti matrix syntactic foam were created by a high speed cutting blade, polished carefully using 1200 grit paper, and cleaned in an ultrasonic water bath for 30 minutes. The samples were dried by hot air and then gold coated with an S-150 sputter coater.

3.2.2.2 Measurements of sample volume and connected porosity

Because of the existence of air voids in the Ti matrix, the actual volume of a Ti matrix syntactic foam sample was different from the design volume. The sample often had an irregular shape after sintering because of shrinkage or damage. Therefore, Archimedes' method was used to measure the actual volume of the sample. To prevent infiltration of water into the sample during the measurement, the surface of the sample was sealed with Vaseline. The sample was then sunk into the water in a container on an electronic balance and held by a thin thread to minimize the error caused by the volume of the thread in the water. The weight increase of the water container is equal to the buoyancy force, which is the product of the volume of the sample and the density of water. Given the density of water, the volume of the sample can be easily obtained.

To measure the connected porosity, the sample was first dehydrated in a furnace at 200°C for 3 hours to remove any moisture in the sample. The weight of the sample was measured

immediately after being taken out of the furnace. The sample was then sunk into water for 5 minutes. Because the wetting angles of ceramic/water and Ti/water are smaller than 90°C (Lim & Oshida 2001; Oh *et al.* 2002b), the connected pores in the sample can be filled with water due to the capillary phenomenon. The weight of the sample together with the absorbed water was measured. The difference between the weights of the sample after and before water absorption was then the weight of the water in the connected pores. The volume of the absorbed water was therefore the volume of the connected pores in the sample.

3.2.2.3 Calculations of Ti volume percentage, density and porosity

The actual volume percentage of Ti in a syntactic foam sample is different from the design Ti volume percentage because of the existence of voids in the Ti matrix. The actual volume percentage of Ti in the sample after sintering was calculated by:

$$f_{Ti} = \frac{W_{Ti}}{\rho_{Ti} V_s} \tag{3.3}$$

where V_s is the volume of the Ti syntactic foam sample, W_{Ti} is the mass of Ti used in making the sample, and ρ_{Ti} is the density of Ti, which is taken as 4.5 g/cm^3 (Welsch *et al.* 1994)

The density of each Ti syntactic foam sample was calculated by dividing the mass of the sample by its volume, which was measured by the Archimedes' method as described in 3.2.2.2.

The total porosity of a sample is the volume of air in the sample divided by the volume of the sample. The volume of air in the sample is the volume of the sample subtracted by the volume of the solid phases in the sample, i.e., Ti and the solid part of the CM particles. The porosity, P, was estimated by:

$$P = 1 - \frac{V_{Ti} + V_{sc}}{V_s} = \frac{V_s - \frac{W_{Ti}}{\rho_{Ti}} - \frac{W_c}{\rho_{sc}}}{V_s} \tag{3.4}$$

where V_{Ti} is the volume of Ti in the sample, V_{sc} is the volume of the solid ceramic in the sample, W_c is the mass of the ceramic microspheres in the sample and ρ_{sc} is the density of the solid ceramic in the CM powder. The solid part of the CMs consisted of approximately 60% SiO_2 and 40% Al_2O_3 by weight. Given the density of SiO_2 of 2.2 g/cm^3 (Shackelford & Alexander 2001) and the density of Al_2O_3 of 3.8 g/cm^3 (Shackelford & Alexander 2001), the density of solid ceramic in the CM powder was estimated to be 2.65 g/cm^3.

The total porosity is composed of closed and connected pores. The volume percentage of the connected pores in the Ti syntactic foam was measured by the water absorption method as described in 3.2.2.2.

3.2.2.4 Estimation of the percentage of the crushed CMs – The volume method

The volume percentage of the crushed CMs discussed here refers to the survival rate of the CMs. It represents the volume percentage of the crushed CMs with respect to the initial volume of all the CMs.

One significant effect from the crushed CMs, which may appear during compaction, is the volume decrease of the sample. To work out the percentage of the crushed CMs, the volumes of the sample with and without crushed CMs need to be calculated. The volume with crushed CMs is the actual volume of the sample, which is obtained by measuring the sample volume directly. The volume without crushed CMs is the ideal volume of the sample, which cannot be obtained directly. Here, a few assumptions are made to estimate this ideal sample volume:

a. The CMs have a uniform distribution in the Ti powder. The Ti matrix forms the major framework of the sample and the CMs are embedded into the Ti matrix.
b. The compaction pressure distribution within the powder preform is uniform, i.e., the pressure applied onto the CMs and Ti powder is the same and equal to the compaction pressure. The deformation of the Ti particles in the Ti matrix is the same as in the pure Ti powder.

With these assumptions, the Ti-CM preform would have an ideal volume composed of the Ti matrix and the CMs. The volume of the Ti matrix can be estimated by a pure Ti powder

of the same mass compacted by the same pressure. The difference between the ideal volume and the actual volume is roughly equal to the air volume in the CMs being crushed. Therefore, the proportion of this decreased volume to the total air volume in the CMs is the percentage of the crushed CMs.

The volume percentage of crushed CMs can be expressed as:

$$\varphi_v = \frac{V_1 - V_2}{V_a} \tag{3.5}$$

where V_1 is the ideal volume of the preform if no CMs are crushed, V_2 is the actual volume of the preform, and V_a is the total volume of pores in the CMs.

The ideal volume of preform, V_1, can be calculated by:

$$V_1 = V_{TM} + V_C = V_{TM} + \frac{W_c}{\rho_c} \tag{3.6}$$

where V_{TM} represents the volume of the Ti matrix in the sample, and V_C and ρ_c are the volume and density of the CMs in the titanium syntactic foam. V_{TM} can be estimated by measuring the volume of a pure Ti powder with the same mass, compacted under the same pressure.

The total volume of air pores in the CMs can be calculated by:

$$V_a = V_c - V_{sc} = \frac{W_c}{\rho_c} - \frac{W_c}{\rho_{sc}} \tag{3.7}$$

The accuracy of this estimation method mainly depends on the accuracy of the measurements of the preform volume and the estimation of the volume of Ti matrix. The volume measurement is reasonably accurate with the standard deviation between 0.6%-1.3%. The volume of the Ti matrix in the preform can be different from that of the Ti powder with the same mass, compacted under the same pressure, because the CMs have a high Young's modulus than the Ti matrix and bear a higher load than the Ti matrix. However, optical microscopic observation of the Ti matrix in a syntactic foam and in a pure Ti powder compact showed that the porosity levels in the two cases are similar. Therefore, it is reasonable to estimate the volume of the Ti matrix in a syntactic foam from the volume of a pure Ti compact under the same compaction pressure.

3.2.2.5 Estimation of the percentage of crushed CMs - The water absorption method

The volume of the sample can be expressed as the sum of the volumes of the Ti, un-crushed CMs, solid ceramic from the crushed CMs, and the connected air pores. The connected pores discussed here include the air pores in the Ti matrix and the air voids in the crushed CMs. The assumptions made to estimate the percentage of crushed CMs by water absorption method are:

a. Both the air pores in the Ti matrix and the air voids in the crushed CMs can be infiltrated by water during water absorption experiment.
b. The air voids in the un-crushed CMs cannot be infiltrated by water during water absorption experiment.

With these assumptions, the volume of the sample can be described as:

$$V_s = V_{Ti} + V_{uc} + V_{cc} + V_{ca} = V_{Ti} + (1-\varphi_w)V_c + \varphi_w V_{sc} + V_{ca} \tag{3.8}$$

where V_{uc} and V_{cc} represent the volume of un-crushed and crushed CMs, respectively, φ_w is the volume percentage of the crushed CMs, V_{ca} is the volume of the connected air pores, which can be measured by the water absorption method discussed in 3.2.2.2. Rearranging equation (3.8) gives:

$$\varphi_w = \frac{V_{Ti} + V_c + V_{ca} - V_s}{V_c - V_{sc}} \tag{3.9}$$

The accuracy of this estimation method depends on the accuracy of the measurements of the volume of the connected pores. It also depends on the validity of the assumptions. In practice, some pores in the Ti matrix and the crushed CMs may be sealed and cannot be penetrated by water. Some uncrushed CMs may have cracks and can be penetrated by water. The assumptions are however reasonable because:

a. The compaction pressures used in this study are relatively low. It is not easy to form too many sealed air pores in the Ti matrix.

b. Observation by optical microscope showed that the CMs have smooth and intact surfaces. The number of cracked CMs is very low.

3.2.3 Mechanical Tests

3.2.3.1 Static compression tests

The Ti matrix syntactic foam samples were first cut to cuboid specimens with a width of 10 mm, depth of 10 mm and height of 20 mm by a high-speed cutting blade. The surfaces of the specimens were ground using 1200 grit paper to remove any surface defects. For each set of samples produced under the same condition, five specimens were prepared and tested. The static compression tests were conducted on a universal testing machine (Instron 4505, U.K.) with a cross-head speed of 0.5 mm/min.

During each compression test, a series of unloading and reloading routes were carried out at 0.4%, 0.6% and 0.8% strains to determine the elastic modulus values. The load and the displacement of the cross-head were measured by a load cell and recorded by a computer connected to the machine. After the test, the recorded load and displacement values were converted into stress and strain values.

The gradients of the unloading curves were taken as the elastic modulus values at the respective strains. This is because during the unloading, the deformation of the specimen

is purely elastic. A set of loading-unloading routes were taken at different strains to examine the amount of plastic deformation occurring during the compression.

3.2.3.2 Three-point bending tests

The Ti syntactic foam samples were cut to cuboid specimens with dimensions of 10 X 5 X 40 mm by a high-speed cutting blade. The length of the specimens was selected to be greater than the span length of the three-point bending test machine. The surfaces of the specimens were ground with 1200 grit paper to remove any surface defects. The opposite sides of the specimen were ensured to be parallel using a square ruler.

The tests were conducted on an Instron 4505 testing machine. The span length was set to 36 mm. The cross-head speed was set to 0.3 mm/min. The maximum load during the test was used to calculate the flexural strength, σ, using equation:

$$\sigma = \frac{3FL}{2bd^2} \tag{3.10}$$

where F is the maximum load applied to the specimen during the test, L is the span length (L = 36 mm), b is the width of the specimen (b = 10 mm) and d is the depth of the specimen (d = 5 mm).

3.2.3.3 Hardness tests

Rockwell hardness tests were conducted on the Ti matrix syntactic foam samples following the guidelines in ASTM 18. A hardened ball indenter with a diameter of 1.588 mm was used for the tests. The choice of this indenter size ensured that the tested area had sufficient Ti powder and CM particles represented. The cross-sectional surface of the sample was ground using 1200 grit paper before testing. The indenter was first forced into the surface of the sample by a light load (10 kg), and then by a heavy load (60 kg). The depth of indentation at the heavy load was determined and converted to a hardness number without measurement units, which is inversely related to the depth. For each sample, ten random test points were measured.

3.2.3.4 Charpy impact tests

Charpy impact tests were conducted on the Ti matrix syntactic foam samples following ASTM E 23. The samples were cut to cuboid specimens with dimensions of 10 X 10 X 50 mm. The surfaces of the specimen were ground using 1200 grit paper to remove any surface defects. A U-notch with 2mm depth and 1mm width was created by cutting in the middle of one side of the specimen using a saw. The specimen was placed in the charpy test machine with a guide device, which ensured the U-notch lay in the route of the striker. The striker was released from a fixed position determined by the intended velocity of striker when it hits the specimen. In this study, the striker hit the specimen with a velocity of 5.0 m/s. The energy absorbed by the specimen during the charpy test was obtained from the meter of the charpy machine.

3.2.4 Biocompatibility tests

3.2.4.1 Cells

The cell used in this study is SaOS-2, a human osteoblast-like cell line. SaOS-2 has been widely used as model system for human osteoblastic cells in biomaterial studies (Akasaka *et al.* 2009). Cells were cultured at 37.5 °C in 5% CO_2 Dulbecco's Modified Eagle Medium, containing 1% penicillin/streptomycin and 10% foetal calf serum. This culture medium is named "complete culture medium" in the later description. When the cells had a confluence upon 70%, the cells were detached and diluted in 15 ml complete culture medium, 3 ml was moved to a new culture flask and diluted in 12 ml complete culture medium.

3.2.4.2 Toxicity test

In this study, the indirect and direct contact cell culture tests were used to test the toxicity of the Ti matrix syntactic foam *in vitro*. The preparation procedure of the specimens used for the indirect and direct contact culture tests were the same. The specimens were thin circular disks with a diameter of 1 cm and a thickness of 1 mm. Using thin disks can help to prevent the infiltration of the cell medium after seeding on the surface of the specimen. The specimen was first cut from the specimen of Ti matrix syntactic foam with a high speed blade. Each side of the specimen was polished carefully to 1 μm. After the polishing, the specimen was placed in an ultra-sonic water bath for 30 minutes to remove any impurity which was introduced into the specimen during the cutting. The specimen

was dehydrated with ethanol for 30 minutes. Afterwards, the specimen was placed in an autoclave and sterilized in 121°C high pressure steam.

Indirect contact tests were carried out using an extraction method, with the following procedure:

a. The Ti matrix syntactic foam specimen was placed in sealed plastic vessels and incubated in the complete culture medium at 37°C for 72 hours.
b. A straw with a connection to a pump was used to aspirate the medium in the flask which contained cells on the inside of the wall.
c. 5 ml phosphate-buffered saline (PBS) was used to wash the cells on the wall of the flask container carefully. After a few seconds, the PBS was aspirated.
d. 3 ml Trypsin (10%) was added into the flask, and the flask was placed in the incubator for 3 minutes. Trypsin can help to detach the cells from the wall of the flask. The incubator, contained 5% CO_2, was set to a temperature of 37±2°C. This setting of the incubator was kept stable during the whole biocompatibility tests.
e. After taking the flask out from the incubator, 12 ml complete culture medium was added to stop the trypsin from further damaging the cells.
f. All the medium was moved to a tube container, and set in a centrifuge. Another tube container with the same volume of water was placed in the opposite side to balance the machine during the rotational operation.

g. The centrifuge was switched on to rotate for 5 minutes. After the centrifugal operation, the cells fell to the bottom of the tube container. The medium above the cells was aspirated.

h. 5 ml complete medium was added into the tube container with a pipette and mixed sufficiently to achieve a uniform distribution of the cells in the medium.

i. 10 μl from this mixture was taken out and dissolved into 90 μl complete medium and blended sufficiently.

j. 10 μl was taken out from the 100 μl mixture and the number of cells was counted using a Haemocytometer (D/C Imp Neubauer). The total number of cells of the whole mixture was obtained by multiplying the counted number by 10.

k. The extract from the specimen was collected and diluted with complete culture medium and used at a ratio of 1:1, 10:1 or 100:1. Moreover, a negative control (100% D-MEM) and 100% extractions from Ti syntactic foam specimens were used respectively. The locations of the diluted medium on the well plate are shown in Fig. 3. 8.

l. SaOS-2 osteocarcinoma cells were seeded at a density of 5×10^4/well in a 24-well plate and grown for 72 hours. The volume needed to satisfy this cell density V_n is calculated as below:

$$V_n = \frac{5\times10^4}{N_c\times10\times10^4}\times10^3 \tag{3.11}$$

Where N_c is the number of cells counted.

m. The well plate was sealed and placed into an incubator for 48 hours.

n. After 48 hours, the well plate was taken out from the incubator. The medium in the well was aspirated.

o. 1 ml PBS was used to wash the cells. After washing, the PBS was removed using a straw.

p. 50 µl live and dead solution (1 ml PBS, 3 µl Calcin and 5 µl Ethidium) was added to each well. Afterwards, the well plate was placed into the incubator for 30 minutes.

q. The cells were observed using an inverted fluorescent microscope (Axiovert 200, Carl Zeiss Ltd).

3.2.4.3 Direct culture

The experimental procedure of the direct contact cell culture was the same as for the indirect contact cell culture from step a to k. The locations of the extracted medium are shown in Fig. 3.9.

After step k, the experimental procedure was as follows:

l. The cells together with the complete medium were placed on the sample surface directly. The volume was determined by the equation 3.11.

m. The well plate was placed into the incubator for 20 minutes. Afterwards, 1 ml complete culture medium was added to each well. The 20 minute period was to let the cells have an initial contact to the specimen surface, and to prevent the cells from moving away from the specimen surface after the complete culture medium was added.

n. The well plate was placed into the incubator again for 48 hours.

o. After 48 hours of culture, the medium in each well was aspirated. 1 ml PBS was used to wash the specimen in the well.

p. 1 ml 2.5% gluteraldehyde was used to fix the cells on the specimen surface for 30 minutes.

q. Continuous dehydration was carried out with ethanol. Firstly, ethanol with a concentration of 70% was added to the well, kept for 30 minutes and then aspirated. Secondly, 90% ethanol was added to each well, kept for 30 minutes and then aspirated. Finally, 100% ethanol was added to the well and kept for 30 minutes.

r. The specimen was taken out from the well plate and point critical drying process was carried out. Afterwards, the specimen was fixed on the conducting rubber for SEM observations (Hitachi S-2460N).

3.2.4.4 Von Kossa stain

The Von Kossa stain is used to quantify mineralization in cell culture and tissue section. During the staining, silver ions are displaced from solution by carbonate or phosphate ions, due to their respective positions in the electrochemical series. As the demonstrable forms of tissue carbonate or phosphate ions are invariably associated with calcium ions, it can be considered as demonstrating sites of tissue calcium deposition. The experimental procedure of conducting Von Kossa stain is below:

a. Specimens were cut first from the Ti matrix syntactic foam samples with a high speed blade, and the dimensions were 5 x 5 x 1 mm. Each surface was polished carefully to 1 μm.

b. Cells were seeded on the surface with a number density of 4×10^5 per well for 21 days in incubator.

c. Specimens were washed with PBS carefully in the well, and fixed with gluteraldehyde for 10 minutes. The amount of the gluteraldehyde needed to cover the top surface of the specimen. In this study, 1 ml gluteraldehyde was added to the culture well.

d. 3% silver nitrate solution was added to the well. The amount of the solution was required to cover the top surface of the specimen in the well. After adding the solution, the culture well was exposed to strong light for 60 minutes. The calcium minerals will be a dark brown or black, which indicated the reaction was complete.

e. The specimen was washed with distilled water three times, and then 5% sodium thiosulfate was placed in for 2 minutes, and washed with distilled water three times.

f. The specimen was counterstained in nuclear fast red for 5 minutes

g. The specimen was dehydrated clearly and mounted for observation.

3.3 Structure

3.3.1 Macro and microstructures

Fig. 3.10 shows the distribution of CMs in a Ti matrix syntactic foam sample with a nominal Ti volume percentage of 70%, fabricated with a compaction pressure of 70 MPa. Fig. 3.10a is the secondary electron (SEI) image, and Fig. 3.10b is the back-scattered electron (BSE) image of the same location. BSE is used to detect contrast between areas with different chemical compositions. Because Ti has a higher atomic number than those of Al, Si and O, the back-scattered electrons signal from Ti is greater than those from the CM particles. Therefore, Ti matrix appears brighter in the image. During the preparation of the surface before SEM observation, the CMs at the surface were damaged and removed. The holes in Fig. 3.10a clearly show the positions of the CMs. The distribution of these holes is uniform. Even if the CMs were removed from the surface, the holes still exhibit a dark colour in Fig. 3.10b.

Fig. 3.11 shows SEI (Fig. 3.11a) and BSE (Fig. 3.11b) images of typical holes with a higher magnification. In Fig. 3.11a, one hole contained part of a CM particle, while another hole was empty, because the CM particle was removed during the grinding process. Both these holes exhibit the same colour in Fig. 3.11b, indicating that their chemical compositions were the same and confirming that these holes are indeed left by the CMs. The traces of CMs in the Ti matrix also indicate that there was some chemical reaction or inter-diffusion at the Ti/CM interface.

Fig. 3.12 shows the CMs at the fracture surface of the Ti matrix syntactic foam with a Ti volume percentage of 60%, fabricated with a compaction pressure of 45 MPa. Because no polishing process was conducted to the surface, the CMs were still embedded in the surface. The distribution of the CMs was uniform. The development of the fracture surface was either transparticle or interparticle. As a consequence, the CMs at the fracture surface were either well embedded, or half removed.

Fig. 3.13 shows the polished cross-sectional surface of the Ti matrix in a sample with a nominal Ti volume percentage of 50%, fabricated with a compaction pressure of 100 MPa. The Ti matrix is formed by the sintered Ti particles containing air voids. At a compaction pressure of 100 MPa, the Ti particles formed a three dimensional structure with necking between Ti particles. On a microstructural scale, sinter bonding is evident as cohesive necks grow at the particle contacts (German 1996), as shown in Fig. 3.14. The boundaries between the Ti particles were visible in some cases and invisible in others, depending on the cohesive neck growth.

Fig. 3.15 shows the images of typical fracture surfaces created by breaking. No obvious plastic deformation was observed on the surface. Fracture could develop across the Ti particles (transparticle) (Fig. 3.15a), or along the bonds between Ti particles (interparticle) (pointed by white arrow in Fig. 3.15b). In Fig. 3.15b, the transparticle fracture also was found (pointed by dark arrow). It proved that both transparticle and interparticle fracture

happened during the fracture procedure. There were a considerable number of pores in the Ti matrix. The pore size was estimated to be in the range between 5-10 μm.

3.3.2 Effect of manufacturing conditions

Figs. 3.16a and b show the details of the surface of the Ti matrix syntactic foam. Fig. 3.16a represents the surface of Ti matrix syntactic foam with low Ti volume percentage and low compaction pressure. Fig. 3.16b represents the surface of Ti matrix syntactic foam with high Ti volume percentage and high compaction pressure. The CMs are indicated with white arrow and the Ti matrix with black. Fig. 3.16c shows optical micrographs of the cross-sectional surface of the Ti matrix syntactic foam samples with five different nominal volume percentages of Ti, 40%, 50%, 60%, 70% and 80%, fabricated by four different compaction pressures, 45 MPa, 70 MPa, 100 MPa and 150 MPa.

Fig. 3.16c is divided into two regions by a solid line depending on the appearance of the Ti matrix. On the left of the line, the Ti matrix had a rough surface after the polishing, indicating a more porous structure. On the right of the line, the Ti matrix exhibited a flat, smooth surface after the polishing, indicating a more dense structure. Fig. 3.16c shows that higher compaction pressures resulted in decreasing amounts of air voids in the Ti matrix, and therefore a more dense structure. Increasing the Ti volume percentage in the syntactic foam also resulted in a more dense structure because of better bonding between

the Ti particles. To achieve a dense Ti matrix, the samples with lower Ti volume percentages required higher compaction pressures, and the samples with higher Ti volume percentages required lower compaction pressures.

Fig. 3.16c is also separated into two regions by a dash-dot line depending on the shapes of the CMs in the Ti matrix. In the samples on the left of the dash-dot line, most CMs remained spherical. In the samples on the right of the dash-dot line, significant deformation of the CMs was observed. The CMs are clearly intact in the samples fabricated with a compaction pressure of 45 MPa. However, in the samples fabricated with higher compaction pressures, more CMs were crushed and lost from the cross-sectional surface, leaving holes in the matrix. This became more serious for the samples with lower Ti volume percentages.

The Ti matrix syntactic foam has three components, Ti matrix, air voids and CM powder particles. The relative proportions of these three components are controlled by the manufacturing conditions. The amounts of Ti matrix and CM powder particles are mainly controlled by their volume percentages used in the powder mixing, and the amount of air voids is controlled by the compaction pressure. Changing the volume ratio of Ti:CMs and compaction pressure can result in a change in the proportions of Ti matrix, CMs and air voids in the syntactic foam.

Since CMs have a lower density than the Ti powder particle, increasing the amount of CMs, or decreasing the Ti, results in a decrease in the density of Ti matrix syntactic foam. Increasing the compaction pressure can result in a decrease in the volume of air voids, and thus an increase in the green density of syntactic foam. However, the distribution of compaction pressure in the preform is not uniform. If the pressure is applied from the bottom, the compaction pressure decreases with the distance from the bottom; thicker powder preforms have a more uniform distribution of pressure than thin powder preforms (Kuno & Kuri 1983). The compressive strength of CMs varies with the internal structure of CMs. After compaction process, the CMs may show different conditions. If the local compaction pressure is higher than the compressive strength of the CMs, the CMs will be broken to small pieces or crushed; if not, the CMs will be intact. The broken CMs may maintain in a spherical shape in the Ti matrix. During the preparation of the cross-section surface or internal surface observation, these broken CMs can fall away from the surface and leave an empty hole in the Ti matrix. The crushed CMs cannot maintain a spherical shape after compaction. No spherical holes can be observed after sintering.

3.3.3 Comparison with metal matrix syntactic foams manufactured by casting

For metals with low melting points (<1200°C), using the casting process to fabricate syntactic foam can achieve an excellent metal matrix, compared with using powder metallurgy. Tao *et al.* (2009) fabricated Al matrix syntactic foam with bimodal ceramic microspheres using an infiltration process and achieved an excellent Al metal matrix and a uniform distribution of embedded CMs. However, in the infiltration process, the volume

percentage of Al metal matrix cannot be changed easily. Daoud (2008) manufactured $ZnAl_{22}$ syntactic foam by casting. In the process, certain amounts of Zn and Al were first placed and melted in a crucible, and microballoons were added manually and stirred to achieve a uniform distribution and a homogeneous structure. The structures of these two syntactic foams and the Ti matrix syntactic foam manufactured in this study are shown in Fig. 3.17. The metal matrix of the syntactic foams fabricated by the casting process has a higher quality than that by the powder metallurgy process, because of the existence of air voids in the metal matrix manufactured by powder metallurgy. In the powder metallurgy process to fabricate the Ti matrix syntactic foam, a compaction pressure is required to shape the preform and to rearrange the Ti particles. During compaction, some of the CMs were damaged and broken to small pieces, leading to a poorer quality than cast syntactic foam.

The advantages of using the powder metallurgy process are that a uniform distribution of CMs and a variable volume percentage of Ti matrix can be achieved. The uniform distribution of CMs in the Ti matrix can result in more homogeneous properties. The variable volume percentage of Ti matrix can achieve varied properties.

3.3.4 Comparison with theoretical properties

3.3.4.1 Ti volume percentage

The relationship between the actual and design Ti volume percentages of the Ti matrix syntactic foam is shown in Fig. 3.18. Generally, the actual Ti volume percentage was different from, often smaller than, the design Ti volume percentage. The difference was a result of the voids in the matrix and the breakage of CMs in the sample. It was a function of the compaction pressure and the design Ti volume percentage. A high compaction pressure can decrease the actual Ti volume percentage due to removal of voids in the Ti matrix. However, a high compaction pressure can also result in crushing of some CMs and therefore a decrease in the whole volume of the sample. As a consequence, the Ti volume percentage can even be higher than the design one. In a sample with a high design Ti volume percentage, there is a large difference between the actual and design Ti volume percentages. This is because the sample with a higher Ti volume percentage has a greater decrease in the metal matrix volume than the sample with a lower Ti volume percentage. Because the CMs are stiff, the decrease in volume of the sample during compaction and sintering is due to the Ti matrix. The structure analysis also showed that there was no deformation at the CM/CM boundaries, little deformation at the CM/Ti boundaries, but significant necking reduction at the Ti/Ti boundaries.

The actual Ti volume percentages of samples with high Ti volume percentages, such as 60%, 70% and 80%, were lower than the design ones. It indicated that fewer CMs are

crushed in a sample with a higher Ti volume percentage than in a sample with a lower Ti volume percentage.

3.3.4.2 Density

Fig. 3.19 shows the relationship between density and norminal Ti volume percentage at different compaction pressures. The theoretical density, which is calculated assuming that there is no porosity in the Ti matrix and no CMs are damaged, is shown as a solid line. The density increases slightly with increasing Ti volume percentage and significantly with increasing compaction pressure. Compared with the theoretical values, most Ti matrix syntactic foam samples have lower densities due to the porosity in the Ti matrix. A small number of samples have densities higher than the theoretical values due to the existence of crushed CMs.

Both porosity and crushed CMs can affect the density of the Ti matrix syntactic foam. Porosity leads to lower densities than the theoretical values and the crushed CMs lead to higher densities than the theoretical values. In Fig. 3.19, the densities of the samples with a compaction pressure of 45 MPa are obviously lower than the others. It is reasonable to believe that most CMs survived at this compaction pressure. When the compaction pressure was increased to 70 MPa, the CMs began to be crushed. With increasing compaction pressure, more and more CMs were crushed and, at the same time, the porosity in the sample decreased. The density was thus increased. When the volume of the

crushed CMs exceeds a certain level, the sample volume may even become smaller than the theoretical volume, and the density of the sample can be higher than the theoretical density.

3.3.4.3 Porosity

Fig. 3.20 shows the relationship between porosity and Ti volume percentage at different compaction pressures. The theoretical porosities of the Ti matrix syntactic foam samples, which are calculated assuming that there is no porosity in the Ti matrix and no CMs are damaged, are shown as a solid line. The actual porosity of a Ti matrix syntactic foam sample is generally higher than the theoretical porosity.

The total porosity includes the air voids in the Ti matrix and the air pores in the CMs. Increasing compaction pressure decreases the volume of the air voids in the Ti matrix due to the Ti powder particle rearrangement and deformation. The air pores in the CMs can be decreased by crushing the CMs, depending on the structure and strength of the CMs. The CMs with the hollow structure are relatively strong, but once crushed, they have greater decrease in volume. The CMs with the porous structure are relatively weak. They are easier to be crushed but have a less decrease in volume.

The porosities of the samples fabricated with a compaction pressure of 45 MPa are significantly lower than the others. The reasons are the same as in the density analysis. Most CMs survived at 45 MPa and began to be crushed when the compaction pressure was increased to 70 MPa. Increasing Ti volume percentage, however, does not affect the porosity very much. It seems the porosity in the Ti matrix is approximately equal to the porosity in the CMs. With increasing compaction pressure, both the porosities in the Ti matrix and the CMs are decreased but still remain approximately equal.

3.3.5 Percentage of broken CMs

Fig. 3.21 shows the relationship between the percentage of crushed CMs, calculated by the volume measurement methods, and the nominal Ti volume percentage at different compaction pressures. The percentage of crushed CMs decreases with increasing the Ti volume percentage and increases with increasing the compaction pressure. Fig. 3.22 shows the relationship between the percentage of crushed CMs, calculated by the water absorption method, and the nominal Ti volume percentage at different compaction pressures. The results obtained by the two methods show a similar trend.

The CM particles are crushed during the compaction process. For the samples with a low Ti volume percentage, the CM particles are more easily crushed because the Ti matrix cannot offer sufficient protection to the CM particles during the compaction. The photographs of the Ti matrix syntactic foams in Fig. 3.16c show that the samples with low

Ti volume percentages have deformed or collapsed holes. For samples with a high Ti volume percentage, the CM particles in the sample can be protected by the flowing, rearranging and deforming of the Ti particles. Thus the percentage of crushed CMs is decreased. However, this protection from the Ti particles is limited, for samples fabricated with a compaction pressure over 150 MPa. Even if the Ti volume percentage is increased to 80%, the volume percentage of crushed CMs in the samples is still higher than 50%.

Fig. 3.23 compares the volume percentages of crushed CMs determined by both the water absorption method and the volume measurement method. The difference in the values obtained by the two methods is affected by the compaction pressure. For the samples fabricated with a low compaction pressure, the volume percentages of crushed CMs calculated by the water absorption method are greater than those calculated by the volume measurement method. For the samples fabricated with a high compaction pressure, the volume percentages of crushed CMs calculated by the water absorption method are smaller than those calculated by the volume measurement method.

The accuracy of the estimation using the volume measurement method depends on the estimation of the volume of the Ti matrix. In the volume measurement method, the stress in the Ti matrix is assumed to be the same as the compaction stress. In practice, the stress distribution in the powder mixture is quite complex. The stress in the Ti matrix can be much different from the compaction stress, depending on the distribution of the CMs within the Ti matrix and the densification of the preform. Increasing the compaction

pressure can significantly increase the densification of the preform, leading to a more similar stress in the Ti matrix with the compaction stress. Therefore, the volume measurement method is likely to have a relatively high accuracy when the samples are fabricated with a high compaction pressure.

The accuracy of the estimation using the water absorption method depends on the extent of the water infiltration within the sample. Although the wetting angles of the water to the ceramic and the Ti are smaller than 90° (Lim & Oshida 2001; Oh *et al.* 2002b), the air in the voids can still prevent the water from full infiltration. The infiltration of the water is easier in a more porous Ti matrix than a dense one. The samples manufactured by low compaction pressures are more porous than those fabricated with high compaction pressures. The volume percentages of crushed CMs measured by the water infiltration method in these samples therefore have a higher accuracy.

3.4 Mechanical Behaviour

3.4.1 Static compressive behaviour

3.4.1.1 Stress-strain curves and unload & reload routes

Fig. 3.24 shows a typical unload & reload routes exhibited in compression testing. The specimen used has a Ti volume percentage of 50%, fabricated with a compaction pressure 45 MPa. During the compression, the unload and reload routes in Fig. 3.24 followed the same routes as the initial loading curve. This is the normal compressive behaviour of the

Ti matrix syntactic foam in the compression tests. Before the maximum stress is reached, no obvious structure failure occurs in the material. Therefore, the unload and reload routes are the same as the initial loading.

Fig. 3.25 shows the fracture surfaces of Ti matrix syntactic foam specimens after the compression tests. These specimens have Ti volume percentages of 40%, 50%, 60%, 70% and 80%, and are fabricated with a compaction pressure of 45 MPa. It is shown that during the compression, the CMs are not damaged. CMs are embedded in the fracture surface and remain in spherical shape after the compression tests. It indicates that the compression pressure did not result in failures of the CMs.

3.4.1.2 Effect of compaction pressure

Fig. 3.26 shows compressive behaviour of Ti matrix syntactic foam specimens with Ti volume percentages of 40% (Fig. 3.26a), 50% (Fig. 3.26b) and 60% (Fig. 3.26c), fabricated with compaction pressures of 45, 70, 100, 150 and 200 MPa.

For the specimens with a Ti volume percentage of 40%, increasing compaction pressure increases the maximum compressive stress. The gradient of the linear part of the stress-strain curve increases with increasing compaction pressure up to 100 MPa, but decreases with increasing compaction pressure further. This indicates that a compaction pressure

over 100 MPa can result in crushing of CMs during compaction process and thus lower elastic modulus of the sample.

The specimens with a Ti volume percentage of 50% have very similar trends to the specimens with a Ti volume percentage of 40%. Increasing the compaction pressure up to 100 MPa results in an increase in the maximum compressive stress. The maximum stresses of the specimens fabricated with compaction pressures of 100 MPa, 150 MPa and 200 MPa are very similar. The gradient of the linear part of the stress-strain curves increases with increasing compaction pressure from 45 MPa to 150 MPa, and then decreases when the compaction pressure is increased to 200 MPa.

The specimens with a Ti volume percentage of 60% have different compressive behaviours from those with lower Ti volume percentages. The stress-strain curves have a region with a large strain at a nearly constant stress. The Ti metal syntactic foams start to show porous metal like behaviour. The maximum stress still increases with increasing compaction pressure. The gradient of the linear part of the stress-strain curve increases when the compaction pressure is increased from 45 MPa to 100 MPa, and decreases when the compaction pressure is increased to 150 MPa and 200 MPa.

3.4.1.3 Effect of Ti volume percentage

Fig. 3.27 shows the compressive stress-strain curves of Ti matrix syntactic foams with Ti volume percentages of 40%, 50% and 60%, fabricated with compaction pressures of 45 MPa (Fig. 3.27a), 70 MPa (Fig. 3.27b), 100 MPa (Fig. 3.27c), 150 MPa (Fig. 3.27d) and 200 MPa (Fig. 3.27e). All specimens are brittle in compression.

The stress-strain curves of the specimens fabricated with compaction pressures of 45 MPa and 70 MPa exhibit an instant drop in stress after the maximum stress. There is a clear effect in increasing the volume percentage of Ti. The maximum stress increases with increasing Ti volume percentage. The gradient of the linear part of the stress-strain curve increases with increasing Ti volume percentage too.

The stress-strain curves of the specimens fabricated with a higher compaction pressure of 100 MPa also exhibits a large instant drop in stress after the maximum stress. However, there are a few small drops before reaching the maximum stress. The stress decreases at these small drops and then increases up to the maximum stress. These small instant area drops indicate that some parts of the metal matrix fractured intermittently. The specimen with a higher Ti volume percentage has a higher maximum compressive stress. However, the gradient of the linear part of the stress-strain curve is lower than that of the specimen with a lower Ti volume percentage.

The specimens fabricated with much higher compaction pressures, 150 MPa and 200 MPa, have a compressive behaviour very similar to that of the specimens fabricated with a compaction pressure of 100 MPa. At these compaction pressures, increasing the Ti volume percentage can still increase the maximum compressive stress, but the effects are not significant.

The effect of Ti volume percentage of the compressive behaviour of the specimens fabricated with 45 MPa was further studied by increasing the Ti volume percentage to 70% and 80%. The compressive behaviours of these two specimens were compared with those with lower Ti volume percentage, as shown in Fig. 3.28. The specimens with Ti volume percentages of 70% and 80% are still brittle. Their maximum compressive stresses are much higher. However, the gradients of the linear part of the stress-strain curves of the specimens with Ti volume percentages of 70% and 80% are very similar to that of the specimen with a Ti volume percentage of 60%.

3.4.1.4 Development of cracks

Fig. 3.29 shows the cracks developed during the compression tests within the specimens. These specimens have Ti volume percentages of 40%, 50%, 60%, 70% and 80%, and were fabricated with a compaction pressure of 45 MPa. The sample with a Ti volume percentage of 80% broke to a few small pieces during the compression test, and the piece shown in the figure is the largest one.

Generally, the compressive failure of metal matrix syntactic foams can be either ductile in the form of collapse and crushing of ceramic spheres (Balch *et al.* 2005; Daoud 2008; Kiser *et al.* 1999; Wu *et al.* 2007; Zhang & Zhao 2007), or brittle in the form of shear failure (Balch *et al.* 2005; Kiser *et al.* 1999) or fracture failure with cracks at an angel to the loading direction (Palmer *et al.* 2007; Tao & Zhao 2009; Zhang & Zhao 2007). When a compressive pressure is applied to the specimen, the stress in the specimen contains tensile stress, shear stress and compressive stress. The fracture inside the specimen can be tensile fracture, shear fracture or compressive fracture. Under pure tensile stresses, a tensile crack develops in the plane perpendicular to the stress direction. Under pure compressive stresses, longitudinal tensile (splitting) cracks appear parallel to the stress direction. Under pure shear stresses, inclined tensile cracks propagate at an angle to the stress direction (Fishman 2008). In the Ti matrix syntactic foam, there exists a complex mixed loading mode during compression. Both longitudinal tensile cracks and inclined shear cracks were found in the specimens. The fracture evolution is illustrated in Fig. 3.30 (Lajtal 1974). The fractures start from the tensile stress concentrations at the flaw boundaries (Fig. 3.30 A and B); inclined shear fractures are initiated (Fig. 3.30 C); the material fails (Fig. 3.31 D); the fault is formed (Fig. 3.30 E). These failure modes are typical for rock, concrete and other brittle materials (Fishman 2008).

Ti volume percentage had a significant effect on the fracture mode of the Ti matrix syntactic foam. The specimens with a lower Ti volume percentage tended to develop tensile fracture, and the specimens with a higher Ti volume percentage tended to develop shear fracture. Whether the fracture is in tensile mode or shear mode depends on the

relative magnitudes of tensile strength and shear strength. If the tensile stress exceeds the tensile strength of the specimen first, the fracture develops in the tensile mode. If the shear stress exceeds the shear strength first, the fracture develops in the shear mode. Ti matrix syntactic foam specimens with a higher Ti volume percentage were more likely to have shear fracture. This indicates that high Ti volume percentage resulted in an increase in the tensile strength more pronounced than the increase in the shear strength.

3.4.1.5 Fracture surface

The specimen with a Ti volume percentage of 50%, fabricated with a compaction pressure of 45 MPa was selected as an example to study the fracture surface. The fracture surfaces of the Ti matrix syntactic foam specimens have very similar features.

Figs. 3.31 and 3.32 show the fracture surfaces of the Ti matrix syntactic foam specimen with a Ti volume percentage of 50%, fabricated with a compaction pressure of 45 MPa. The fracture surfaces of the other Ti matrix syntactic foam specimens have very similar features. Generally, the fracture develops not only across the Ti particles, but also across the CM particles. The fracture surface is very smooth and flat, characteristic of brittle fracture.

Crack growth in a monolithic material, such as steel and aluminum, is predictable. However, the crack growth in syntactic foams is more difficult to predict. There are many factors that can affect the crack growth within the composite material, such as the properties of the matrix, distribution of the CMs, the thickness of the CM particle wall, etc. Pure Ti is a ductile material (Williams 1973b). However, the Ti matrix syntactic foam shows brittleness in compression. This may be caused by the contamination of Ti during the manufacturing. Ti can easily react with many elements at high temperatures. Even with a good vacuum during the whole manufacturing process, Ti can still react with the residual oxygen and nitrogen in the furnace chamber and the compounds in the CM particles. All these reaction products decrease the ductility of Ti and increase the brittleness.

3.4.1.6 Compressive strength

Fig. 3.33 shows the relationship between compressive strength and Ti volume percentage for the specimens fabricated with different compaction pressures of 45, 70, 100, 150 and 200 MPa. Two additional Ti volume percentages, 70% and 80%, were also studied for the specimens manufactured at the compaction pressure of 45 MPa. The relationship is shown in Fig. 3.34. It is shown that the specimen with a higher Ti volume percentage and a higher compaction pressure has a higher compressive strength.

The compressive strength of metal matrix syntactic foams depends not only on the mechanical properties of the metal matrix and the ceramic particles but also on the volume fraction, structure, distribution of the ceramic particles, and the amount of defects in the syntactic foam (Zhao & Tao 2009). In Ti matrix syntactic foam, both the Ti matrix and the CMs contribute to the compressive strength of the syntactic foam. Our results suggest that the compressive strength of the Ti matrix syntactic foam is mainly determined by the Ti volume percentage. This is because the Ti matrix has a higher strength than the CM particles. When the Ti volume percentage is increased to 70% and 80%, the compressive strength of the Ti matrix syntactic foam is significantly increased.

Increasing the compaction pressure can result in decreased porosity in the Ti matrix syntactic foam. As a consequence, the matrix becomes more and more dense, and the compressive strength is thus increased.

3.4.2 Flexural strength

Fig. 3.35 shows the relationship between flexural strength and Ti volume percentage for specimens fabricated with compaction pressures of 45, 70, 100, 150 and 200 MPa. Two additional Ti volume percentages, 70% and 80% were studied for the specimens fabricated with the compaction pressure of 45 MPa. The relationship is shown in Fig. 3.36. It is shown that the specimens with higher Ti volume percentages and higher compaction pressures have higher flexural strengths.

In the three-point bending test, the upper half of the rectangular specimen is subject to compression, and the bottom half is subject to tension. For compression, both Ti matrix and CMs contribute to the strength. For tension, only the Ti matrix contributes to the strength. This is because the syntactic foam is virtually like two matrices, Ti and CMs, intermingled together, the CMs are in contact with each other but no bonding between them. They can bear compressive load but not tensile load, nearly all tensile load will be borne by the Ti matrix. As a consequence, the flexural strength of the specimen is mainly determined by the Ti volume percentage. A higher compaction pressure can result in a much denser specimen and therefore a higher flexural strength.

3.4.3 Elastic modulus

Fig. 3.37 shows the relationships between the elastic modulus and Ti volume percentage (Fig. 3.37a) and compaction pressure (Fig. 3.37b) for Ti matrix syntactic foam specimens with Ti volume percentages of 40%, 50% and 60%, fabricated with compaction pressures of 45, 70, 100, 150 and 200 MPa. In the low compaction pressure range, increasing the volume percentage of the Ti can increase the elastic modulus of Ti matrix syntactic foam. When the compaction pressure is over 100 MPa, increasing the volume percentage of Ti decreases the elastic modulus of the Ti matrix syntactic foam. The effects of the compaction pressure and volume percentage of Ti on the elastic modulus of Ti matrix syntactic foam are not simple. If all the CM particles remain intact during the manufacturing, increasing the Ti volume percentage, or decreasing the CM volume percentage, can result in a decrease in the elastic modulus of the Ti matrix syntactic foam.

This is because the elastic modulus of the CM particles is much higher than that of the Ti matrix. Increasing the compaction pressure can result in a more dense Ti matrix syntactic foam. The elastic modulus is thus increased. However, the CM particles are quite brittle. During the manufacturing, especially during the compaction process, some CM particles can be crushed. These crushed CMs can significantly affect the elastic modulus of Ti matrix syntactic foam. The effect depends on the internal structure of the CM particles. The CMs with the hollow structure are more likely to lose all strength after being crushed and cannot support the compression load. The CMs with the porous structure can still maintain a nearly spherical shape after being crushed. These CMs can still support the compression load after deformation.

The percentages of crushed CM particles have already been estimated in Chapter 3.3.3. At the compaction pressure of 70 MPa, the CM particles begin to be crushed during the compaction. The general trend is that a higher compaction pressure and a higher CM volume percentage result in more crushed CM particles.

Increasing the compaction pressure has two different effects on the elastic modulus of Ti matrix syntactic foam. On the one hand, the specimens with higher compaction pressures have more crushed CM particles, leading to lower elastic moduli of specimens. On the other hand, the specimens with higher compaction pressure are more dense, leading to higher elastic moduli. When the compaction pressure is relatively low, the specimens have less crushed CM particles and the elastic moduli of these specimens are high. When the

compaction pressure is increased, more and more CM particles begin to be crushed. However, the decrease in the elastic modulus due to the crushed CMs is very small, and the elastic modulus of the specimen can still increase. When the compaction pressure reaches 100 MPa, the volume of crushed CMs in the specimen becomes very high. The decrease in the elastic modulus due to the crushed CMs is greater than the increase due to the densification effect. The elastic modulus of the specimen is decreased.

Increasing the Ti volume percentage also has two different effects on the elastic modulus of the Ti matrix syntactic foam. Increasing the Ti volume percentage can decrease the volume of the crushed CM particles, and therefore increase the elastic modulus. However, because the elastic modulus of Ti matrix is lower than that of the CM particles, increasing the Ti volume percentage can decrease the elastic modulus of specimens. The final effect depends on the compaction pressure. At a relatively low compaction pressure, increasing the Ti volume percentage can decrease the amount of the crushed CMs in the specimen, and thus increase the elastic modulus. When the compaction pressure is relatively high, increasing the Ti volume percentage can still decrease the amount of the crushed CMs in the specimen. However, because of the high compaction pressure, the amount of the crushed CM particles in the specimen is very large. The elastic modulus of specimen is thus decreased.

3.4.4 Rockwell Hardness and impact toughness

Fig. 3.38 shows the Rockwell hardness of Ti matrix syntactic foam specimens with Ti volume percentages of 40%, 50%, 60%, 70% and 80%, fabricated with compaction pressures of 70, 100, 150 and 200 MPa. The specimen with a Ti volume percentage of 40%, fabricated at a compaction pressure of 70 MPa was crushed by the indenter during the hardness test. The hardness of this specimen was not included in Fig. 3.39. In general, the Rockwell hardness of the specimens increased slightly with increasing both the Ti volume percentage and the compaction pressure.

Hardness is defined as an ability of a material to resist permanent indentation or deformation when in contact with an indenter under load (Revankar 2003). The Rockwell hardness of the Ti matrix syntactic foam represented the ability to resist local compressive load during the test. A higher compaction pressure can result in a decrease in the volume of the voids formed between the CMs and the Ti particles in the Ti matrix syntactic foam. As a consequence, the hardness was increased.

Fig. 3.39 shows the specimens after charpy tests. The specimens have Ti volume percentages of 40%, 50%, 60%, 70% and 80% and were fabricated with a compaction pressure of 45 MPa. The specimens were broken into many small pieces after the charpy tests. The number of pieces decreased with increasing the Ti volume percentage. Optical microscopy observation has shown that there are no strong bonds between the CM

particles and the Ti matrix. The strength mainly comes from the sintered Ti matrix. The specimens with higher Ti volume percentages have stronger Ti matrix network, and are therefore not easy to be broken to small pieces during the charpy test.

Fig. 3.40 shows the relationship between the impact toughness and Ti volume percentage of the Ti matrix syntactic foams with Ti volume percentages of 40%, 50%, 60%, 70%, and 80%, and fabricated with a compaction pressure of 45 MPa. Fig. 3.41 shows the absorbed energy of each broken interface in the specimens. The impact toughness and the absorbed energy of each broken interface increase significantly with increasing the Ti volume percentage. As discussed previously, this is because the tensile properties of the Ti syntactic foam mainly come from the Ti matrix.

3.4.5 Comparison with human bone

Table 3.2 compares the mechanical properties of the Ti matrix syntactic foam and the cortical and trabecular bones. Compared with human bone, the Ti matrix syntactic foam has a higher density and a porosity between that of cortical bone and trabecular bone. The elastic modulus of the Ti matrix syntactic foam is similar to that of cortical bone, but higher than that of trabecular bone. However, the compressive and flexural strengths of Ti matrix syntactic foam are much lower than those of cortical bone, but higher than those of trabecular bone.

Table 3.2 The mechanical properties of Ti matrix syntactic foam, cortical bone and trabecular bone.

	Ti matrix syntactic foam	Cortical bone	Trabecular bone
Denstiy (g/cm^3)	1.5-3.0	1.30±0.03 (1)	0.34-0.35 (6)
Porosity	25-60%	4-26% (2)	75% (7)
Pore size (μm)	5-10, 125-250	10-100 (3)	
Elastic Modulus (GPa)	2.6-4.4	3.88-11.7(4)	0.127-0.43 (6)
Compressive strength (MPa)	20-90	88.3-163.8 (4)	1.6-4.5 (6)
Flexural strength (MPa)	10-30	88.9-113.8 (5)	

(1) Orvieto *et al.* (1992); (2) Wachter *et al.* (2001); (3) Wang & Ni (2003); (4) Ascenzi & Bonucci (1967); (5) Ascenzi & Bonucci (1968); (6)Giesen *et al.* (2001); (7) Gilbert *et al.* (2009)

As evidenced in the literature, the elastic modulus of human bones varies considerably. The requirement of the implant material depends on where it is applied. This study develops an efficient and economic method to fabricate a material with controlled elastic modulus. As a potential implant material, Ti matrix syntactic foam can decrease the stress shielding effect by providing a close elastic modulus to the human bone; it is expected to have wide applications in implant surgery.

3.5 Biological Performance

3.5.1 Toxicity

Fig. 3.42, Fig. 3.43 and Fig. 3.44 show the live/dead cell culture of the Ti matrix syntactic foam sample with nominal Ti volume percentages of 40%, 60% and 80%, fabricated with

a compaction pressure of 70 MPa. There are three different proportions of the extracted material from the Ti matrix syntactic foam sample, which are 1%, 10%, 50%. The figures in left column were the results of cells cultured in standard culture medium, and the figures in the right column were those cultured in the mixture of extraction from Ti matrix syntactic foam and standard culture medium with a set of different volume ratio. The live/dead test results show that the cells have near same exhibition. The cells in standard complete culture medium after the same culture period are shown in Fig. 3.45. The green particles represent the living cells and the red particles show the dead cells. The distribution of cells is not uniform. After culture for 48 hours, the areas with a high concentration resulted in cell clumping. The cells in these areas have an approximately spherical shape after culture. However, the cells in the areas with a low cell concentration exhibit an excellent spreading after culture. This non-uniform distribution and confluence of the cells happen to the control culture well too. After 48 hours in complete culture medium, the dead cell percentages in the well cultured with extraction from samples with different Ti volume percentages are approximate same. This result proved that both Ti and the ceramic used in this study were chemically inert after the sintering process, and there were no toxic elements released from the material. Increasing the compaction pressure cannot introduce new elements into the material, and therefore, samples with different compaction pressure were considered non-toxic.

Ti and Ti alloys have a very low toxicity for living animals, including human beings. Histological studies have shown that Ti has practically no toxicity for bones (Matsunaga *et al.* 2000; Nociti *et al.* 1997). Additionally the ceramic has shown its chemical inertness

in human body fluid and therefore was taken as a potential implant material (Park & Lakes 2007). The toxicity test conducted on the Ti matrix syntactic foam to examine the chemical inertness of Ti matrix syntactic foam after the sintering process is reliable.

3.5.2 Biocompatibility

3.5.2.1 Cell adhesion

The exhibition of cells on the Ti matrix syntactic foam depends on surface morphology. Generally, areas consisting of a larger number of sintered Ti powder particles have smoother performance after the polishing. The spreading of cells on these smooth areas was good with numerous filopodia and microvilli, as shown in Fig. 3.46. However, on the surface of individual Ti powder particles, the spreading of the cells is much less due to the surface morphology being less smooth than the flat area, as shown in Fig. 3.47. On the CM surface, the spreading of the cells is very poor. The cells exhibit spherical shape generally, as shown in Fig. 3.48.

Ti has already shown an excellent biocompatibility with cells, leading to osteoblast proliferation. *In vivo* and *in vitro* studies on the differentiation, and maturation around Ti implants (Davies 1998; Schwartz *et al.* 1999; Stanford & Keller 1991; Swart *et al.* 1992) showed that the surface of Ti implants can modulate phenotypic expression and metabolism of osteoblast cells (Brunette 1988; Cooper 2000; Degasne *et al.* 1999). The interactions between cells and implants, such as the attachment, morphology, proliferation,

and function of the cells, are affected by the surface properties of the implant material, for example the size and the shape of the surface features (Curtis & Wilkinson 1997; Myllymaa *et al.* 2009; Puleo & Nanci 1999; Schwartz *et al.* 1997). Generally, on a smooth surface, cells have flat, well-spread morphology, and on a rough surface, cells exhibit a round or cuboidal shape (Boyan *et al.* 2001). The ability to control cell orientation and morphology through topographical patterning, now referred to as contact guidance, was first observed in the early 1900s (Harrison 2005). Recent research has already shown that the adhesion of SaOS-2 cells on Ti can be affected by the roughness of the surface, SaOS-2 cells are flattened with numerous filopodia and microvilli, and on a rough sandblast surface, cells are less flattened with visible filopodia, as shown in Fig. 3.49 (Degasne *et al.* 1999).

Most cells on the surface of CM particles maintained a spherical shape, which indicated that the cells did not exhibit good spreading. The number density was obviously lower than that on the Ti surface. These spheres have an approximate dimension of 5-10 μm. A very small amount of cell spreading was observed, as shown in Fig. 3.50. After the cell spreading, it has a similar dimension, shape, filopodia and microvilli with those on the surface of Ti.

Generally, there was not too much adhesion of cells on the CM particles after cell culture, compared with the adhesion of cells on the Ti surface. This is because the composition of

the CM particles was not designed for clinical application initially, and thus the CM particles exhibited very low biocompatibility with to the cell adhesion. Recently, a number of pieces of research on the biocompatibility of ceramics with composition suitable for clinical applications have already been conducted. Calcium phosphate ceramics and bioactive glasses were introduced into implants more than 30 years ago as bone substitutes because of bioactive bonding to the bone and enhanced bone tissue formation (El-Ghannam 2004). The bioactive glass, which contains approximate 45 wt% of silica in addition to calcium and phosphorous, is known to have the most stimulatory effect on bone cell function (El-Ghannam *et al.* 1999; Garcia *et al.* 1998; Klein *et al.* 1983; Ogino *et al.* 2004; Oonishi *et al.* 2000; Schepers *et al.* 1991).

3.5.2.2 Cell calcification

Ti and its alloy have been successfully used in dentistry and orthopaedics because bone is able to form in close approximation to the material surface. Many pieces of research have shown that the surface of an implant material has profound effects on the success of an implant because the surface characteristics modulate the adsorption of the proteins, lipids, sugars, and ions present in the tissue fluid onto the material (Tengvall 2001). 1-3 weeks after a successful implant surgery, calcification will occur in Osteoblast cells (Boyan *et al.* 2001). The von Kossa stain can demonstrate the calcification in the extracellular matrix during the culture of human osteoblast cells (Kassem *et al.* 1992). Therefore, using von Kossa to examine the calcification of the osteoblast on the surface of the Ti matrix syntactic foam can examine the potential for implant application.

The Von Kossa stain was conducted on the Ti matrix syntactic foam sample with a Ti volume percentage of 60%, fabricated with compaction pressures of 45 MPa (Fig. 3.51) and 100 MPa (Fig. 3.52).

Generally, on the surface of specimen fabricated with a compaction pressure of 45 MPa, the dark area (pointed by black arrow) which indicates the calcium distribution connected each other and form a large dark area. However, to the specimen fabricated with a compaction pressure of 100 MPa, the dark area (pointed by black arrow) was individually in the surface. The pores of CM were point out by white arrow. These dark areas are formed by the reaction of silver ions and the phosphate. This phenomenon indicates that the osteoblast cells on the surface of Ti matrix syntactic foam specimen with higher compaction pressure have less calcification than those on the Ti matrix syntactic foam specimen with lower compaction pressure. This is because the higher compaction pressure can result in a much denser specimen. As a consequence, after polishing, the specimen fabricated with higher compaction pressure has much more smooth surface. This is because the osteoblast cells exhibits an increased calcification of the rough Ti surface (Groessner-Schreiber & Tuan 1992).

The performance of the osteoblast cell lines on the surface of Ti matrix syntactic foam can be summarized in Table 3.3.

Table 3.3 The performance of osteoblast cell lines on the surface of Ti matrix syntactic foam.

		Cell spreading	Calcification
Ti matrix	Smooth surface	More	Less
	Rough surface	Less	More
Ceramic microspheres (CMs)		Poor	------

Most cells concentrated on the surface of the Ti matrix. Depending on the surface morphology, the cells have different spreading. On the smoother surface, better spreading and lower calcification of the cells can be achieved. However, on the surface of CMs, the spreading of the cells is very poor.

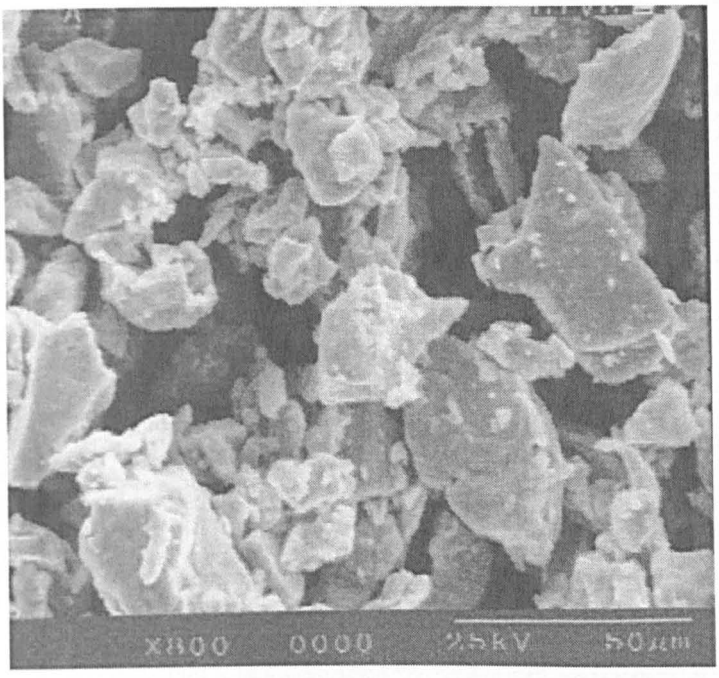

Fig. 3.1 SEM image showing the morphology of the Ti powder used to fabricate the Ti matrix syntactic foams.

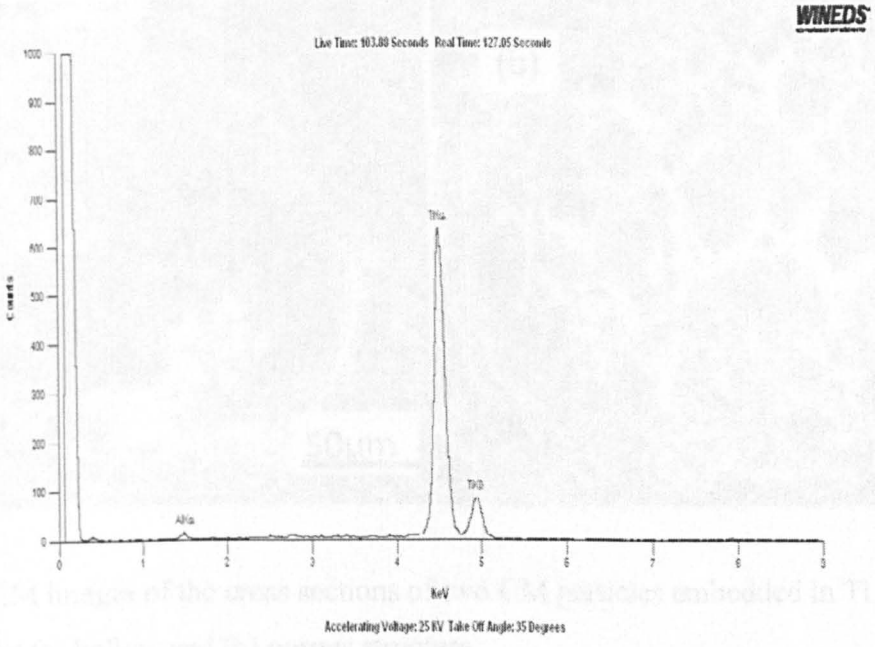

Fig. 3.2 The EDX spectrum of the Ti powder.

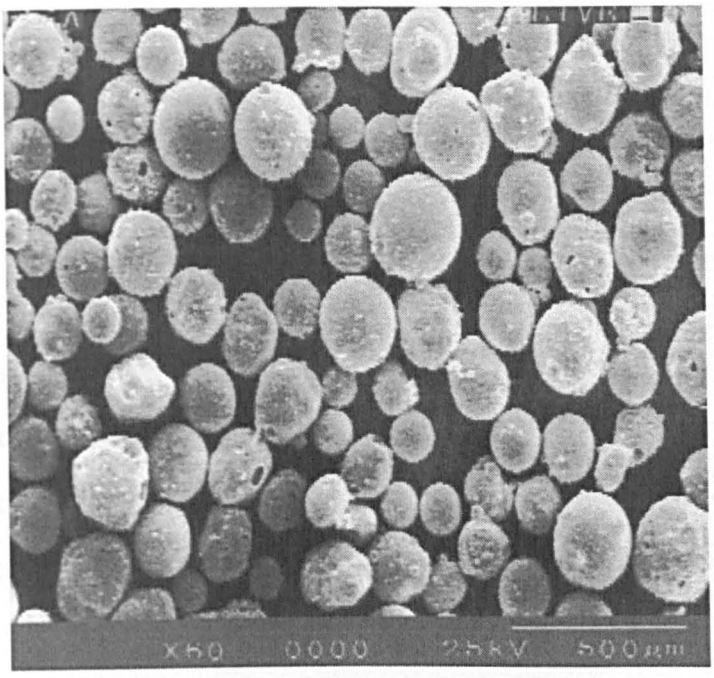

Fig. 3.3 SEM image showing the morphology of the CM powder used to fabricate the Co-Cr-Mo matrix and Ti matrix syntactic foams.

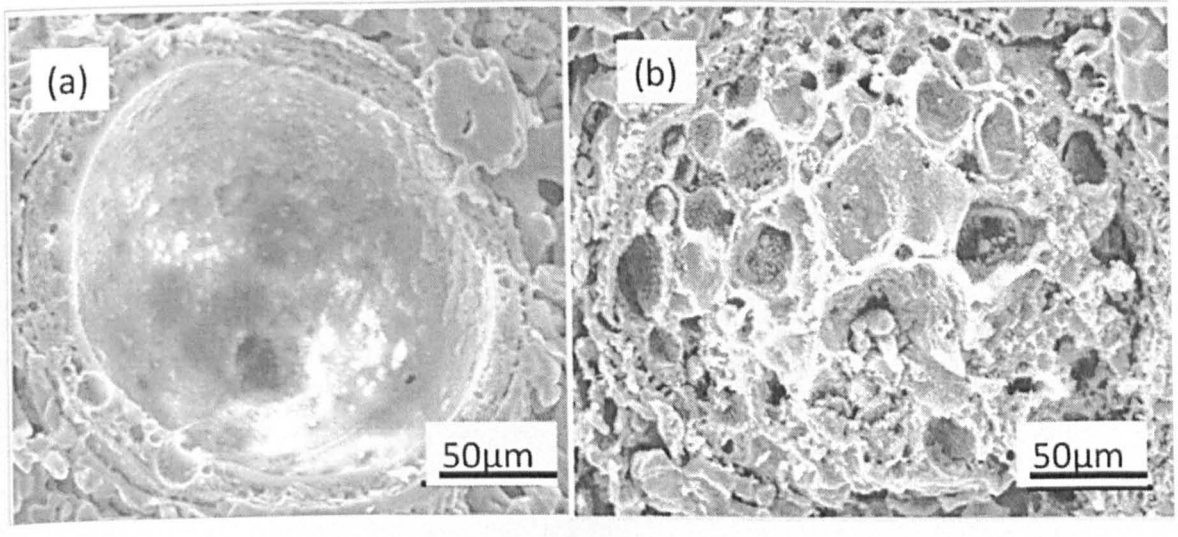

Fig. 3.4 SEM images of the cross sections of two CM particles embedded in Ti matrix, showing the (a) hollow and (b) porous structure.

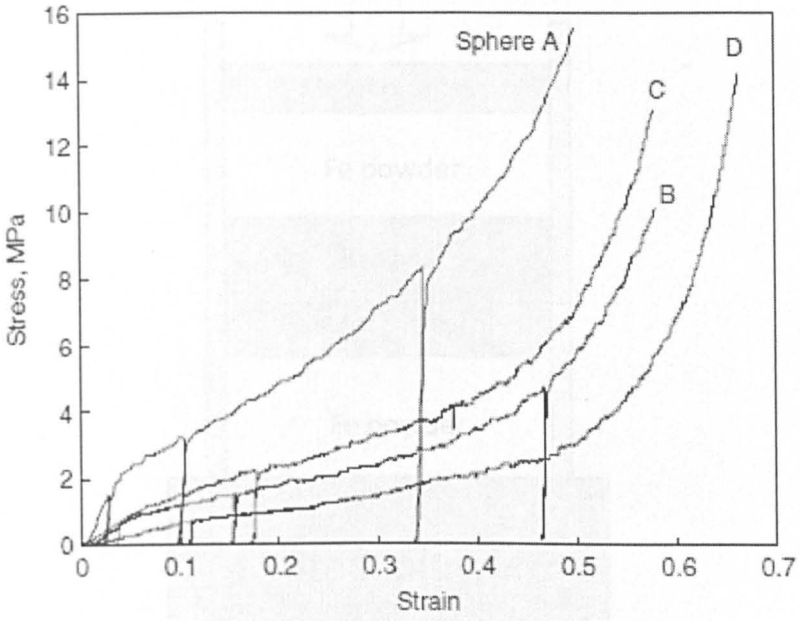

Fig. 3.5 The compressive behaviour of CMs in static compression (Zhang & Zhao 2007).

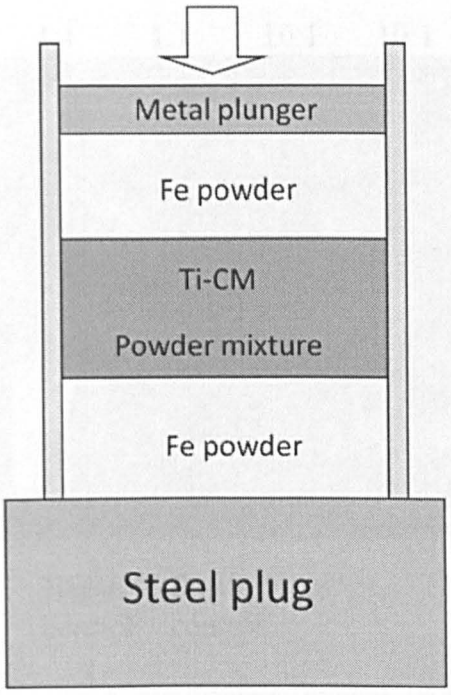

Fig. 3.6 Schematic diagram showing the process of preparing the Ti–CM preform.

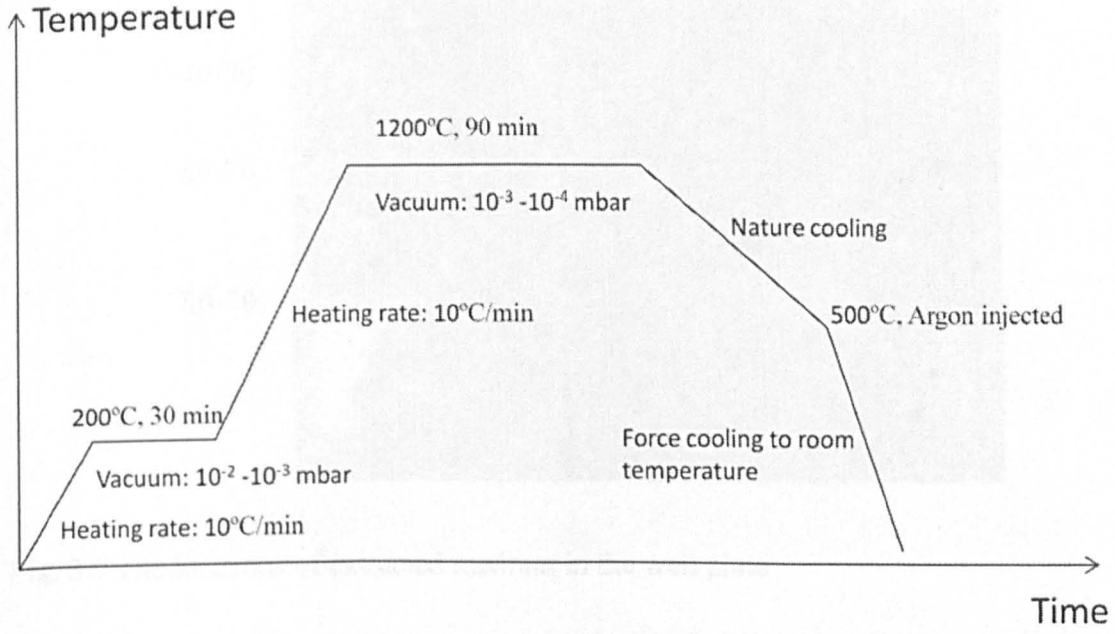

Fig. 3.7 The heating program of the sintering process

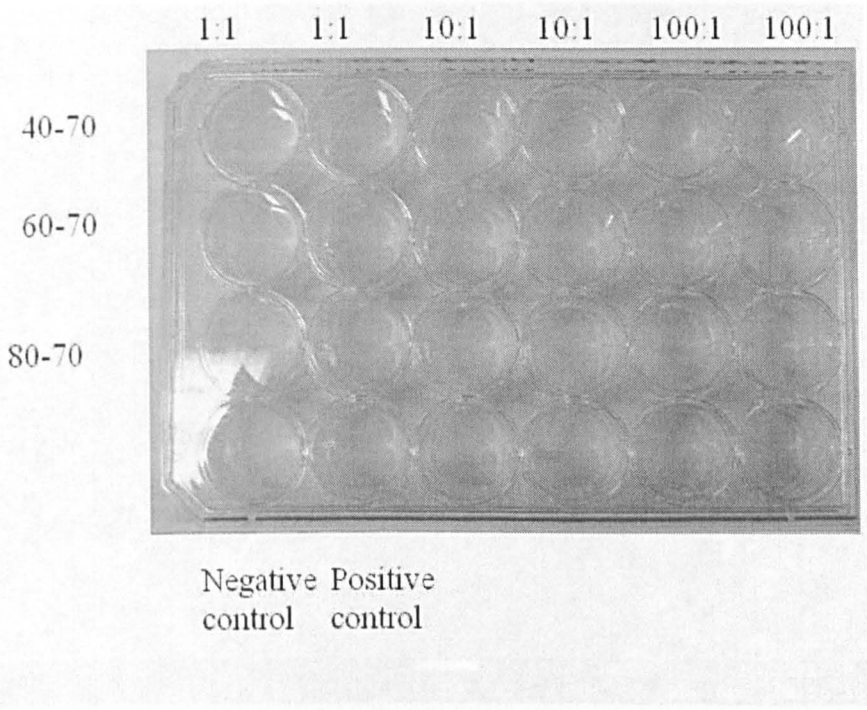

Fig. 3.8 The locations of diluted medium in the well plate.

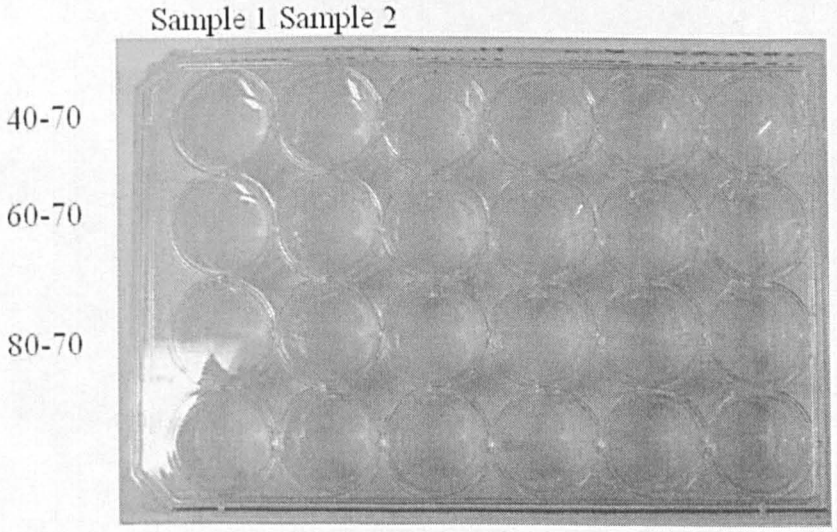

Fig. 3.9 The locations of extracted medium in the well plate

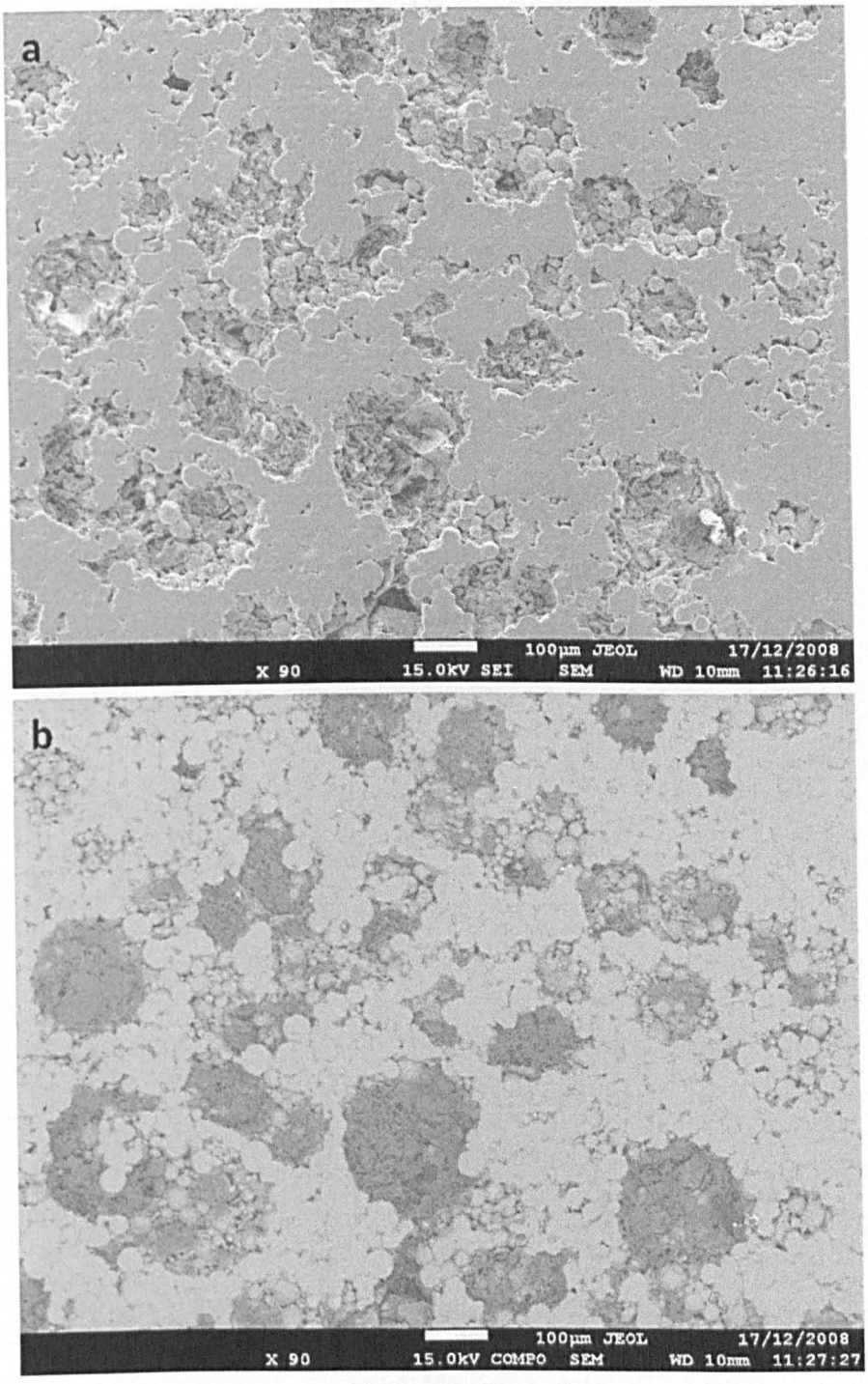

Fig. 3.10 (a) Secondary electron and (b) back scattered electron images of the surface of a Ti matrix syntactic foam sample with a Ti volume percentage of 70%, fabricated with a compaction pressure of 70 MPa.

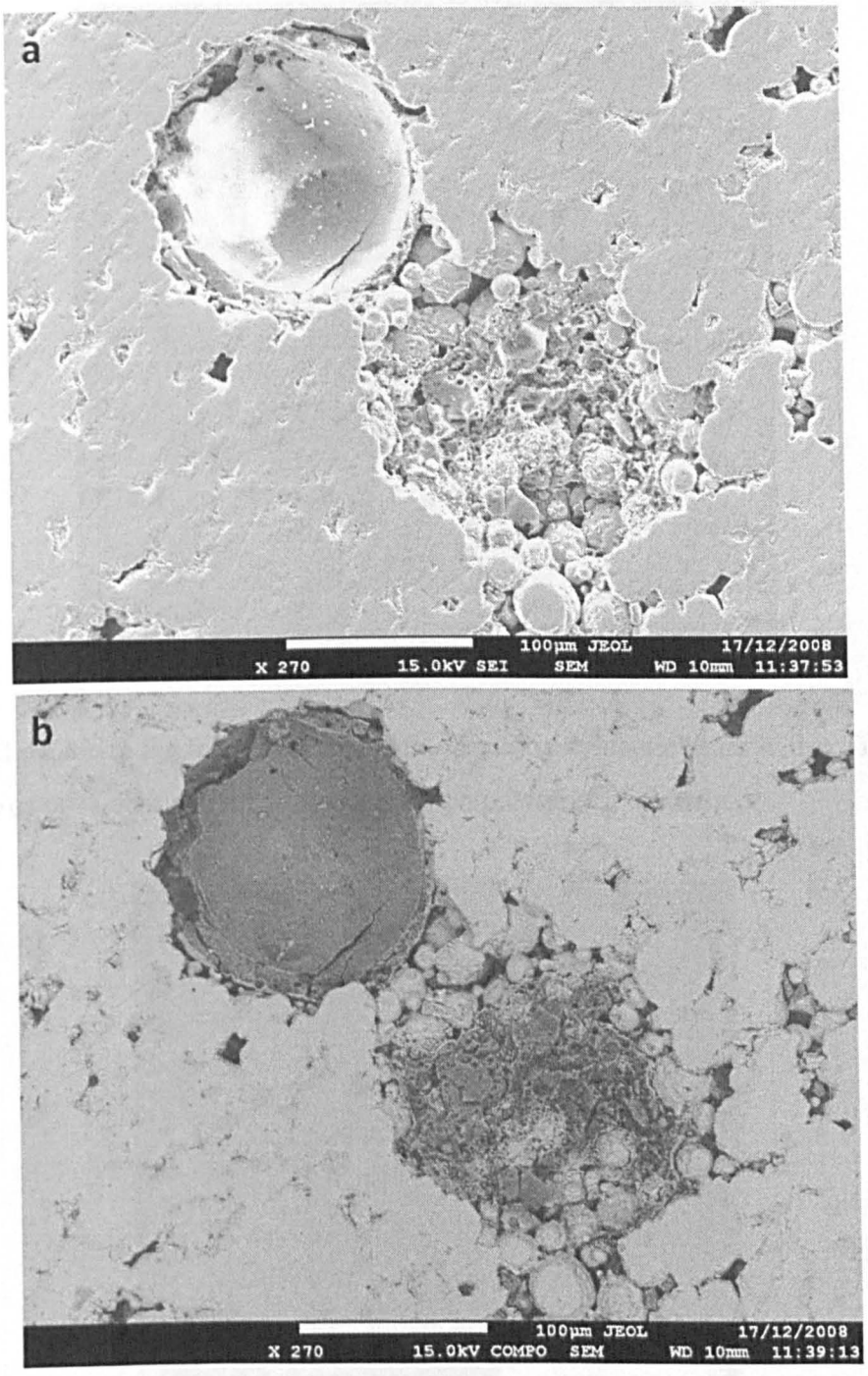

Fig. 3.11 (a) Secondary electron and (b) back scattered electron images of the CMs in a Ti matrix syntactic foam sample with a Ti volume percentage of 70%, fabricated with a compaction pressure of 70 MPa.

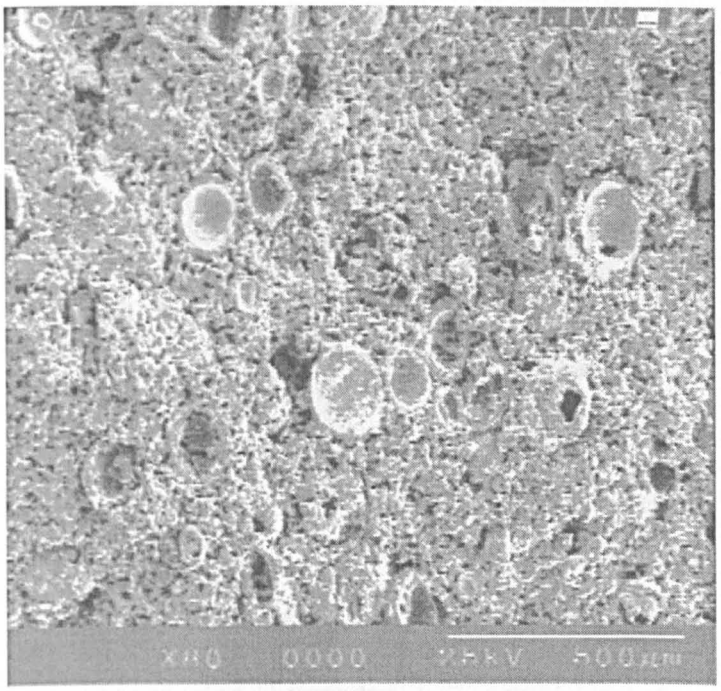

Fig. 3.12 The CMs in the fracture surface of a Ti matrix syntactic foam with a Ti volume percentage of 60%, fabricated with a compaction pressure of 45 MPa.

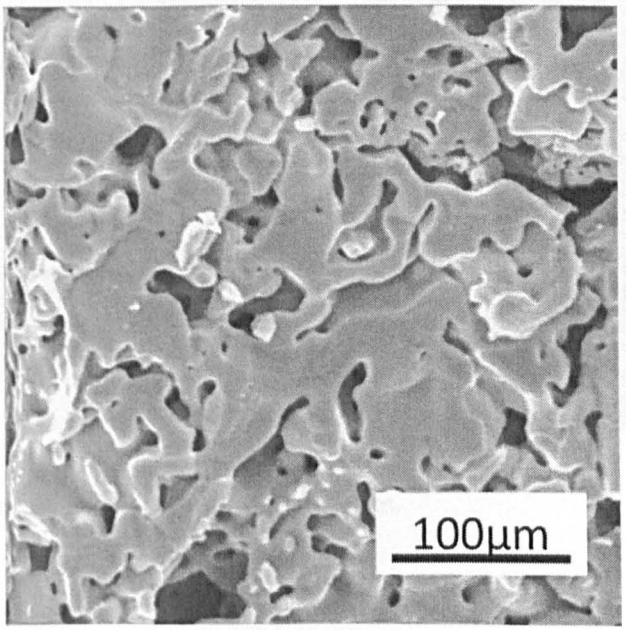

Fig. 3.13 A typical SEM image of the Ti matrix in a Ti matrix syntactic foam with a Ti volume percentage of 50%, fabricated with a compaction pressure of 100 MPa.

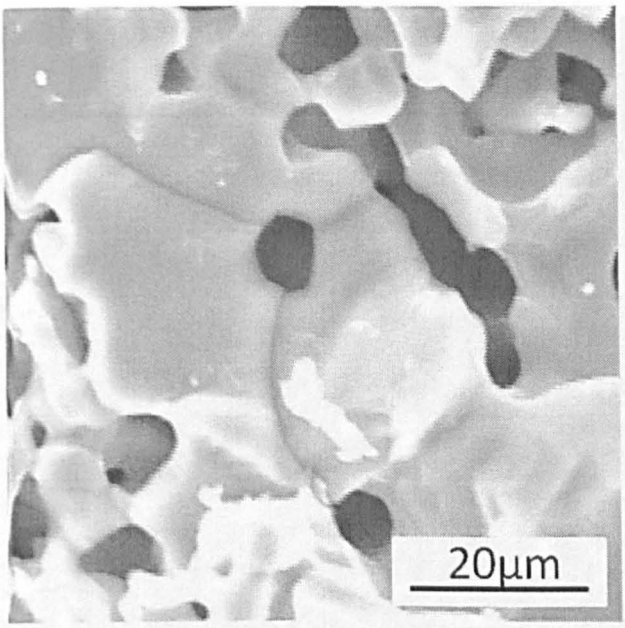

Fig. 3.14 SEM images of connected Ti particles.

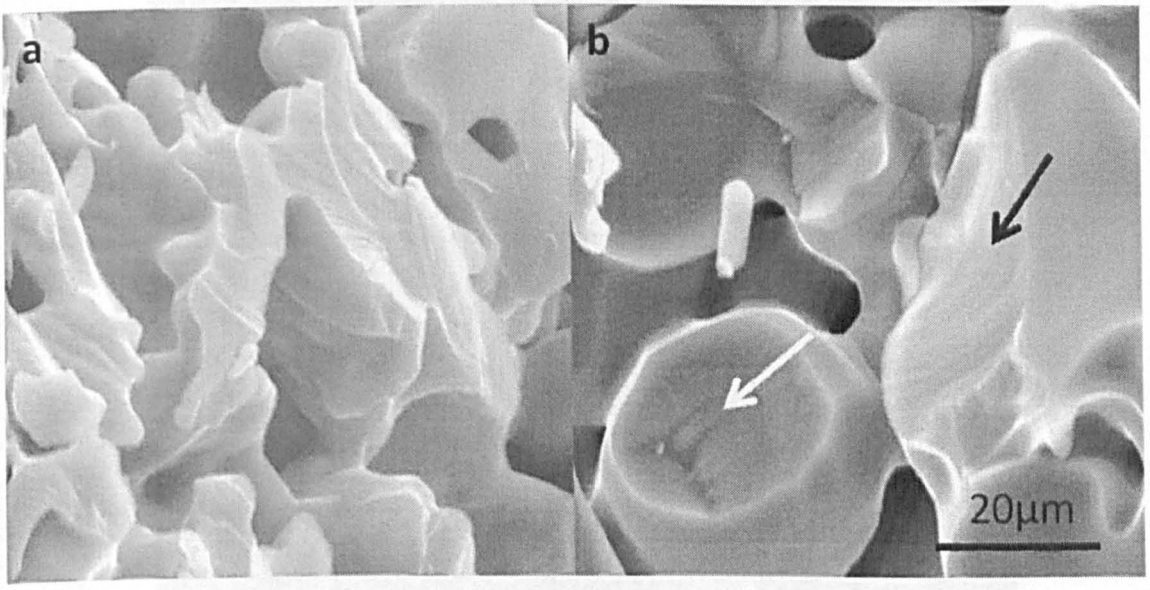

Fig. 3.15 SEM images of fractured internal surfaces.

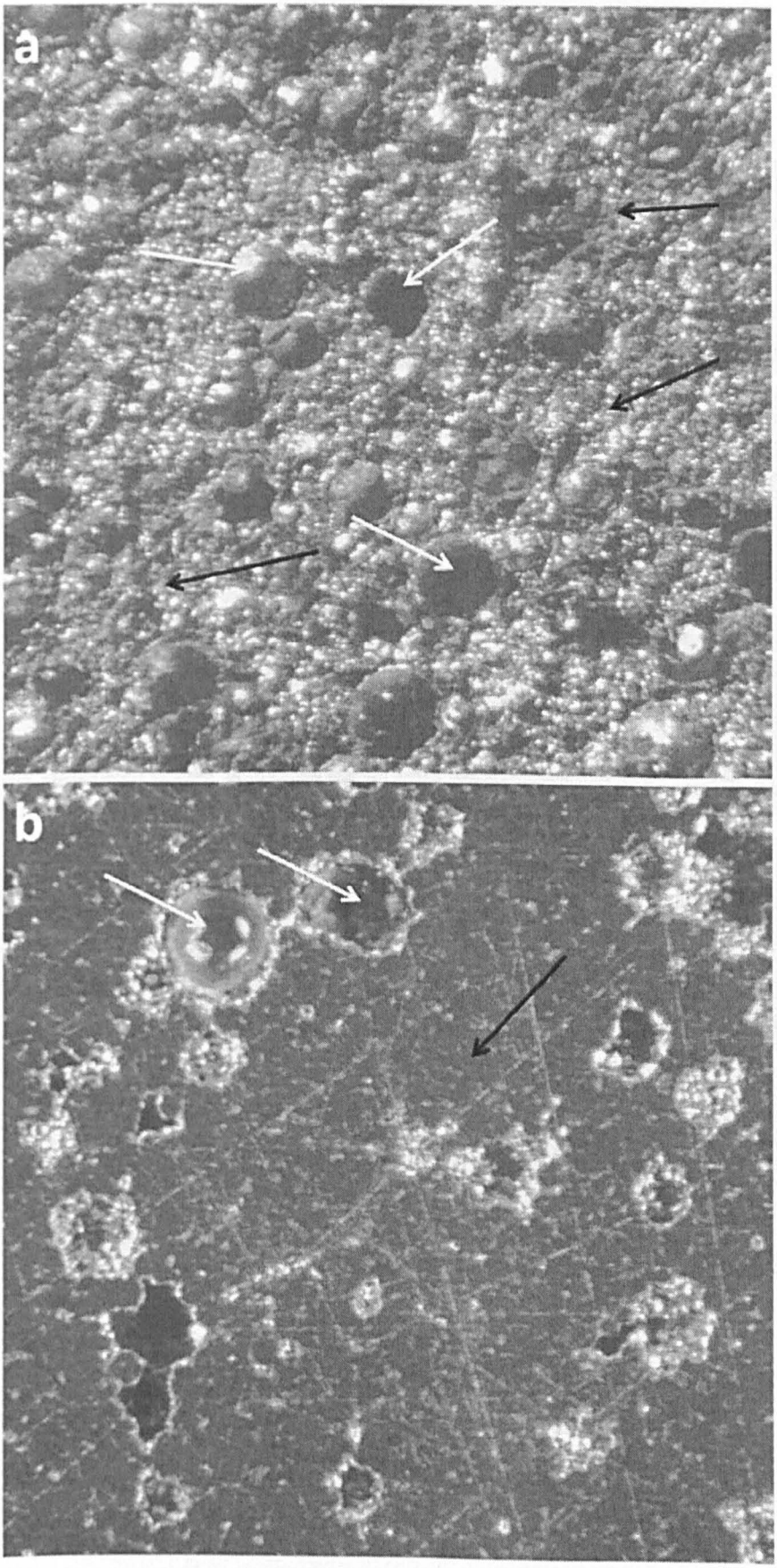
a
b

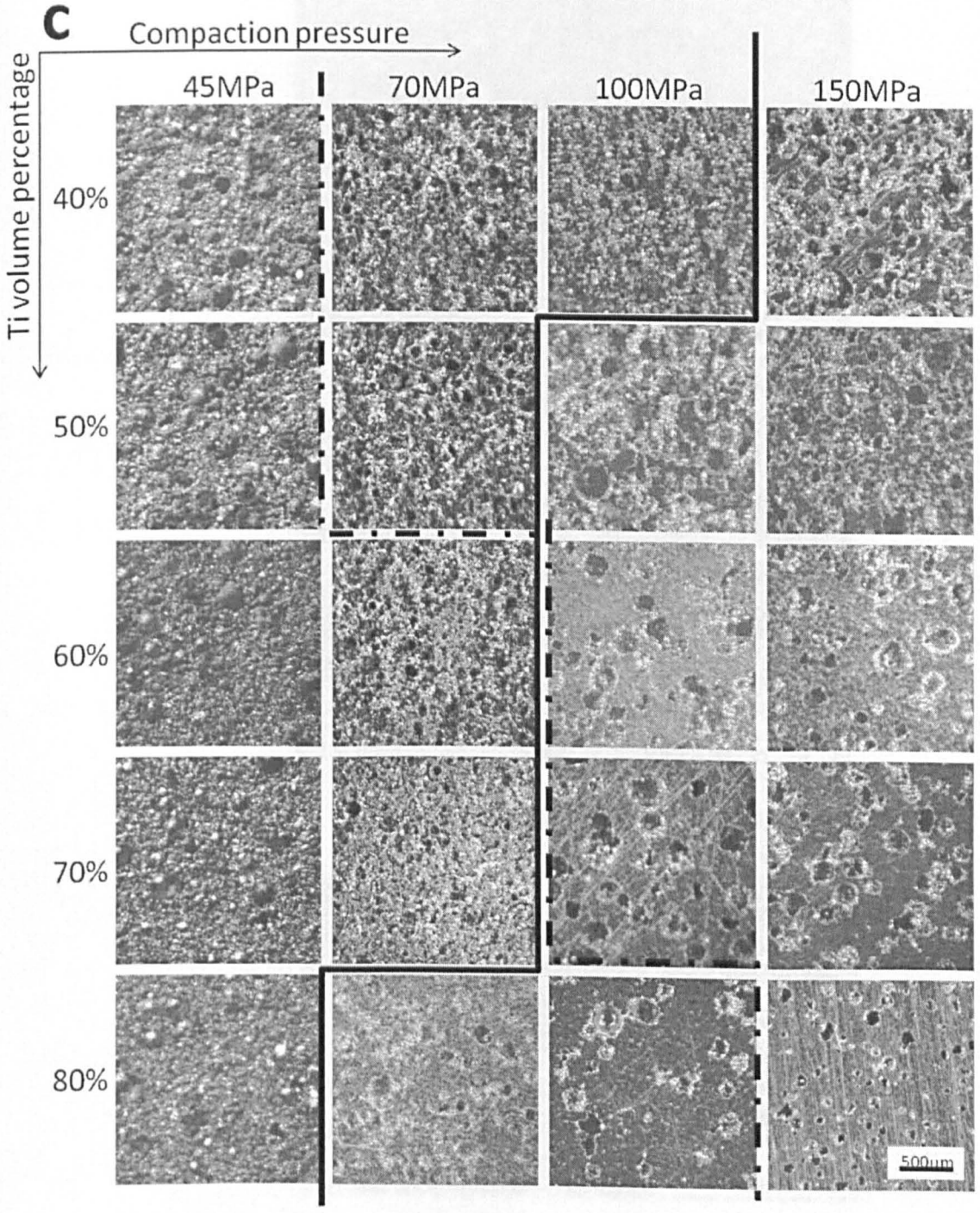

Fig. 3.16 The optical images of the Ti matrix syntactic foam surfaces with a series of Ti volume percentage of 40%, 50%, 60%, 70% and 80%, fabricated with compaction pressures of 45, 70, 100 and 150 MPa.

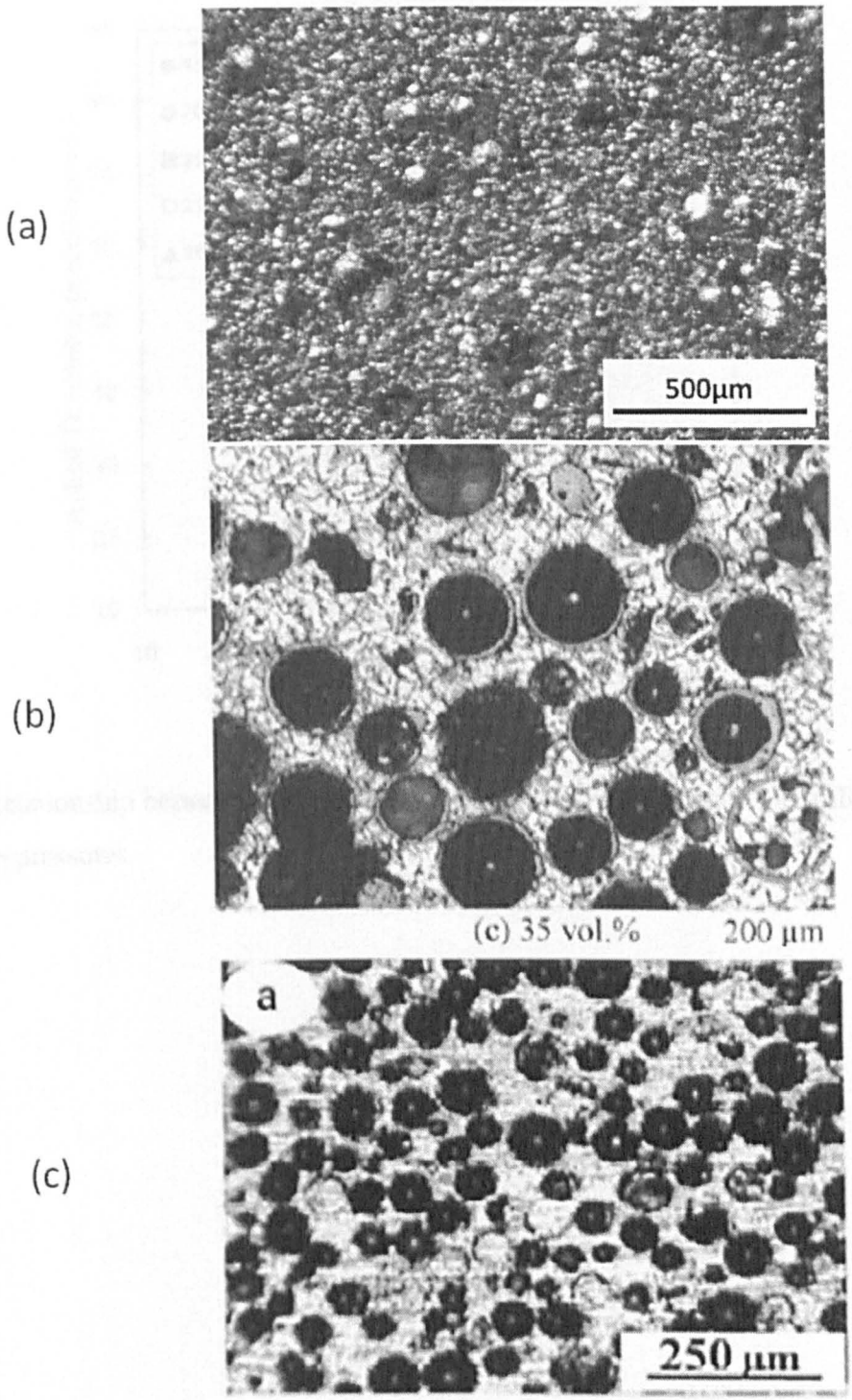

Fig. 3.17. Cross-sections of (a) Ti matrix syntactic foam, (b) ZnAl22 matrix syntactic foam (Daoud 2008) and (c) Al matrix syntactic foam (Tao *et al.* 2009).

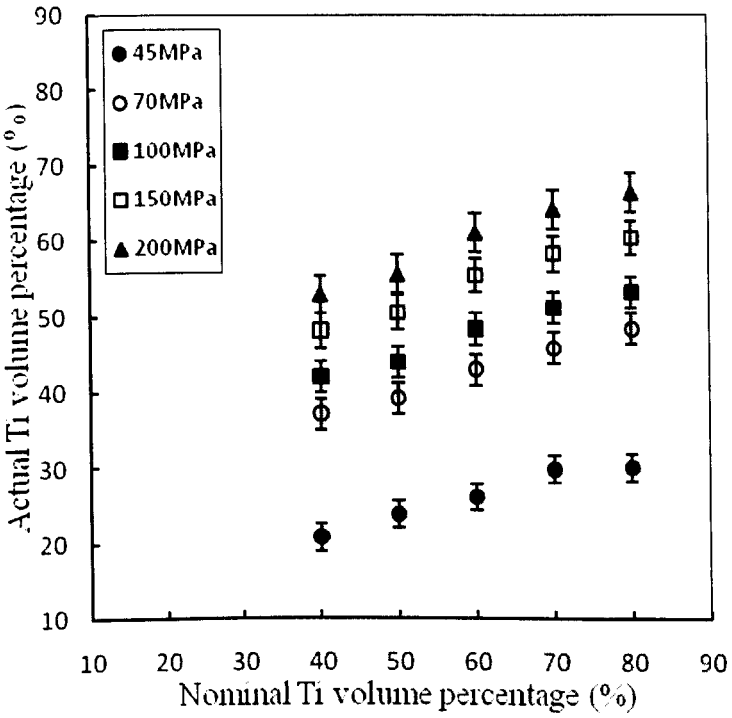

Fig. 3.18 Relationship between nominal and actual Ti volume percentages at different compaction pressures.

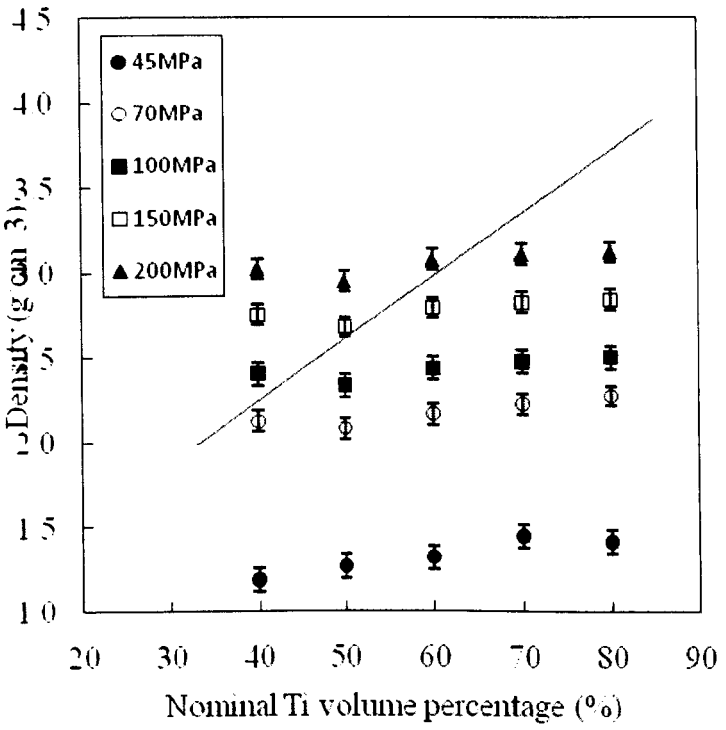

Fig. 3.19 Relationship between density and Ti volume percentage at different compaction pressures.

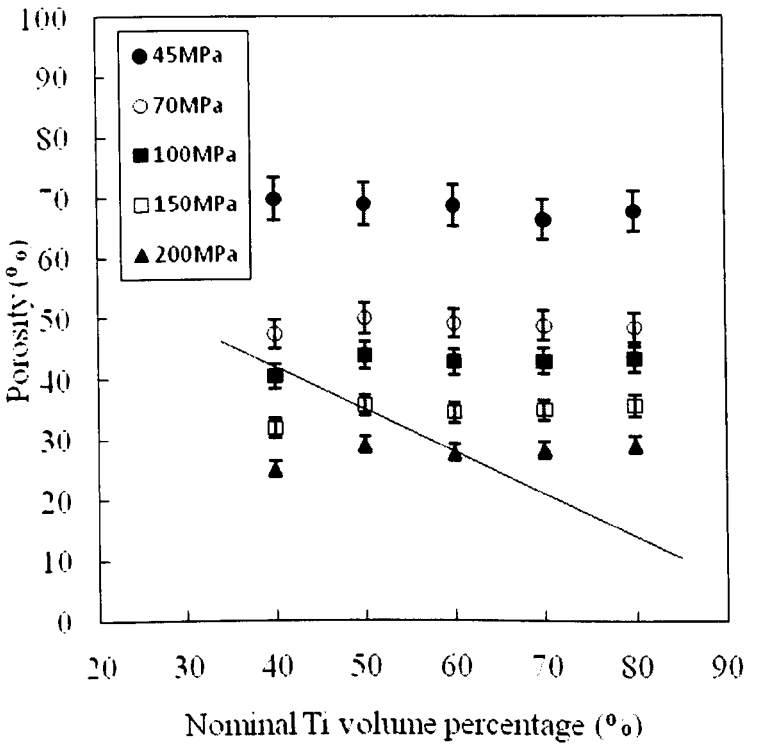

Fig. 3.20 Relationship between porosity and Ti volume percentage at different compaction pressures.

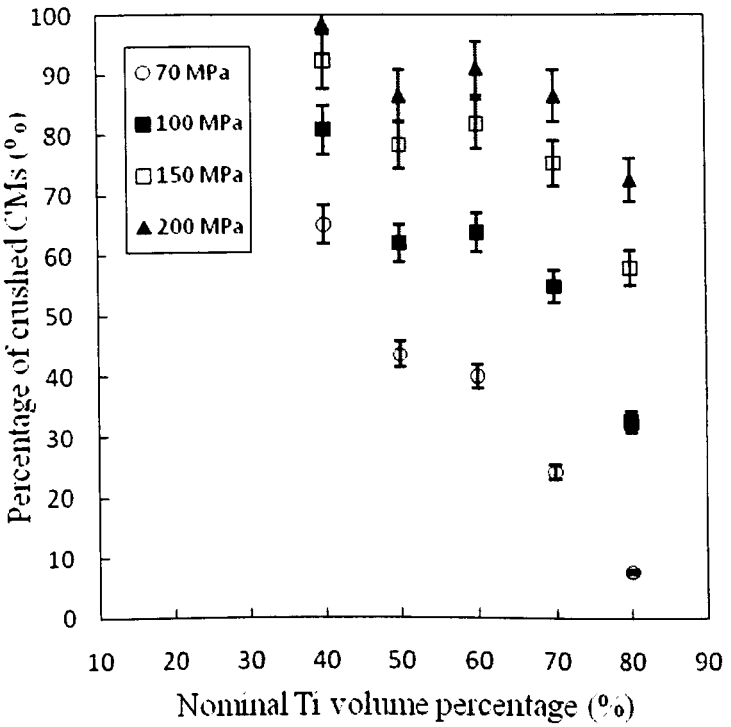

Fig. 3.21 Relationship between the percentage of broken CMs, calculated by the volume measurement method, and the nominal Ti volume percentage at different compaction pressures.

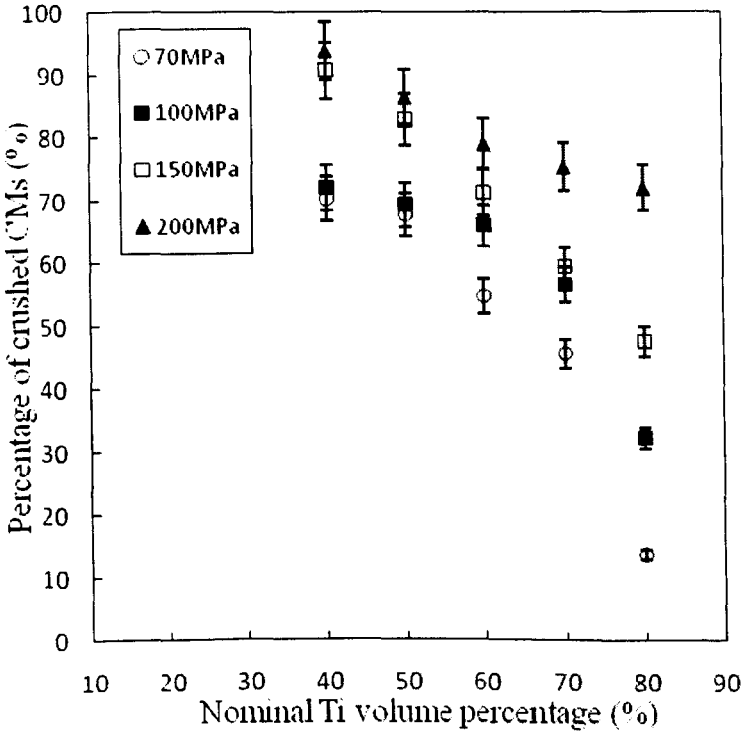

Fig. 3.22 Relationship between the percentage of crushed CMs, calculated by the water absorption method, and the nominal Ti volume percentage at different compaction pressures.

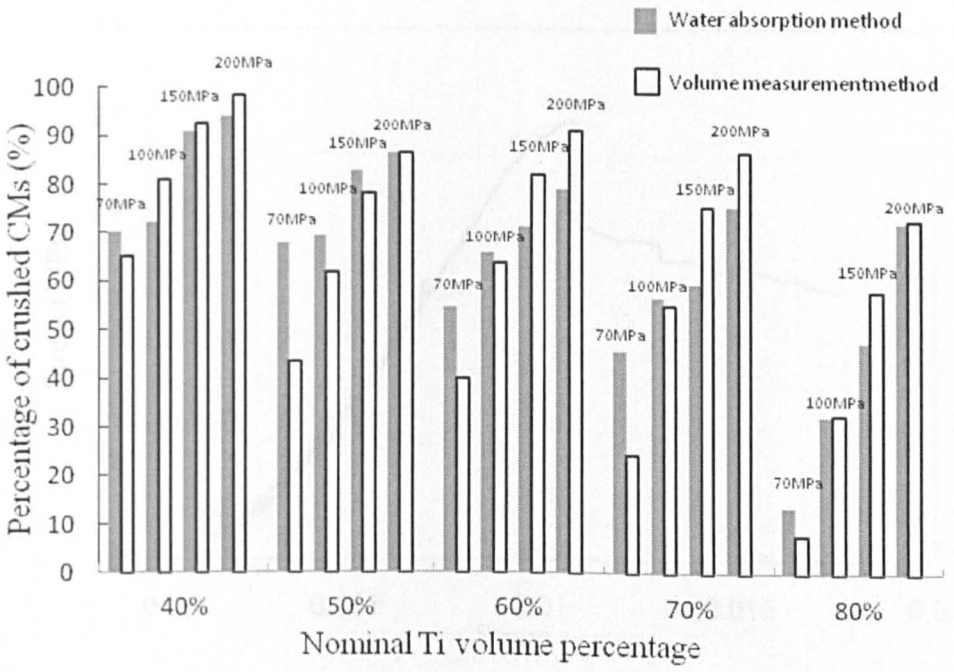

Fig. 3.23 Comparisons between the percentages of crushed CMs obtained by the two different methods for samples with different nominal Ti volume percentages fabricated with different compaction pressures.

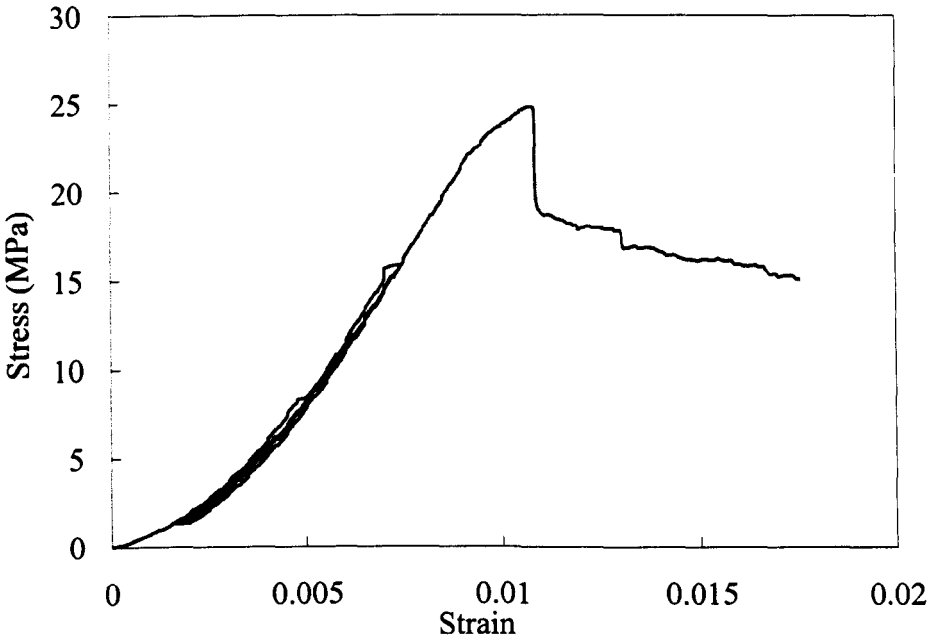

Fig. 3.24 Two typical compressive stress-strain curves of Ti matrix syntactic foam specimens with a Ti volume percentage of 50%, fabricated with a compaction pressure of 45 MPa.

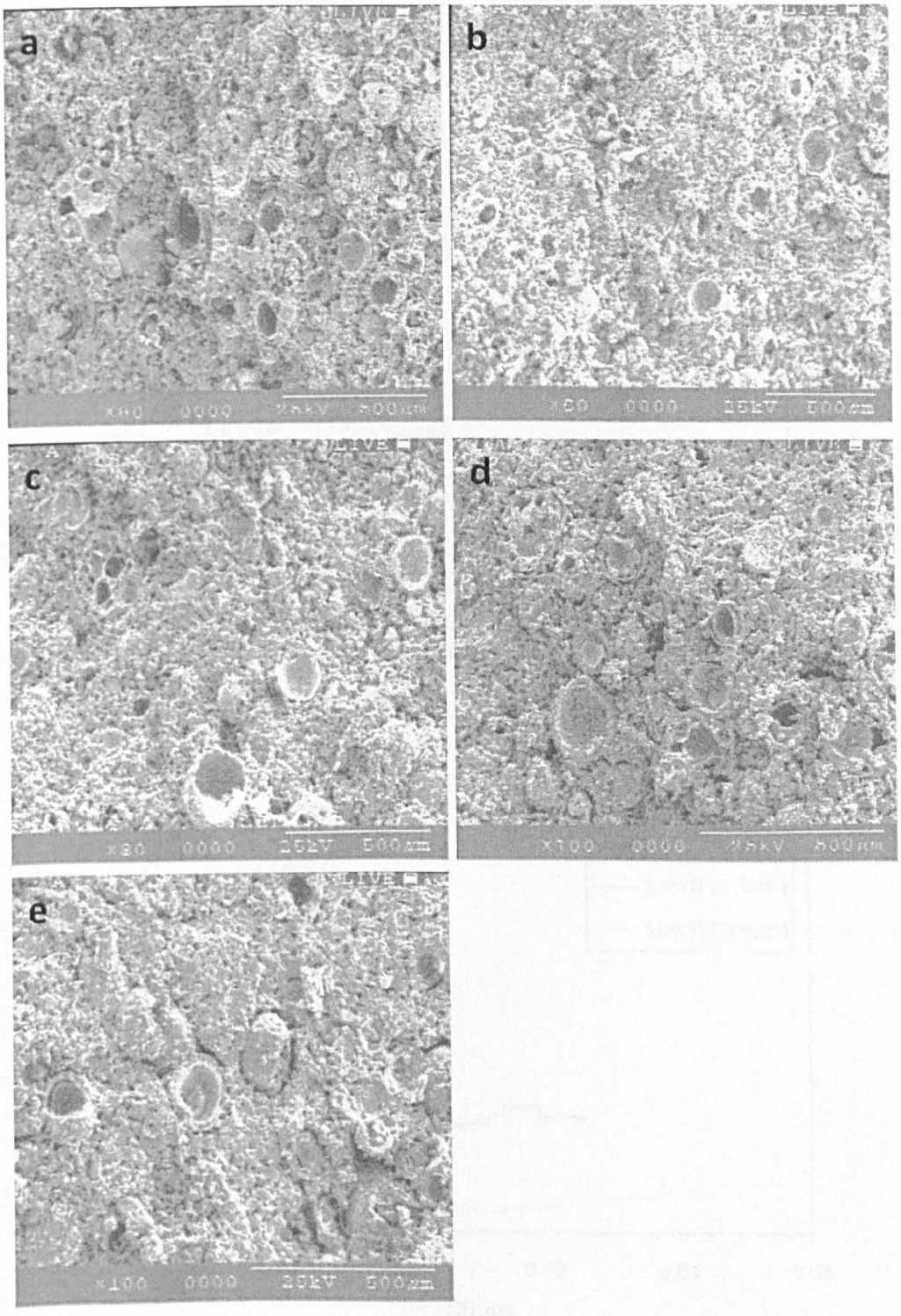

Fig. 3.25 The optical images of fracture surfaces of Ti matrix syntactic foams with Ti volume percentages of (a) 40%, (b) 50%, (c) 60%, (d) 70% and (e) 80%, fabricated with a compaction pressure of 45 MPa.

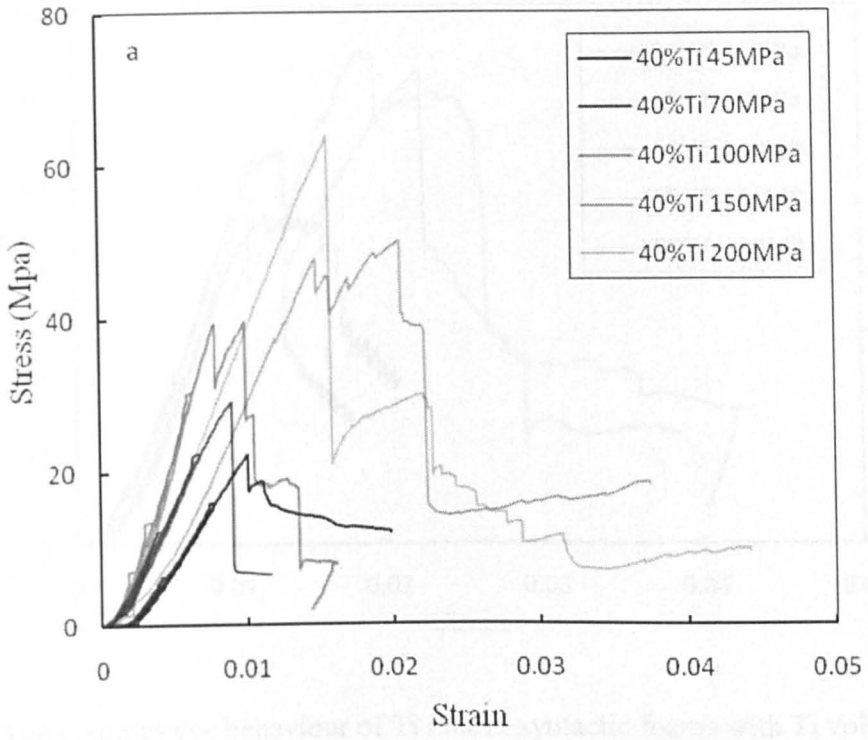
a
40%Ti 45MPa
40%Ti 70MPa
40%Ti 100MPa
40%Ti 150MPa
40%Ti 200MPa
Stress (Mpa)
Strain
0
20
40
60
80
0
0.01
0.02
0.03
0.04
0.05

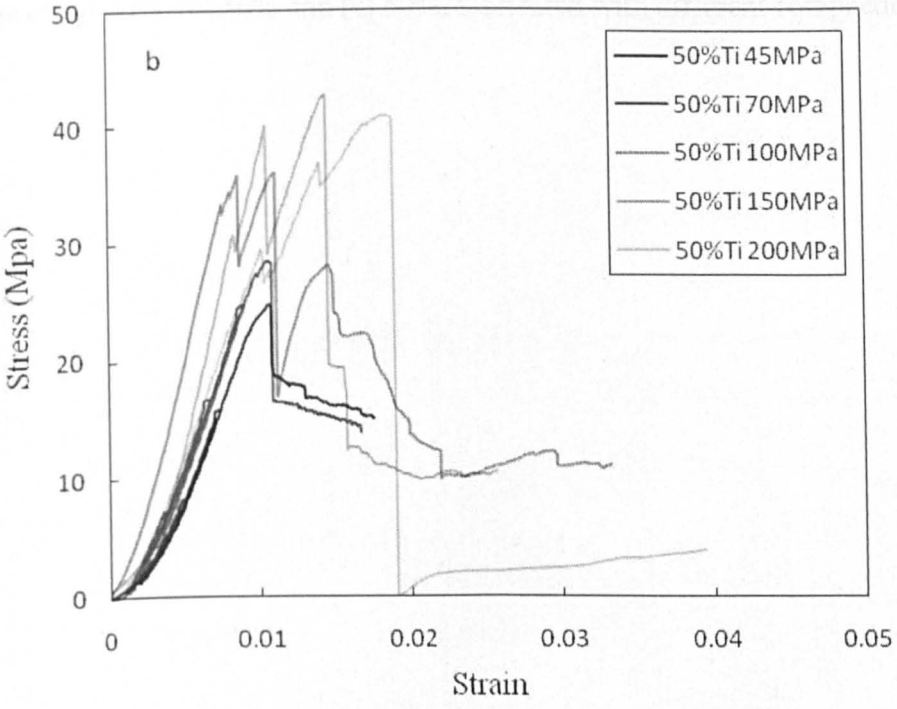
b
50%Ti 45MPa
50%Ti 70MPa
50%Ti 100MPa
50%Ti 150MPa
50%Ti 200MPa
Stress (Mpa)
Strain
0
10
20
30
40
50
0
0.01
0.02
0.03
0.04
0.05

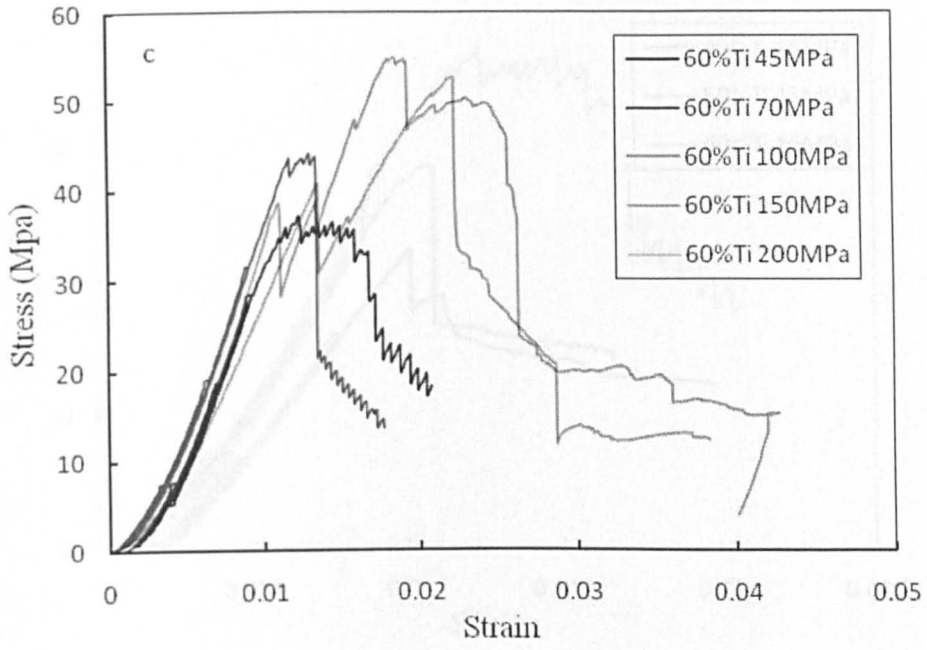

Fig. 3.26 The compressive behaviour of Ti matrix syntactic foams with Ti volume percentage of (a) 40%, (b) 50% and (c) 60%, fabricated with different compaction pressures.

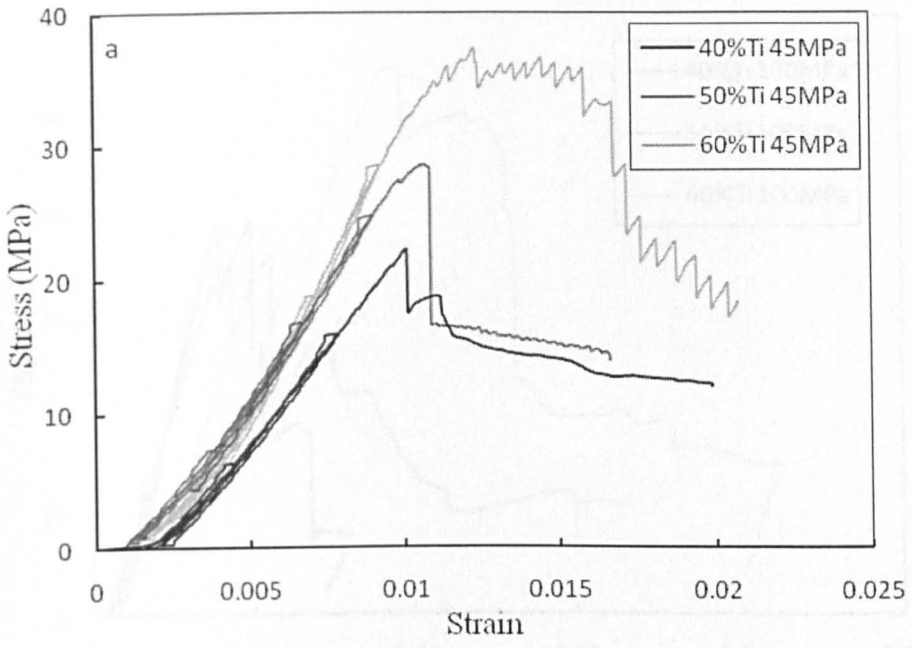
a
40%Ti 45MPa
50%Ti 45MPa
60%Ti 45MPa
Stress (MPa)
Strain
0
10
20
30
40
0
0.005
0.01
0.015
0.02
0.025

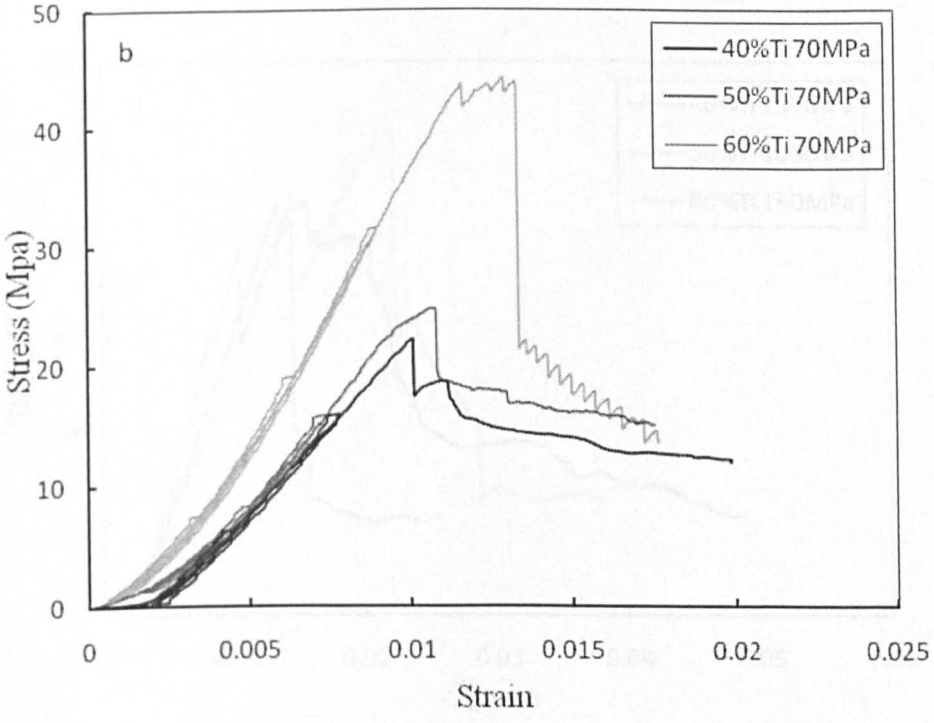
b
40%Ti 70MPa
50%Ti 70MPa
60%Ti 70MPa
Stress (Mpa)
Strain
0
10
20
30
40
50
0
0.005
0.01
0.015
0.02
0.025

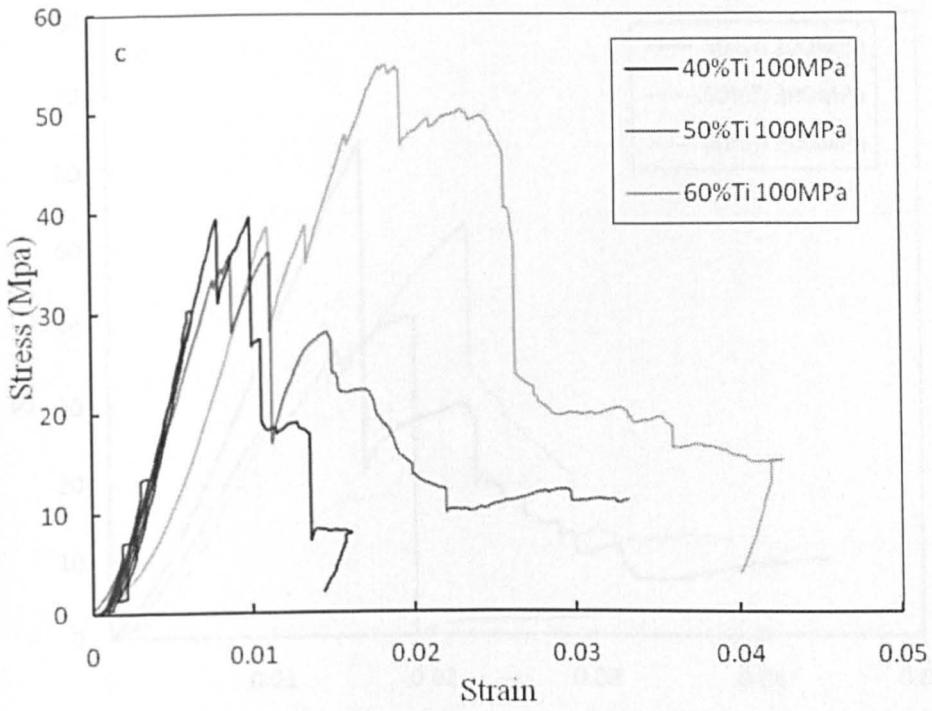
c
40%Ti 100MPa
50%Ti 100MPa
60%Ti 100MPa
Stress (Mpa)
Strain
0
10
20
30
40
50
60
0
0.01
0.02
0.03
0.04
0.05

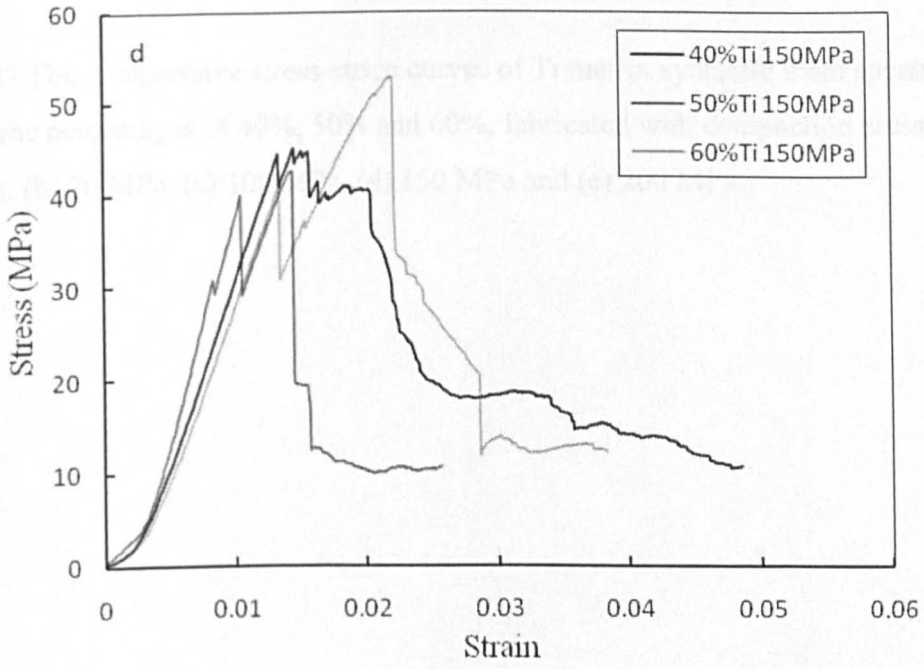
d
40%Ti 150MPa
50%Ti 150MPa
60%Ti 150MPa
Stress (MPa)
Strain
0
10
20
30
40
50
60
0
0.01
0.02
0.03
0.04
0.05
0.06

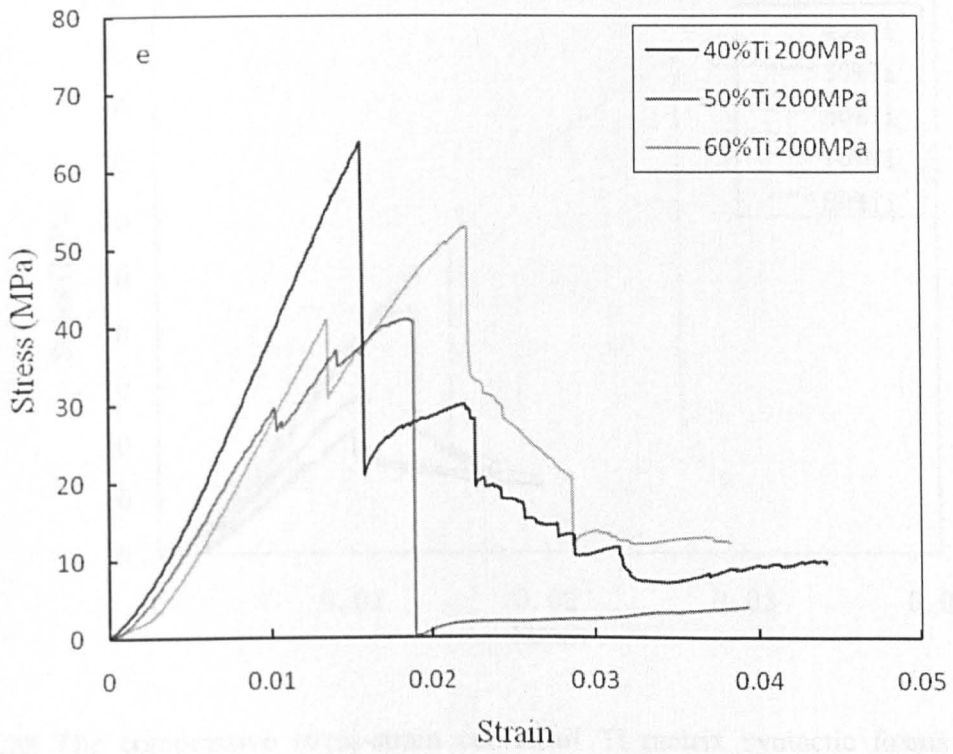

Fig. 3.27 The compressive stress-strain curves of Ti matrix syntactic foam specimens with Ti volume percentages of 40%, 50% and 60%, fabricated with compaction pressures of (a) 45 MPa, (b) 70 MPa, (c) 100 MPa, (d) 150 MPa and (e) 200 MPa.

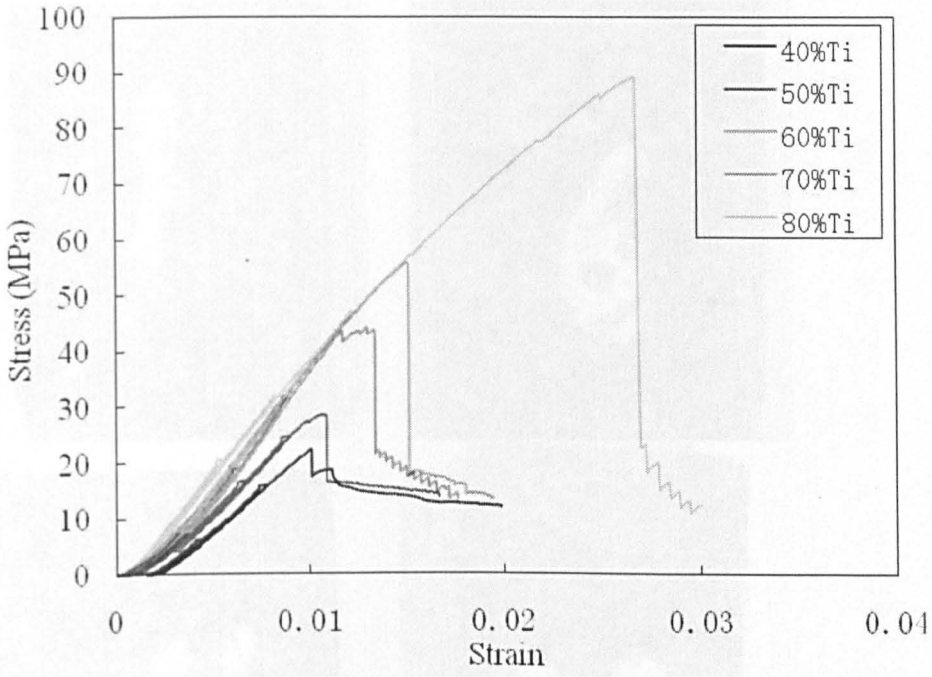

Fig. 3.28 The compressive stress-strain curves of Ti matrix syntactic foams with Ti volume percentages of 40%, 50%, 60%, 70% and 80%, fabricated with a compaction pressure of 45 MPa.

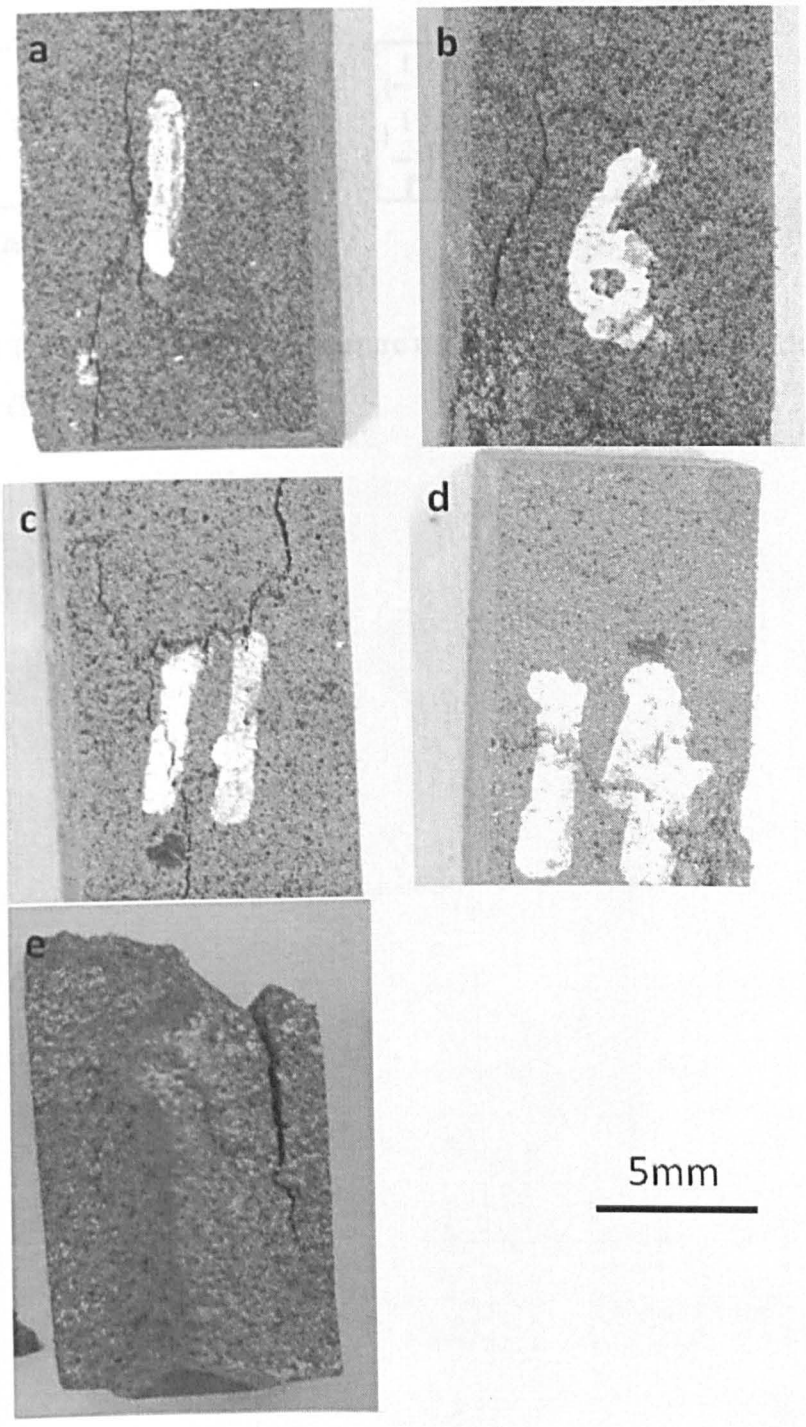

Fig.3.29 Optical images of the Ti matrix syntactic foam specimens after compression test. The specimens had Ti volume percentages of (a) 40%, (b) 50%, (c) 60%, (d) 70% and (e) 80% and were fabricated with a compaction pressure of 45 MPa.

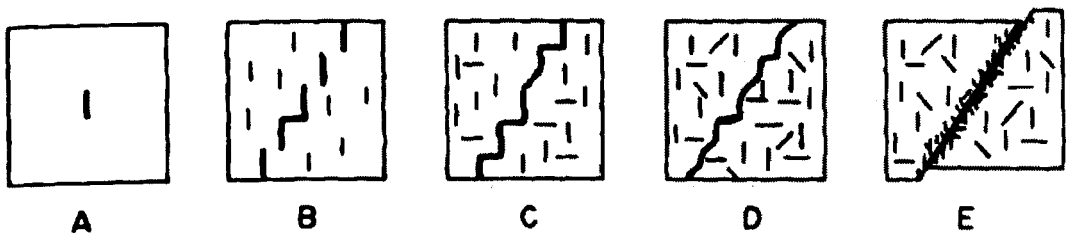

Fig. 3.30 The evolution of brittle fracture under triaxial compression at low confining pressure. (Lajtal 1974)

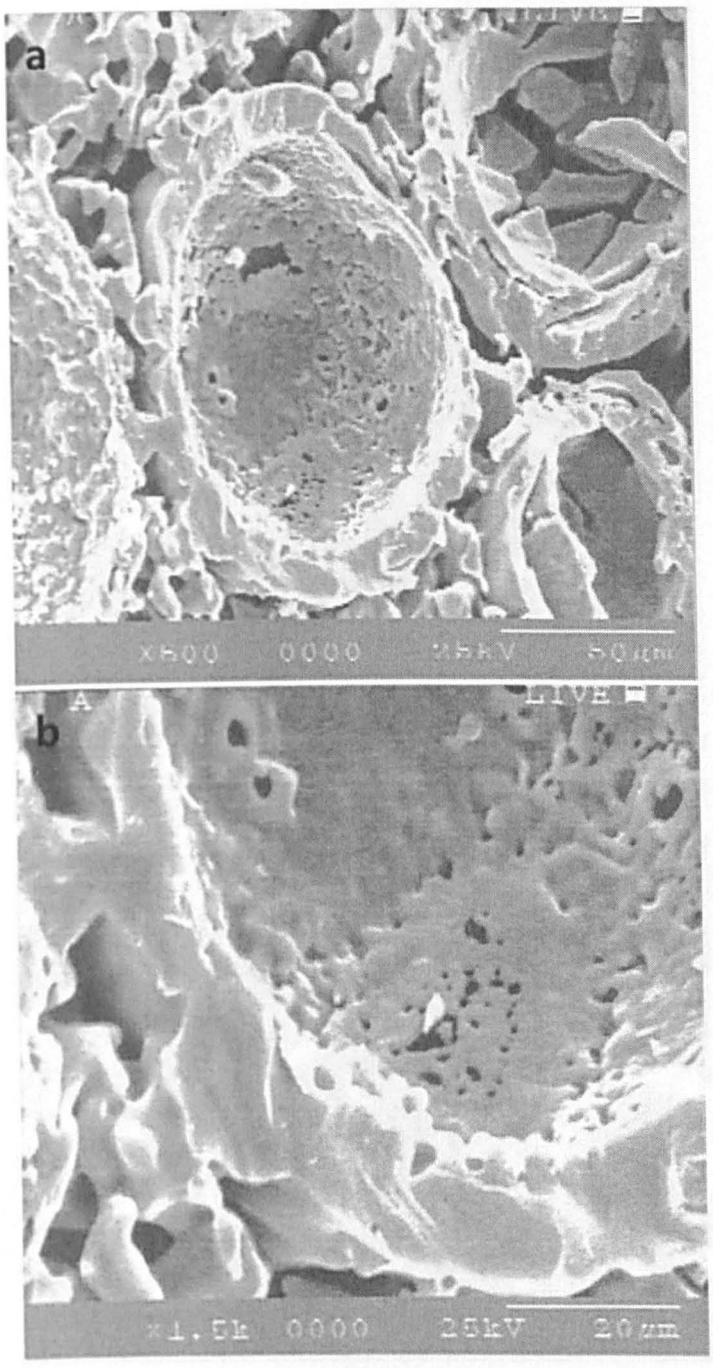

Fig. 3.31 SEM images of a fracture surface of a Ti matrix syntactic foam specimen after compression test showing fractured CMs. The specimen had a Ti volume percentage of 50% and was fabricated with a compaction pressure of 45 MPa.

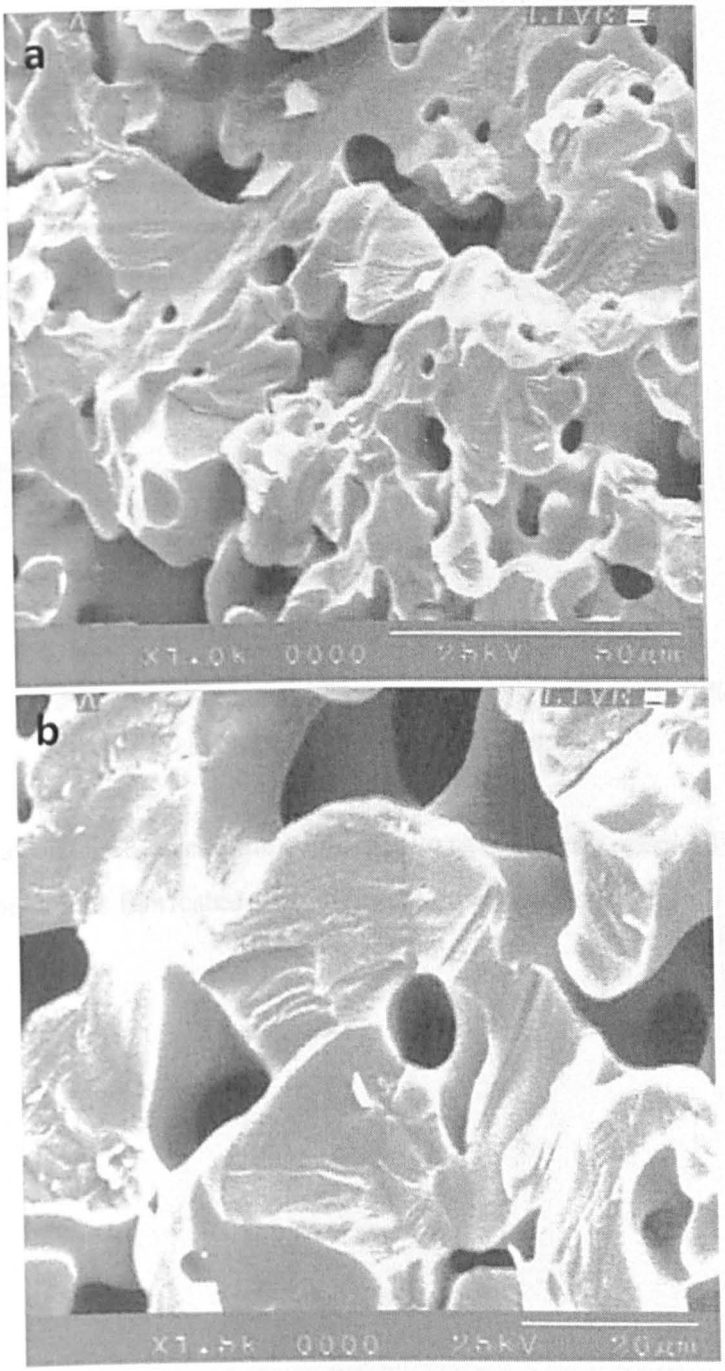

Fig. 3.32 SEM images of a fracture surface of a Ti matrix syntactic foam specimen showing the fractured Ti matrix. The specimen had a Ti volume percentage of 50% and was fabricated with a compaction pressure of 45 MPa.

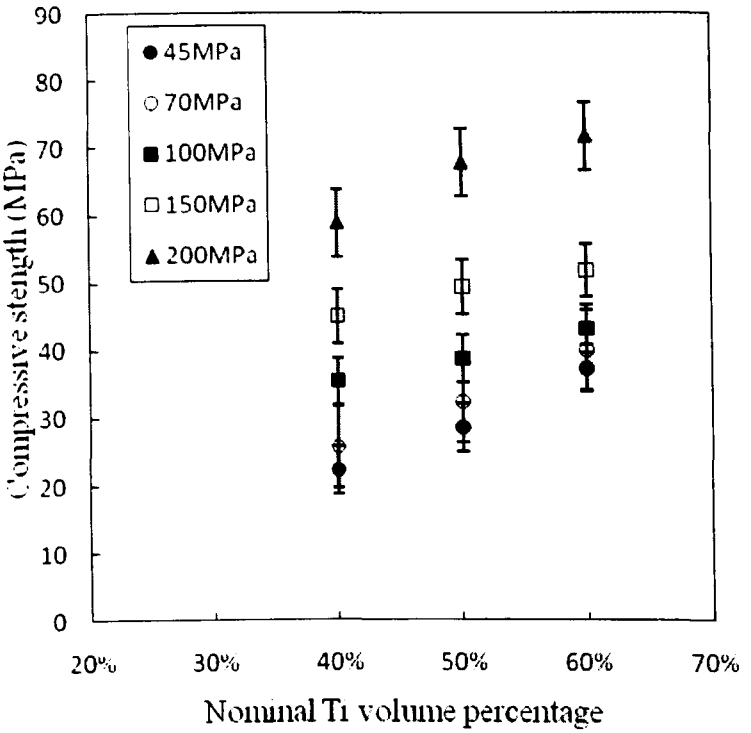

Fig. 3.33 The relationship between the compressive strength and nominal Ti volume percentage for specimens fabricated with different compaction pressures.

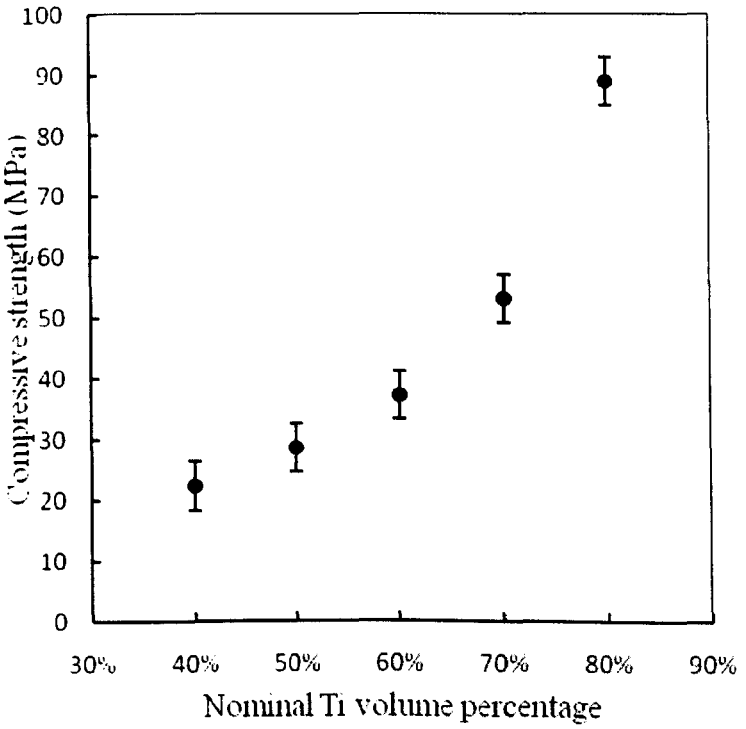

Fig. 3.34 The relationship between compressive strength and nominal Ti volume percentage for specimens fabricated with a compaction pressure of 45 MPa.

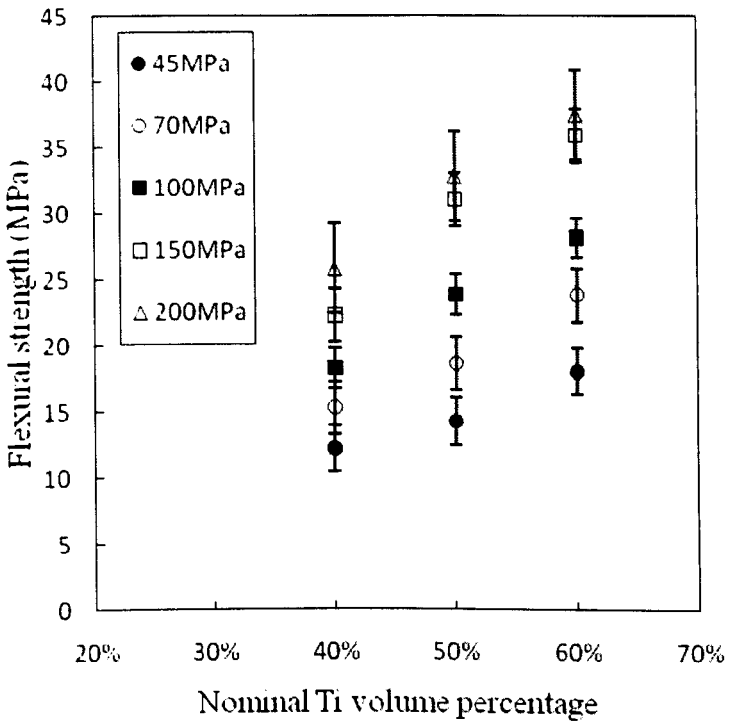

Fig. 3.35 The relationship between flexural strength and nominal Ti volume percentage for specimens fabricated with different compaction pressures.

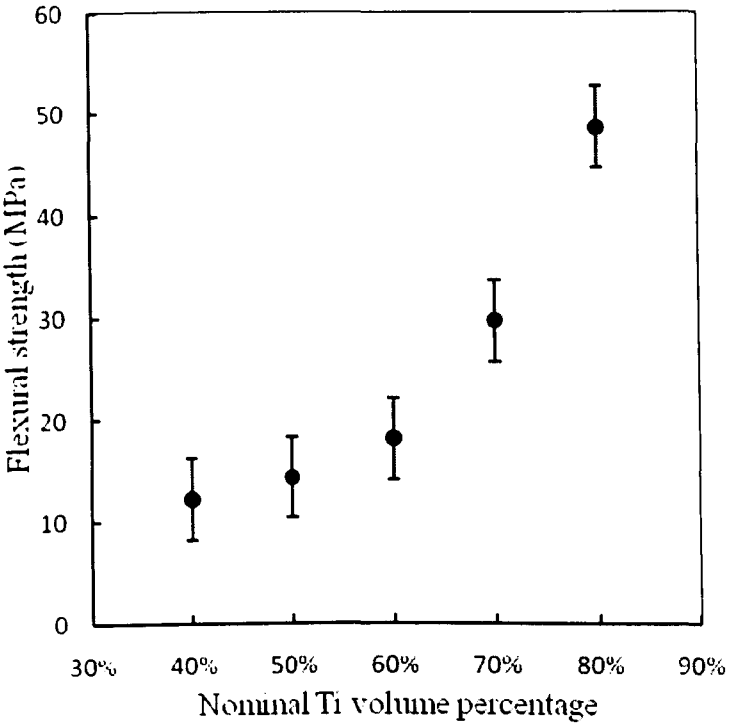

Fig. 3.36 The relationship between flexural strenght and nomial Ti volume percentage for specimens fabricated with a compaction pressure of 45 MPa.

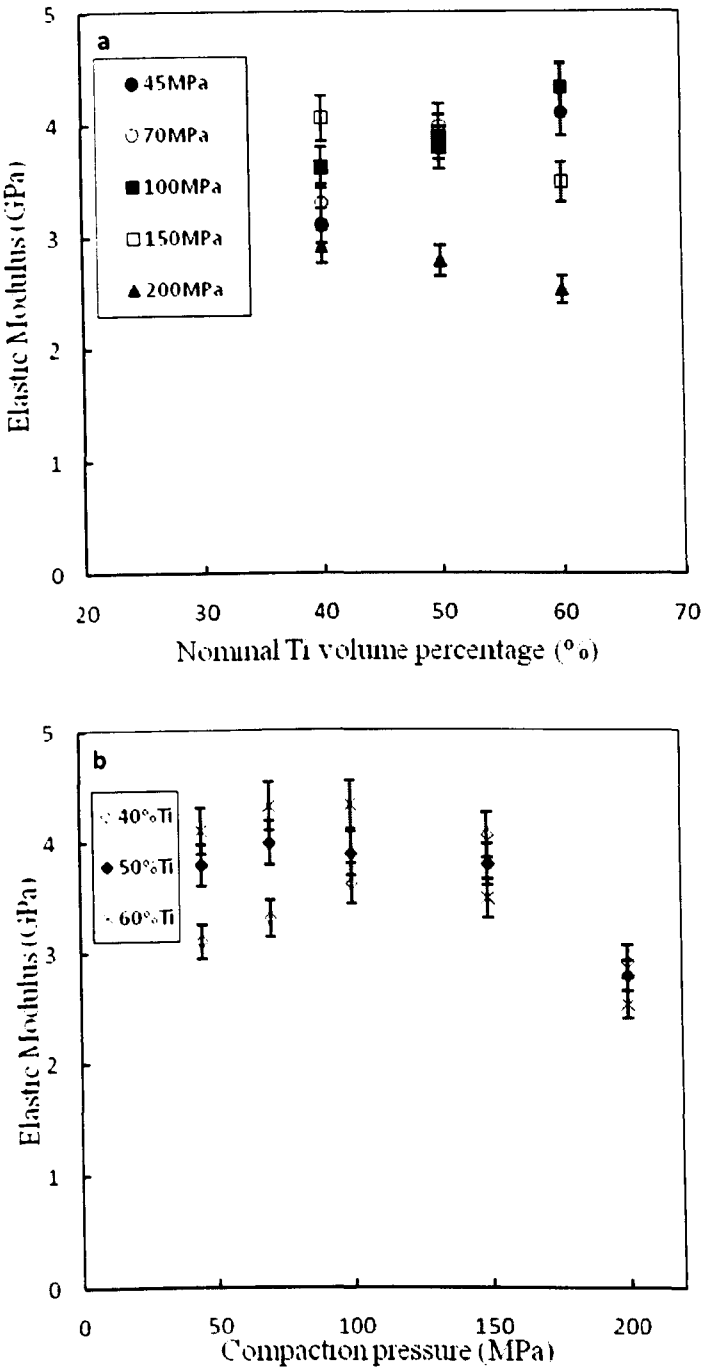

Fig. 3.37 The relationships between elastic modulus and (a) Ti volume percentage, and (b) compaction pressure for Ti matrix syntactic foam specimens with Ti volume percentages of 40%, 50% and 60%, fabricated with compaction pressures of 45, 70, 100, 150 and 200 MPa.

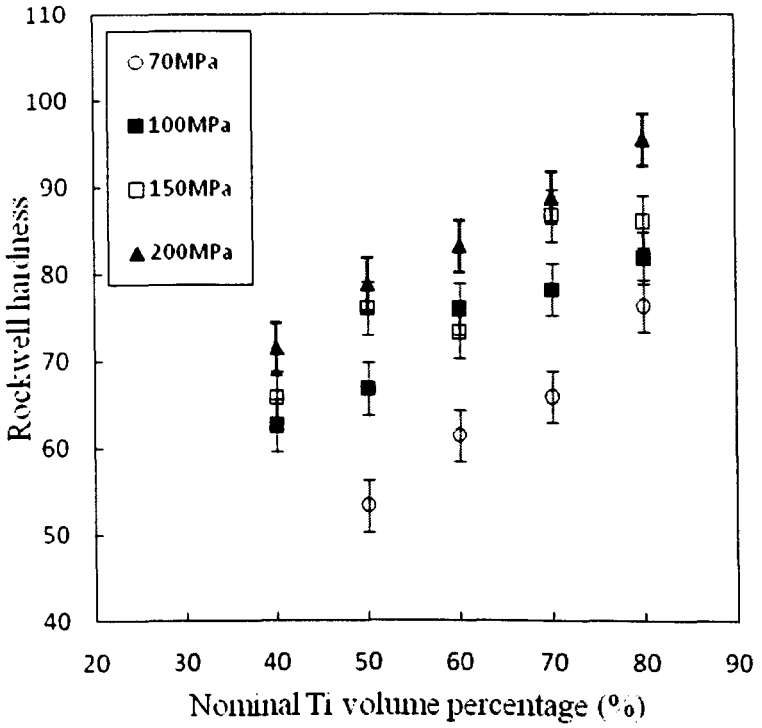

Fig. 3.38 The relationship between the Rockwell hardness and the Ti volume percentage for Ti matrix syntactic foam specimens fabricated with compaction pressures of 70, 100, 150 and 200 MPa.

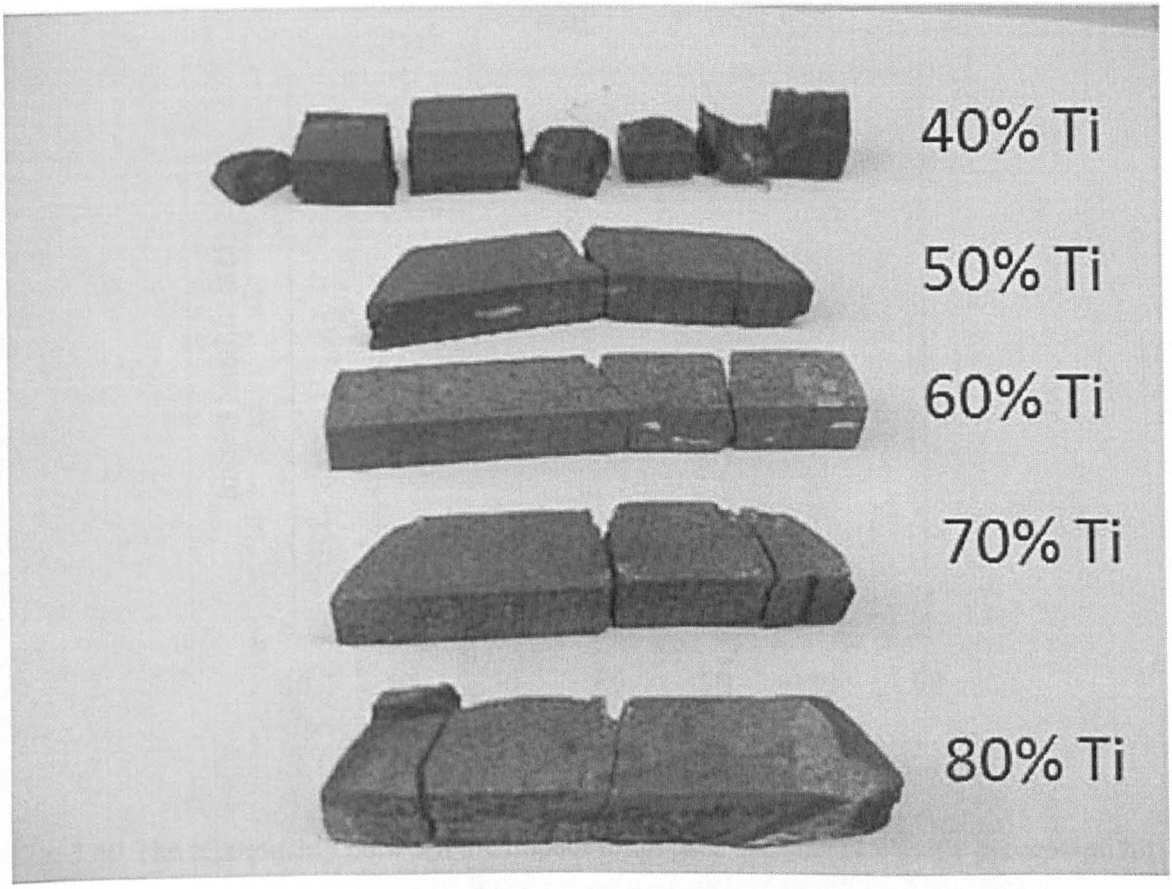

Fig. 3.39 Ti matrix syntactic foam specimens after charpy test. The specimens had Ti volume percentages of 40%, 50%, 60%, 70% and 80%, and were fabricated with a compaction pressure of 45 MPa.

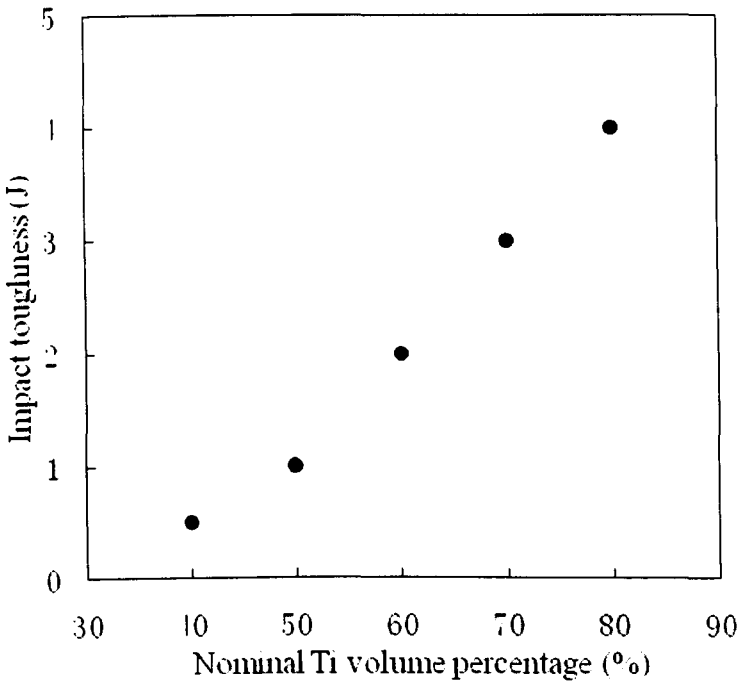

Fig. 3.40 The relationship between the impact toughness and the Ti volume percentage for Ti matrix syntactic foam specimens fabricated with a compaction pressure of 45 MPa.

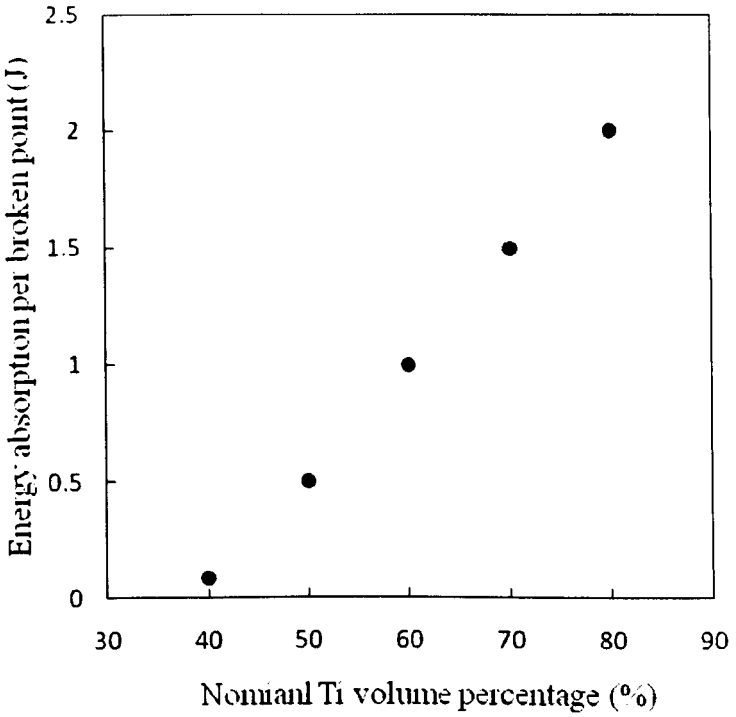

Fig. 3.41 The relationship between the absorbed energy of each broken interface and Ti volume percentage, for specimens fabricated with a compaction pressure of 45 MPa.

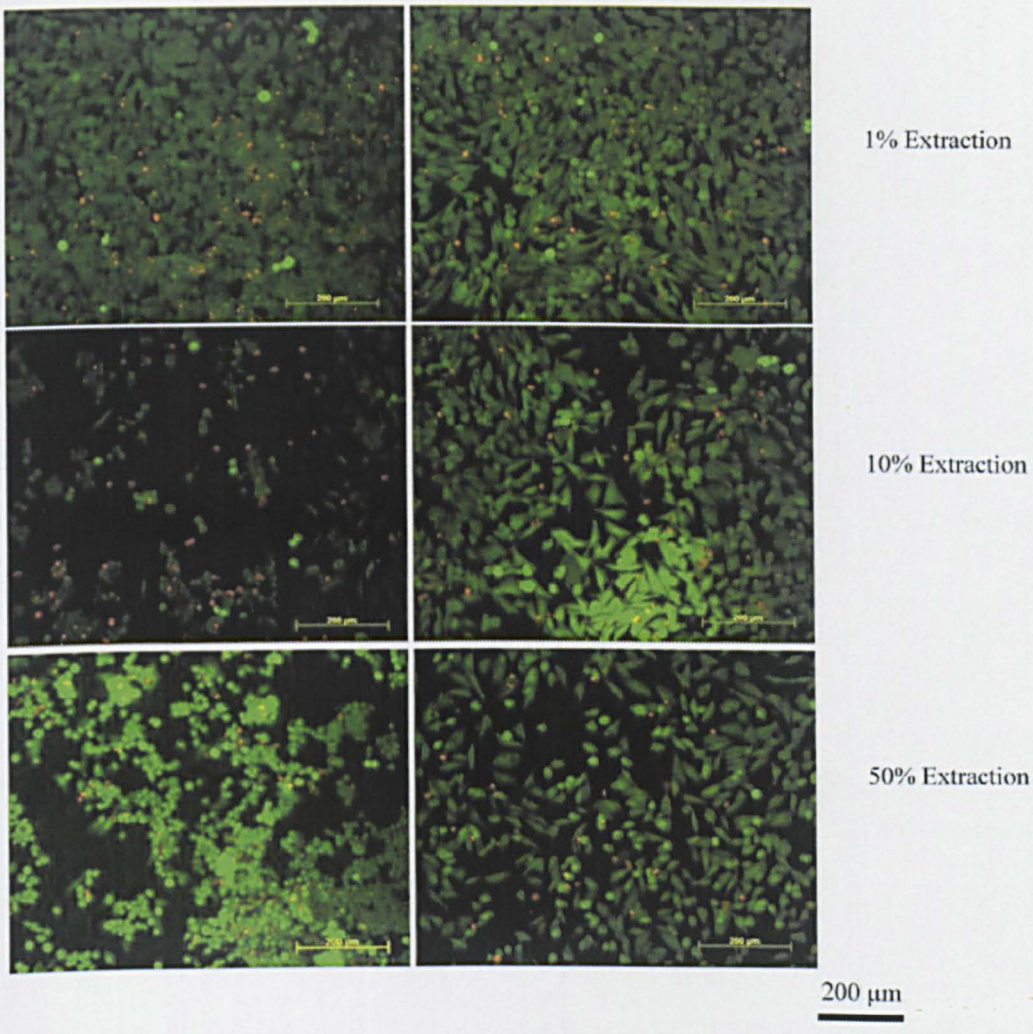

Fig. 3.42 The cytotoxicity test of Ti matrix syntactic foam sample with a Ti volume percentage of 40%, fabricated with a compaction pressure of 70 MPa. The micrographs in the left column were show the cells cultured in the standard culture medium, and those in the right column show the cells cultured in the mixture of extraction from Ti matrix syntactic foam and standard culture medium with different volume ratios.

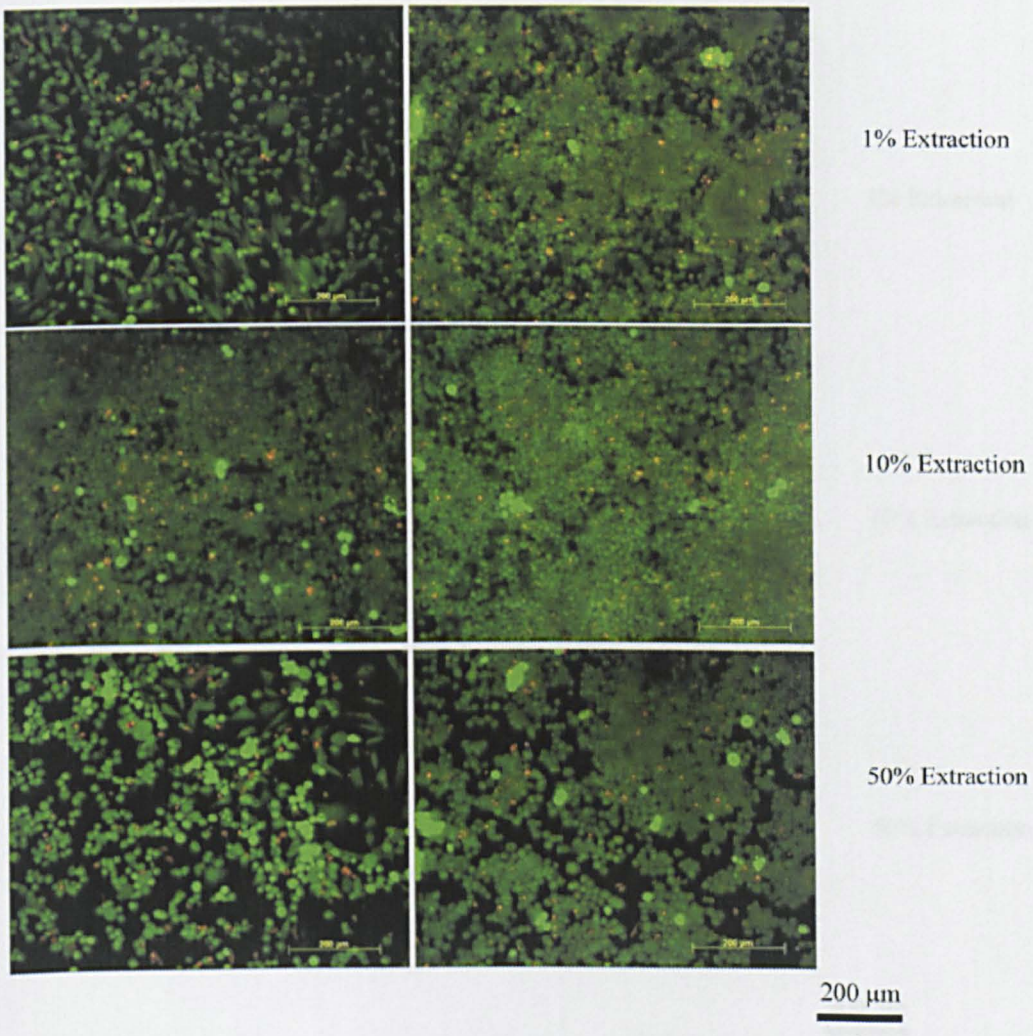

Fig. 3.43 The cytotoxicity of Ti matrix syntactic foam sample with a Ti volume percentage of 60%, fabricated with a compaction pressure of 70 MPa. The micrographs in the left column were show the cells cultured in the standard culture medium, and those in the right column show the cells cultured in the mixture of extraction from Ti matrix syntactic foam and standard culture medium with different volume ratios.

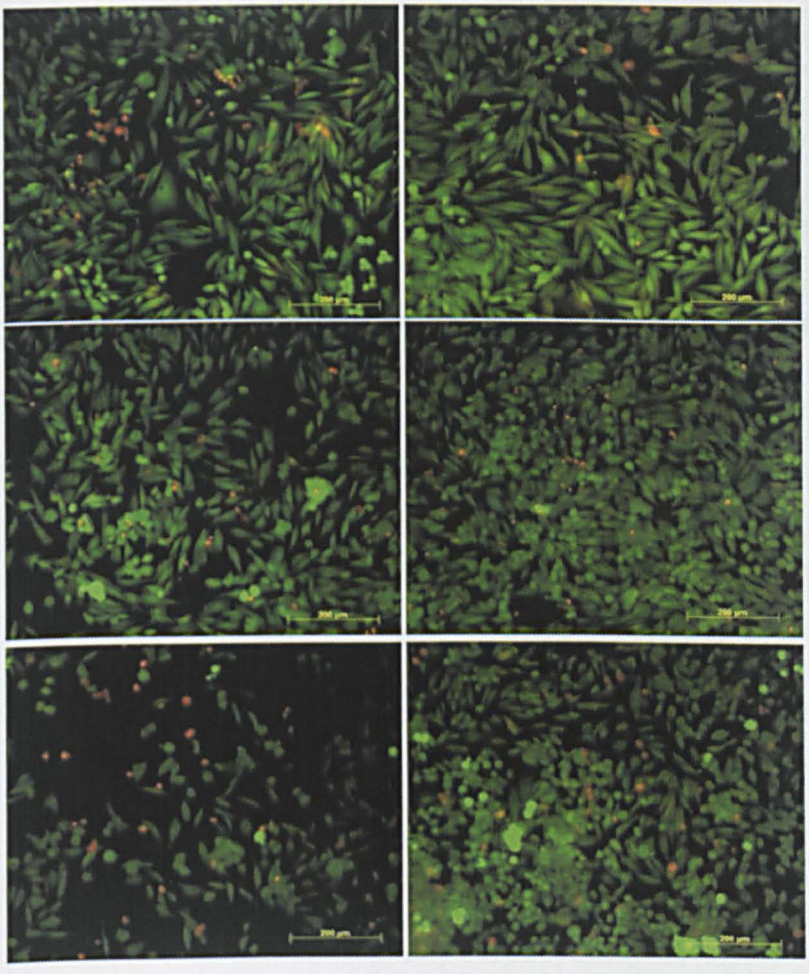

Fig. 3.44 The cytotoxicity of Ti matrix syntactic foam sample with a Ti volume percentage of 80%, fabricated with a compaction pressure of 70 MPa. The micrographs in the left column were show the cells cultured in the standard culture medium, and those in the right column show the cells cultured in the mixture of extraction from Ti matrix syntactic foam and standard culture medium with different volume ratios.

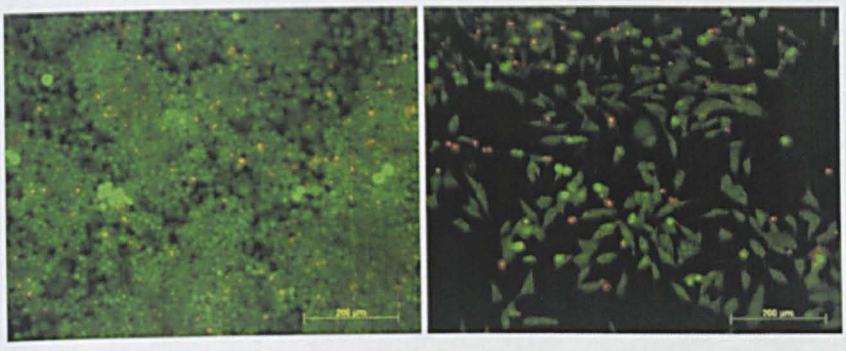

Fig. 3.45 The cytotoxicity test of standard culture medium. The micrographs in the left column were show the cells cultured in the standard culture medium, and those in the right column show the cells cultured in the mixture of extraction from Ti matrix syntactic foam and standard culture medium with different volume ratios.

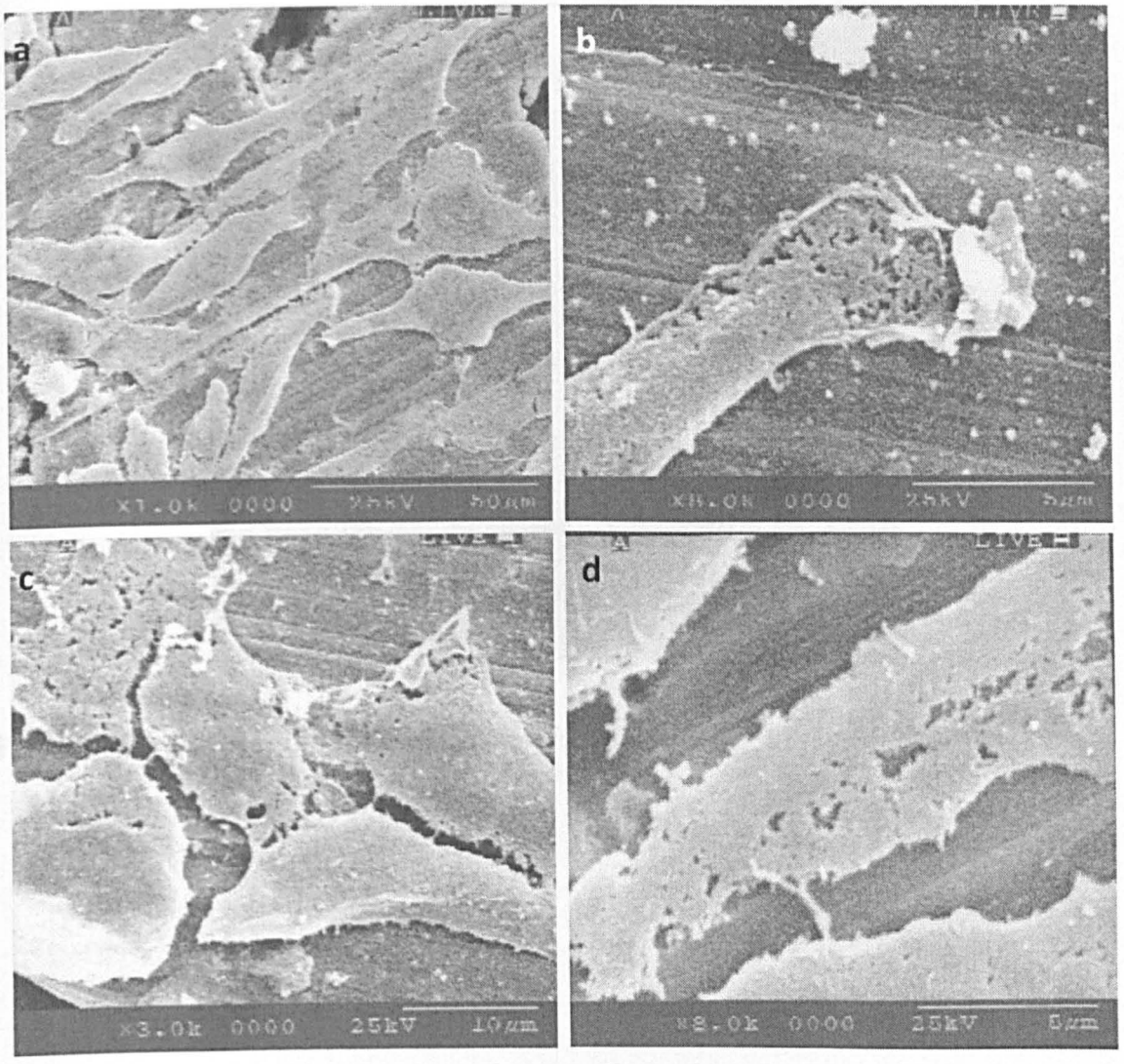

Fig. 3.46 The performance of the cells on the flat surface of Ti matrix syntactic foam sample.

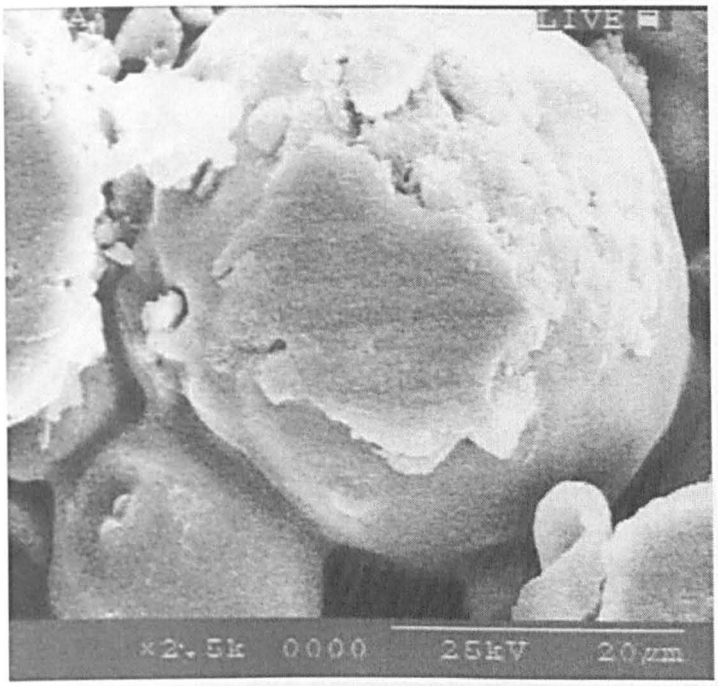

Fig. 3.47 The adhesion of SaOS-2 cells on sphere Ti particle.

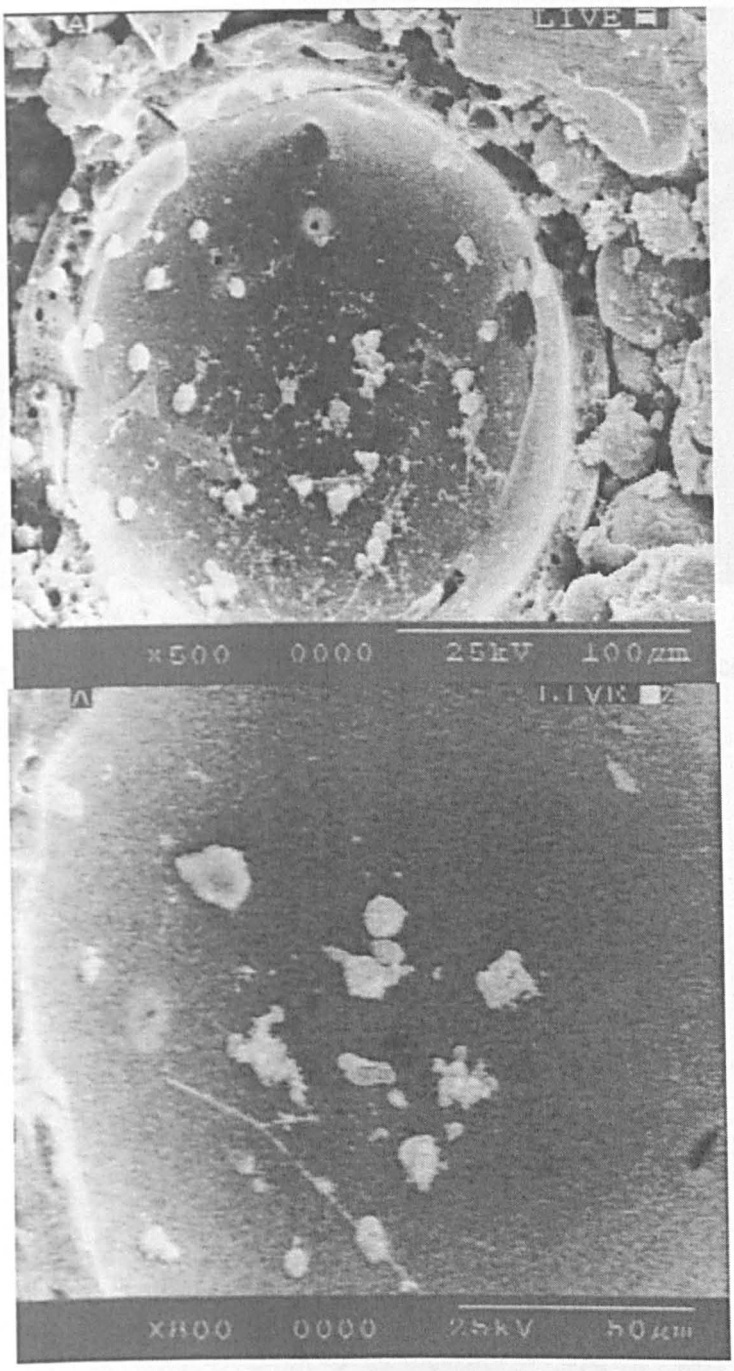

Fig. 3.48 The performance of cells on the surface of CM particle in the Ti matrix syntactic foam specimen.

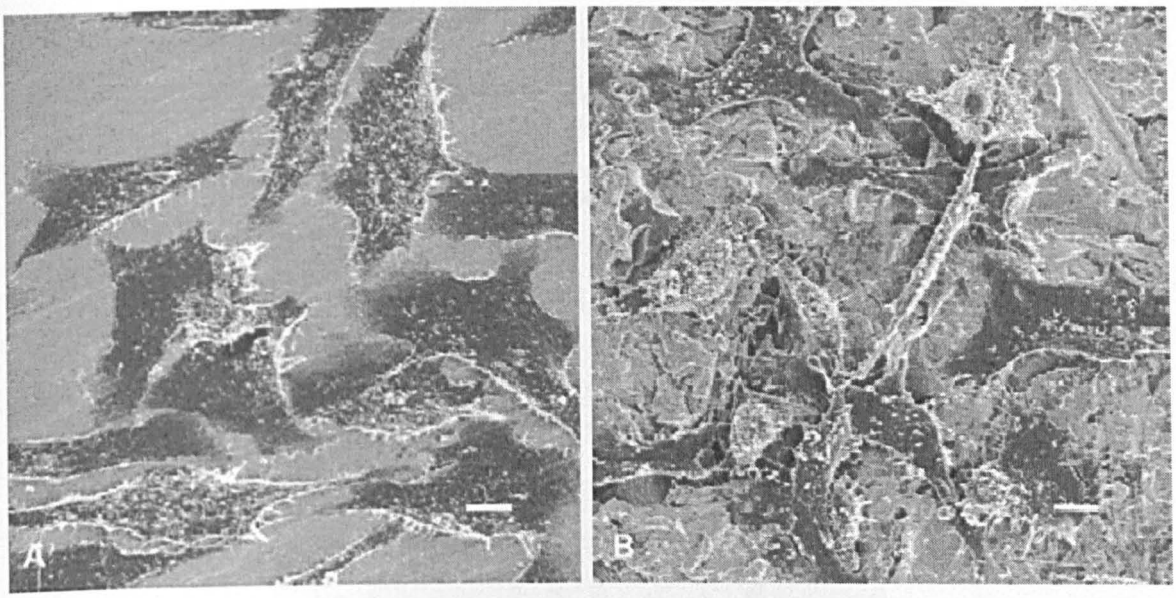

Fig. 3.49 The performance of SaOS-2 cells on (A) non-sandblast Ti surface and (B) rough sandblast Ti surface (Degasne *et al.* 1999).

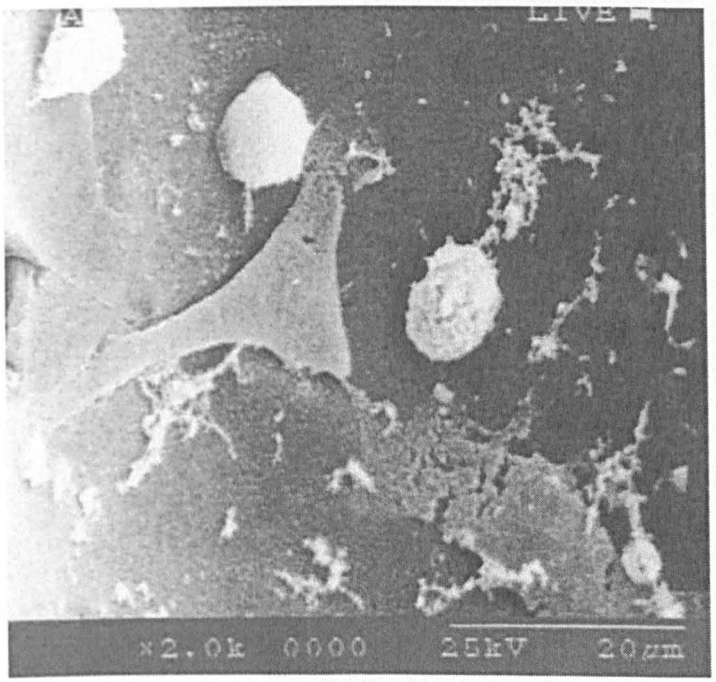

Fig. 3.50 The spreading cells on the surface of CMs.

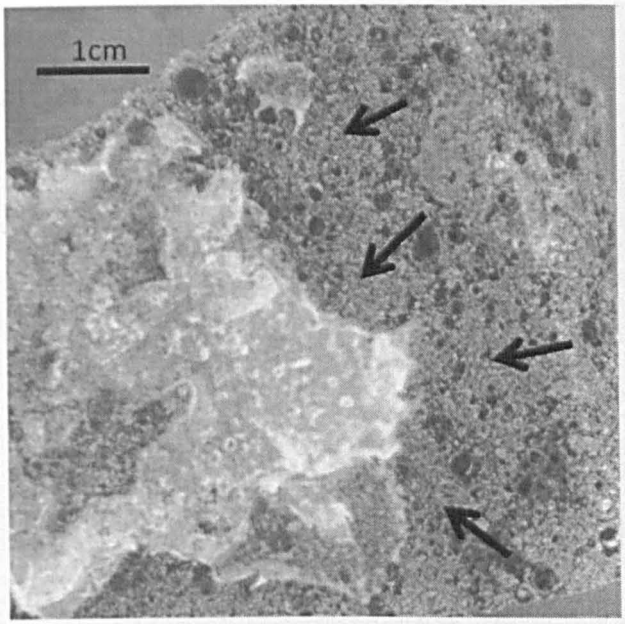

Fig. 3.51 The Von Kossa stain on the Ti matrix syntactic foam sample with a Ti volume percentage of 60%, fabricated with a compaction pressure of 45 MPa.

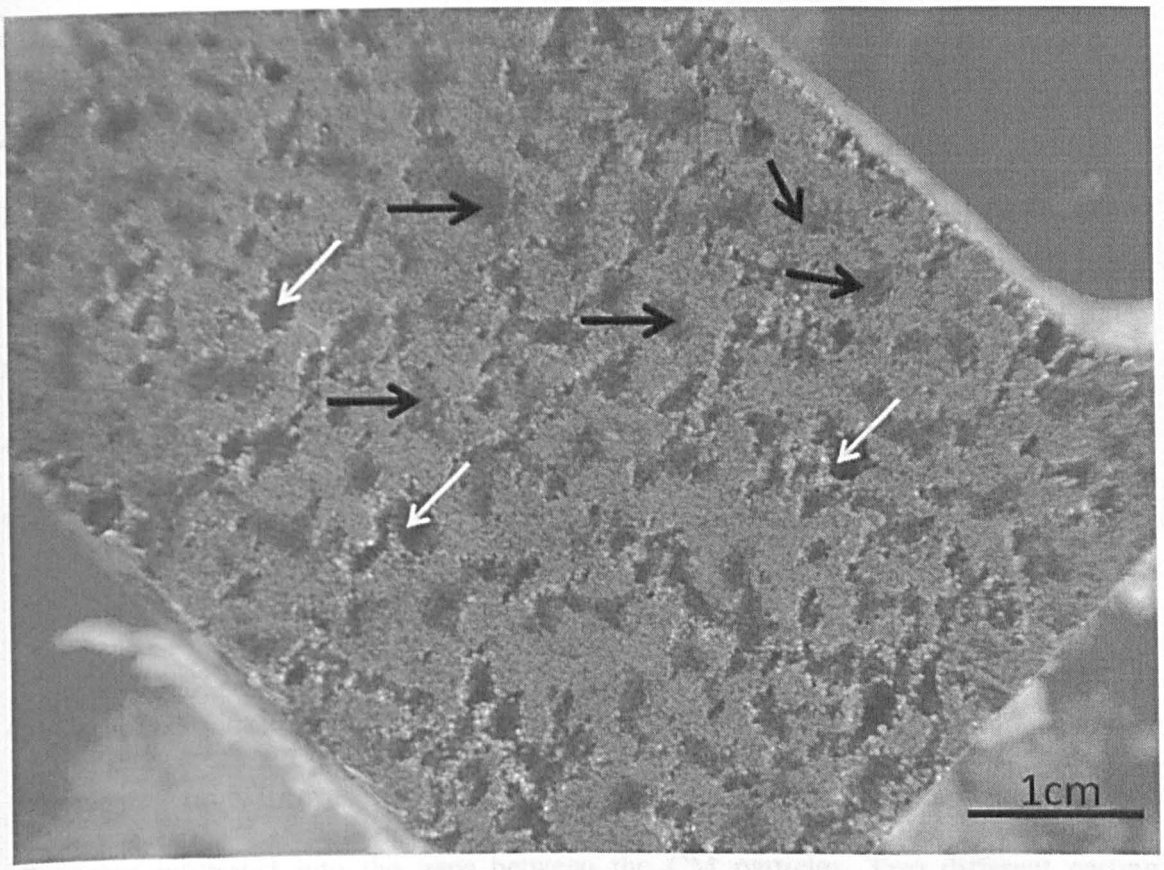

Fig. 3.52 The Von Kossa stain on the Ti matrix syntactic foam sample with a Ti volume percentage of 60%, fabricated with a compaction pressure of 100 MPa.

Chapter 4 Co-Cr-Mo matrix syntactic foam

4.1 Introduction

In this chapter, a feasibility study on the fabrication of Co-Cr-Mo matrix syntactic foams using casting processes is conducted. Co-Cr-Mo is one of the popular biomaterials used nowadays. Its good biocompatibility and corrosion resistance are well documented (Park & Lakes 2007; Williams 1976; Williams 1973b). It has been widely applied as an orthopedic implant material (Katti 2004).

Co-Cr-Mo alloy has a lower melting temperature than Ti. In this study, Co-Cr-Mo alloy matrix syntactic foam was fabricated with casting processes, i.e., the molten Co-Cr-Mo alloy was infiltrated into the gaps between the CM particles. Two different casting processes were used in this study, pressure casting and centrifugal casting. The distribution of the CM particles in the sample was analyzed using an optical microscope.

4.2 Manufacturing Procedure

4.2.1 Raw materials

The raw materials used for fabricating the Co-Cr-Mo alloy matrix syntactic foam were Heraenium CE, a Co-Cr-Mo alloy designed for fabricating removable dentures, and ceramic microspheres (CMs), as described in Chapter 3. The Heraenium CE alloy has a composition of 63.5% Co, 27.8% Cr and 6.5% Mo by weight, a density of 8.0 g/cm^3, and a melting temperature range between 1330-1380 °C.

4.2.2 Preparation of sample pattern and casting mould

The Co-Cr-Mo matrix syntactic foam was manufactured by investment casting where liquid Co-Cr-Mo alloy was poured into a mould containing CMs. This process consisted of two steps, mould preparation and casting.

Fig. 4.1 shows how the pattern and mould was built. The sample pattern was made by blending molten casting wax (S-U-Flexible wax, SCHULER-DENTAL, Germany) with 4g CM powder. At first, the wax was placed in a steel tube container with a diameter of approximate 1cm, and then was placed in a furnace and heated to 200°C. After the wax was taken out from the furnace, 4g CM powder particles were added to the tube container. Because the wax has a high viscosity during the cooling process to room temperature, it is easy to blend the wax and force the CM powder to embed in the wax during this stage. A steel stick was used for blending to achieve a uniform distribution of CM powder. After the wax completely solidified, the pattern was removed from the tube container. The two ends of the cylinder were attached with two plastic cylinders with a diameter of 3.5 mm and a length of 30 mm. The assembly was placed in the investment mould builder. Gypsum was used to fill the builder. After the gypsum was consolidated, the plastic cylinders were removed. Feeder sprues with a reservoir were added, resulting in a complete investment casting mould.

4.2.3 Casting

A Co-Cr-Mo alloy ingot was preheated to above its melting temperature in a vacuum induction casting machine with a pressure of 250 mbar. The weight of this liquid Co-Cr-Mo alloy was measured. The liquid Co-Cr-Mo alloy was injected into the investment mould either by high pressure inert gas, as shown in Fig. 4.2, or by centrifugal force, as shown in Fig. 4.3. To inject liquid Co-Cr-Mo alloy into the mould by inert gas, the investment mould was kept in the induction casting machine after the liquid Co-Cr-Mo alloy floated to the feeder reservoir. An inert gas with a pressure of 5 bar was then applied to the liquid Co-Cr-Mo alloy to force it to infiltrate into the investment mould. To inject liquid Co-Cr-Mo alloy into mould by centrifugal force, the investment mould was taken out from the induction casting machine with a sealed device to prevent the liquid Co-Cr-Mo alloy in the feeder sprues from reacting with oxygen. It was set in a centrifugal casting machine with a rotating speed of approaching 2000 rpm and a lever length of 25 cm.

During the infiltration of the liquid Co-Cr-Mo alloy into the investment mould, the wax in the pattern was burned and replaced by liquid Co-Cr-Mo alloy. The specimen was cooled to room temperature either in the induction casting machine or in the centrifugal casting machine. The specimen was taken out from the mould afterwards, and sandblasted using 250μm Al_2O_3 Special Abrasive at a pressure of 4 bar. The sandblast can ensure optimum edge definition and good surface structure of the casting. A Co-Cr-Mo matrix syntactic foam was thus obtained.

4.2.4 Structural analysis

The weight of the Co-Cr-Mo sample was measured immediately after manufacturing by a digital balance. The fraction of CMs lost during casting, W_L, was calculated using:

$$W_L = \frac{(W_c + W_I) - W_s}{W_c} \tag{4.1}$$

where W_c is the weight of the CMs in the sample pattern, W_I is the weight of the injected Co-Cr-Mo alloy in the sample and W_s is the weight of the sample after casting.

A high speed blade was used to cut the specimen to obtain a cross-sectioned surface of a Co-Cr-Mo alloy matrix syntactic foam sample. The cross-sectional surface was polished using 1200 grit paper. A small piece containing homogeneously embedded CMs in the surface was cut from the sample and polished to 1μm. An optical microscope was used to observe the structural details in the cross-sectional surface. The distribution of CMs in the cross-sectional surface was used to evaluate the distribution of CMs in the sample.

4.3 Results and Discussion

4.3.1 Distribution of CMs

Fig. 4.4 shows the exterior of a Co-Cr-Mo matrix syntactic foam sample fabricated by pressure casting. Fig. 4.4(a) is taken from the side with sprues, and Fig. 4.4(b) is taken from the opposite side. The distribution of the CMs is not uniform. The CMs mainly

concentrate at the place in connection with the two sprues, as shown in Fig. 4.4(a). In the opposite side, there are very few CMs distributed.

Fig. 4.5 shows the cross-sectional surfaces of a Co-Cr-Mo alloy matrix syntactic foam sample fabricated by the pressure casting method. The CMs are mainly distributed at the edge, especially the position in connection with the sprues, as well as the outside surface. In the centre of the horizontal cross-sectional surface, as shown in Fig. 4.5(a), there are a few CMs embedded in the Co-Cr-Mo alloy matrix. However, in general, the distribution of the CMs is very poor. In the vertical cross-sectional surface, the distribution of the CMs is still very poor. Only a thin layer has the CMs, as shown in Figs. 4.5(b) and (c).

Fig. 4.6 shows the exterior of the Co-Cr-Mo alloy matrix syntactic foam sample fabricated by the centrifugal casting method. Fig. 4.6(a) is taken from the sprues side, and Fig. 4.6(b) is taken from the opposite side. The CMs mainly concentrate at the place in connection with the sprues. On the opposite side, there are nearly no CMs.

Fig. 4.7 shows the cross-sectional surfaces of the Co-Cr-Mo alloy matrix syntactic foam sample fabricated by the centrifugal casting method. The distribution of CMs is very poor and no CMs are found to be embedded in the cross-sectional surface. All the CMs are situated at the place in connection with the sprues. No Co-Cr-Mo alloy infiltrated into the gaps between the CMs.

Fig. 4.8 shows an optical image of the cross-sectional surface of the Co-Cr-Mo alloy matrix syntactic foam sample fabricated by the pressure casting method at a higher magnification. The CMs are in a dark colour due to the rough surface, and the Co-Cr-Mo alloy is in a bright colour due to the flat surface. The Co-Cr-Mo alloy infiltrated between the CMs and filled some of the internal voids of the CMs. However, the CMs were not in a spherical shape, indicating that they were deformed or squeezed. This is because during casting, the high temperature liquid Co-Cr-Mo alloy softened the non-crystalline CMs. The thermal properties of the CMs used in this study are not available. However, the temperature of the molten Co-Cr-Mo alloy is likely to be higher than the softening point of the CMs. No embedded CMs were found in the sample fabricated by the centrifugal casting method.

4.3.2 Casting defects

The major casting defect of the two manufacturing methods is gas porosity. The gas porosity is formed during cooling of the liquid metal. Because the Co-Cr-Mo alloy ingot was melted in a vacuum furnace, the amount of gas dissolved in the molten Co-Cr-Mo alloy should be very small. However, the pattern contained a large amount of wax. After the molten Co-Cr-Mo alloy was poured into the chamber, the wax was melted and could produce a large amount of gas, which can form gas porosity into the sample. Examples of large air voids are shown in Figs. 4.5(b) and (c).

The sample fabricated by pressure casting has more gas porosity than the sample fabricated by centrifugal casting. This is possibly because of the different pressure application times. In the pressure casting process, the pressure was removed after the molten alloy was pressed into the chamber. In the centrifugal casting process, the pressure was applied during the whole centrifugal process.

Misrun casting defects are observed in the samples fabricated by the centrifugal casting method, as shown in Fig. 4.6. The defects are mainly located at the positions in connection with the sprues. They are caused by the agglomeration of CMs. The Co-Cr-Mo alloy matrix is heavier than the CMs. As a consequence, the Co-Cr-Mo alloy is forced to move away from the centrifugal centre by the centrifugal force more than the CMs. The CMs had a segregated distribution, resulting in misrun casting defects.

4.3.3 Loss of CMs

Some CMs were lost during the pouring of the molten alloy. Estimation using equation 4.2 shows that there are approximately 70% of the CMs were lost during pressure casting and nearly 50% of the CMs were lost during centrifugal casting. The pressure casting method caused more lost CMs, possibly because it has a more rapid infiltration of the molten alloy and a higher pressure than the centrifugal pressure applied to the molten alloy. The high pressure and fast infiltration can expel more CMs away.

4.3.4 Problems and suggested solutions

The problems of the Co-Cr-Mo alloy matrix syntactic foams fabricated by the two methods are listed in Table 4.1.

Table 4.1 Problems of samples fabricated by pressure casting and centrifugal casting.

	Pressure casting	Centrifugal casting
Casting defects	Gas porosity	Gas porosity and misrun
Distribution of CMs	Embedded in the alloy matrix	Agglomeration, no CMs are embedded in alloy matrix
Condition of CMs	Softened and deformed	
Loss of CMs during casting	~70%	~50%

The casting defects, gas porosity and casting misrun, can be reduced using a higher vacuum condition. After the molten Co-Cr-Mo alloy was poured into the casting chamber, the wax degraded and released gas. Using a higher vacuum can remove the gas produced during the degradation of wax from the casting chamber.

A possible way to prevent the non-uniform distribution of CMs is to fill the casting chamber with CMs completely. The liquid alloy can be infiltrated into the gaps between the CMs with assisted gas pressure. In this case, the amount of metal matrix equals the volume of the gaps between the CMs, which is determined by the packing and the sizes of

the CMs. Changing the packing density or the sizes of the CM particles can change the volume of the gaps between the CM particles and therefore the volume percentage of the metal matrix. However, this change is very small. For random packing, the volume fraction of the CMs is approximately 63%. For close-packing, the volume fraction of the CMs is approximately 74% (Hartmann *et al.* 1999). Changing the size distribution of the CMs can also change the volume fraction of the CMs in the syntactic foam (Tao *et al.* 2009). By using a mixture of fine and coarse CMs, the volume percentage of the CMs can be changed from 60% to 75% (Tao *et al.* 2009).

The CMs in the samples were damaged because the softening temperature is lower than the melting temperature of the Co-Cr-Mo alloy. This problem can be solved by choosing hollow spheres with a higher softening temperature range. An appropriate choice would be SiO_2 microspheres.

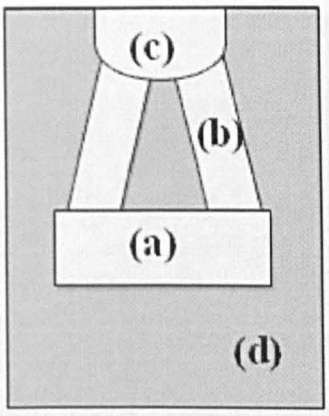

Fig. 4.1 Schematic of the cross-section of the mould builder for manufacturing Co-Cr-Mo matrix syntactic foam using investment casting. (a) Sample pattern, (b) sprues, (c) reverse feeder, and (d) gypsum. The builder was removed after the gypsum solidified.

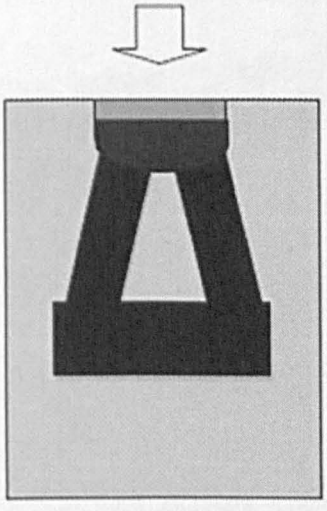

Fig. 4.2 Schematic of the pressure casting process, where liquid Co-Cr-Mo alloy infiltrated into the casting mould under pressure.

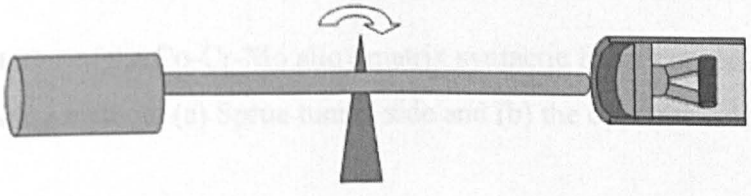

Fig. 4.3 Schematic of the centrifugal casting process.

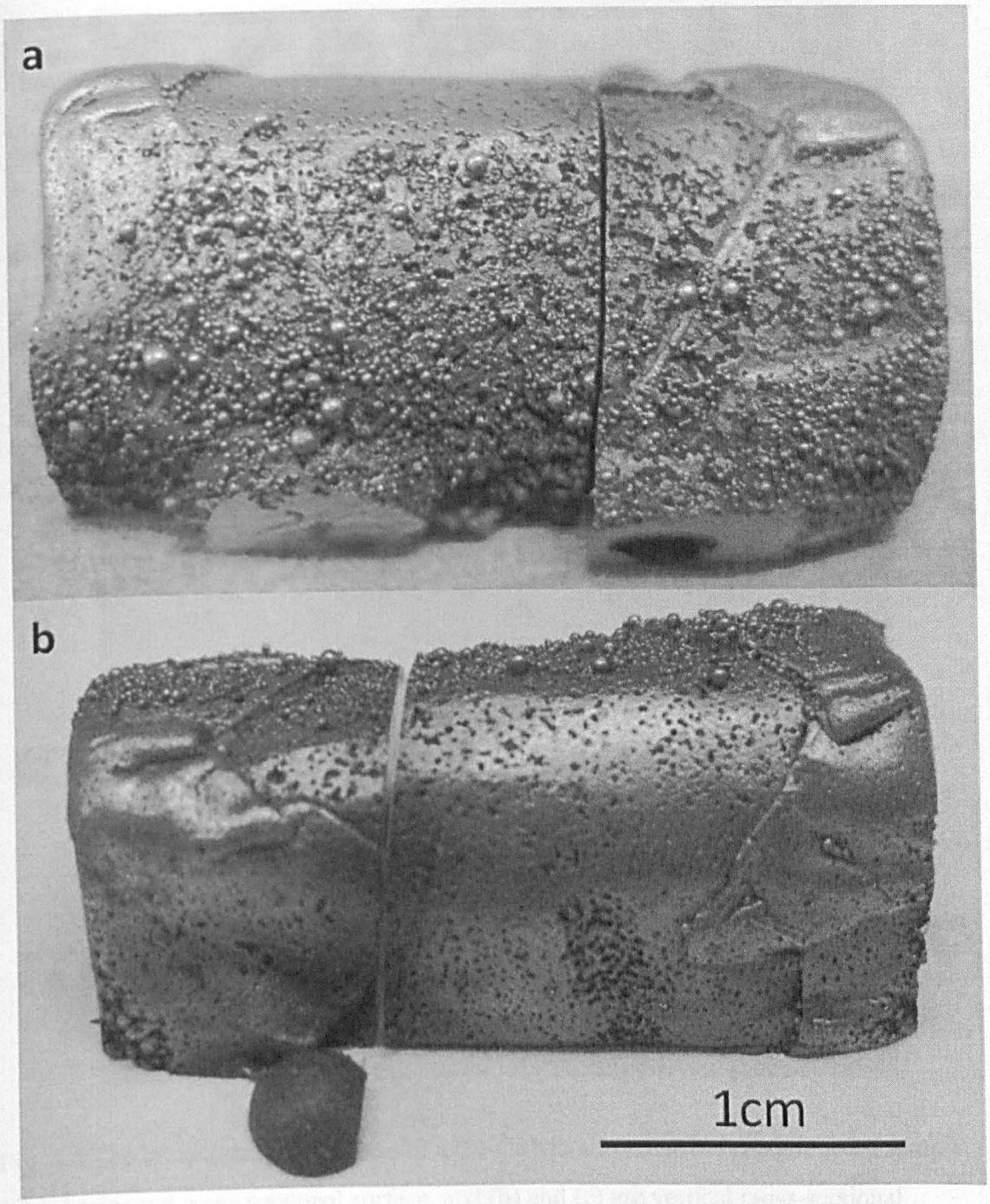

Fig. 4.4 The exterior of the Co-Cr-Mo alloy matrix syntactic foam sample fabricated by the pressure casting method. (a) Sprue tunnel side and (b) the opposite side.

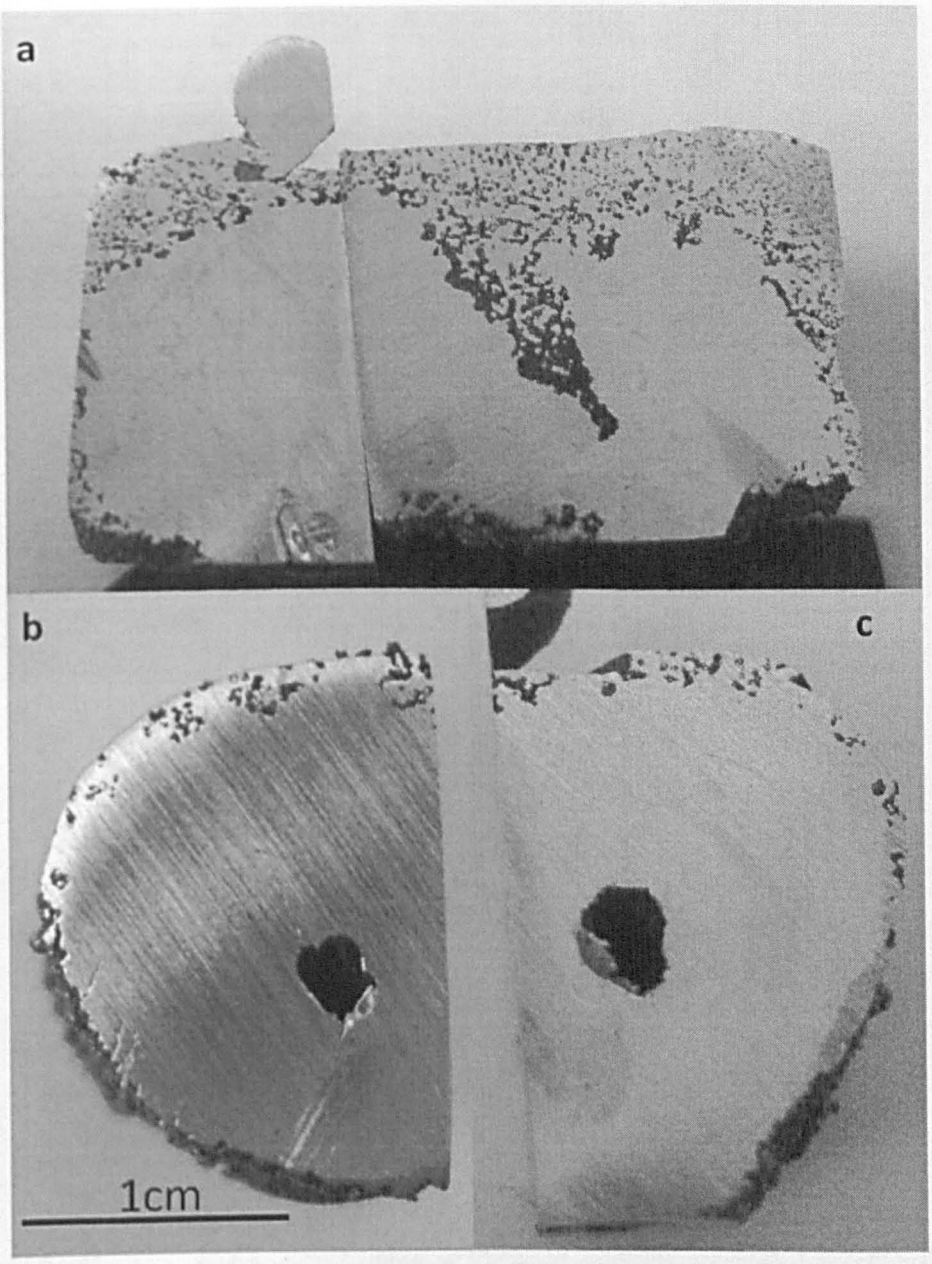

Fig. 4.5 The cross-sectional surfaces of a Co-Cr-Mo alloy matrix syntactic foam sample. (a) is horizontal cross-sectional surface, and (b) and (c) are vertical cross-sectional surfaces.

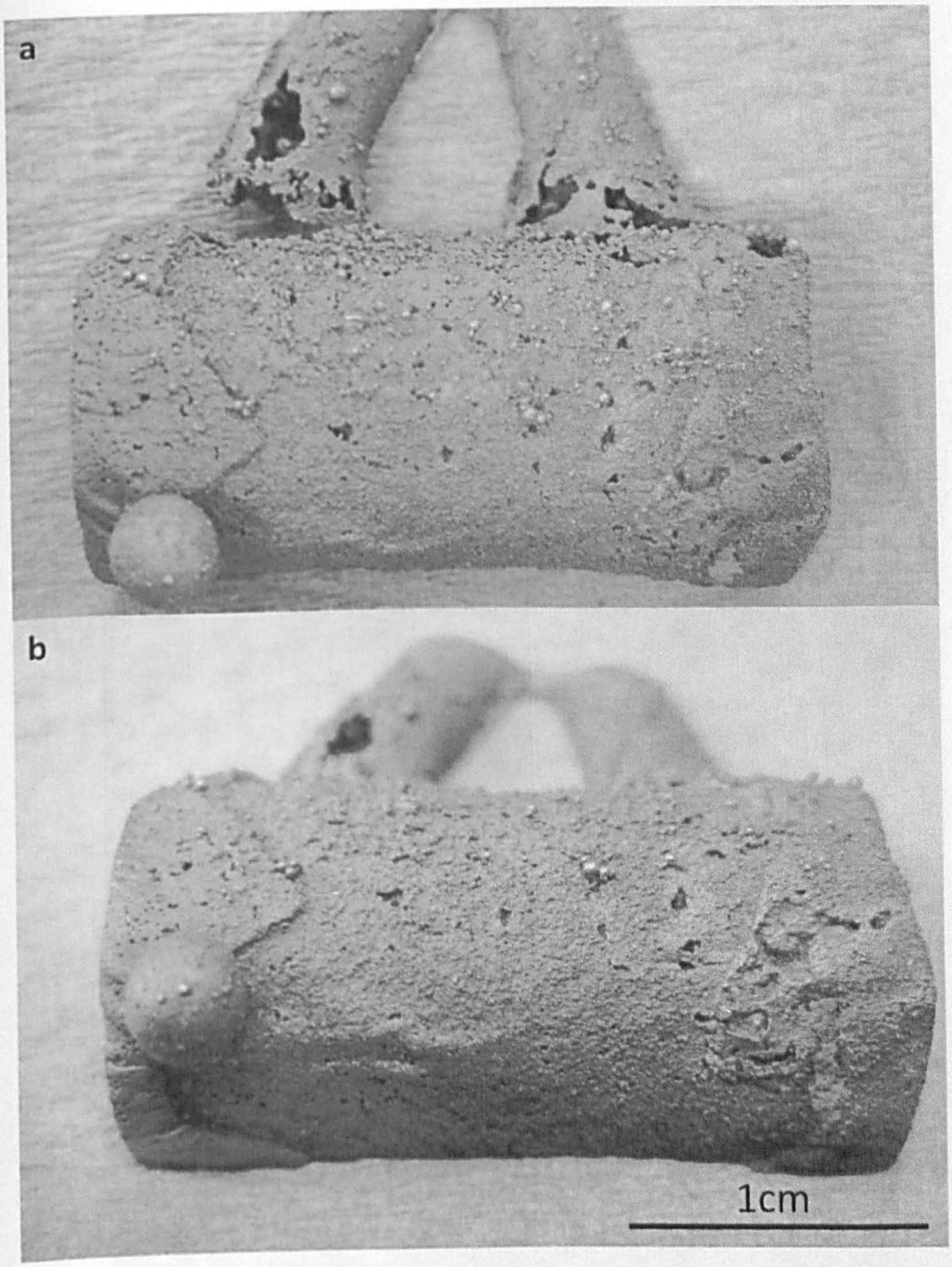

Fig. 4.6 The exterior of a Co-Cr-Mo alloy matrix syntactic foam sample fabricated by the centrifugal casting method. (a) From the sprue tunnel side, and (b) from the opposite side.

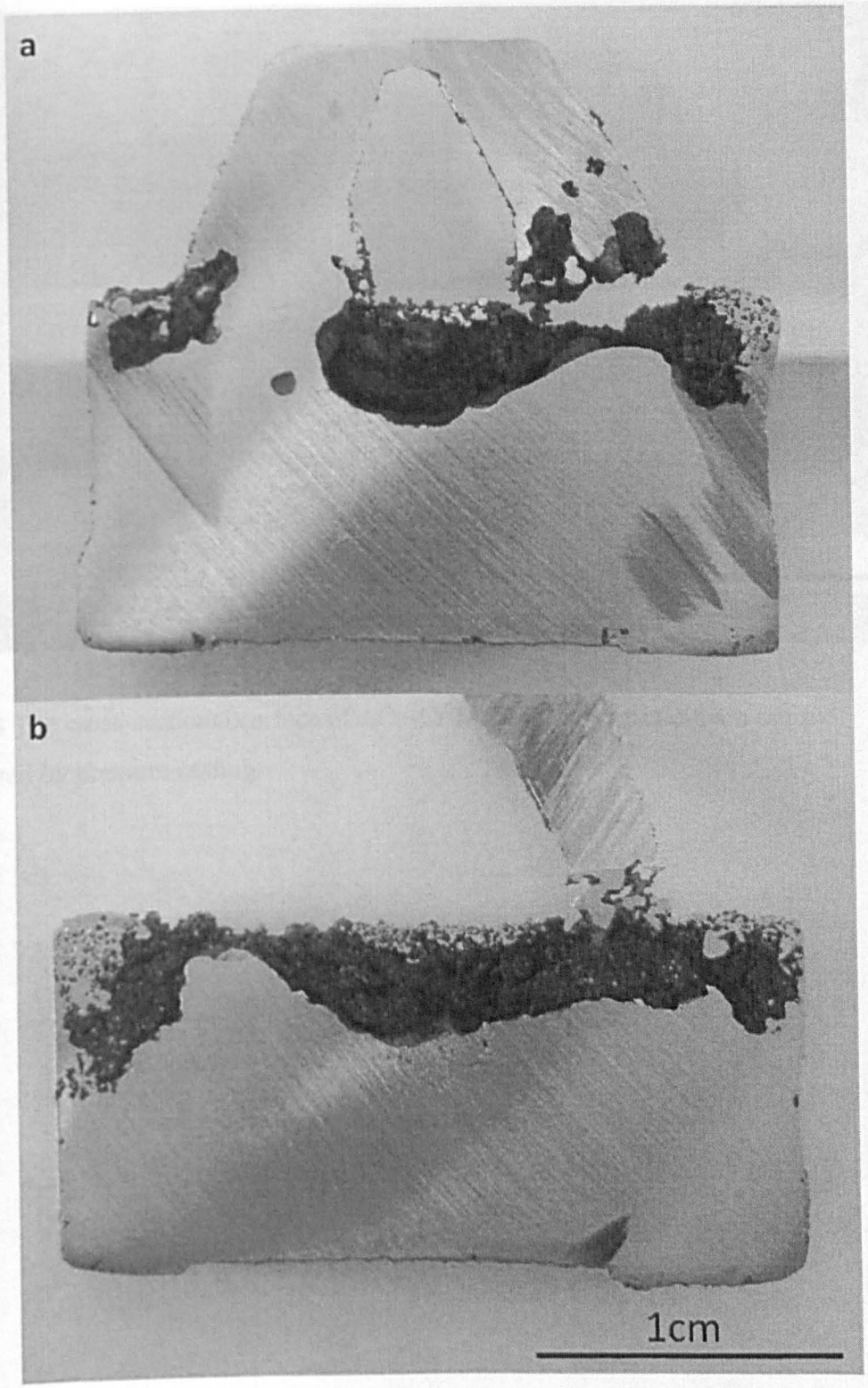

Fig. 4.7 The cross-sectional surfaces of the Co-Cr-Mo alloy matrix syntactic foam sample fabricated by centrifugal casting.

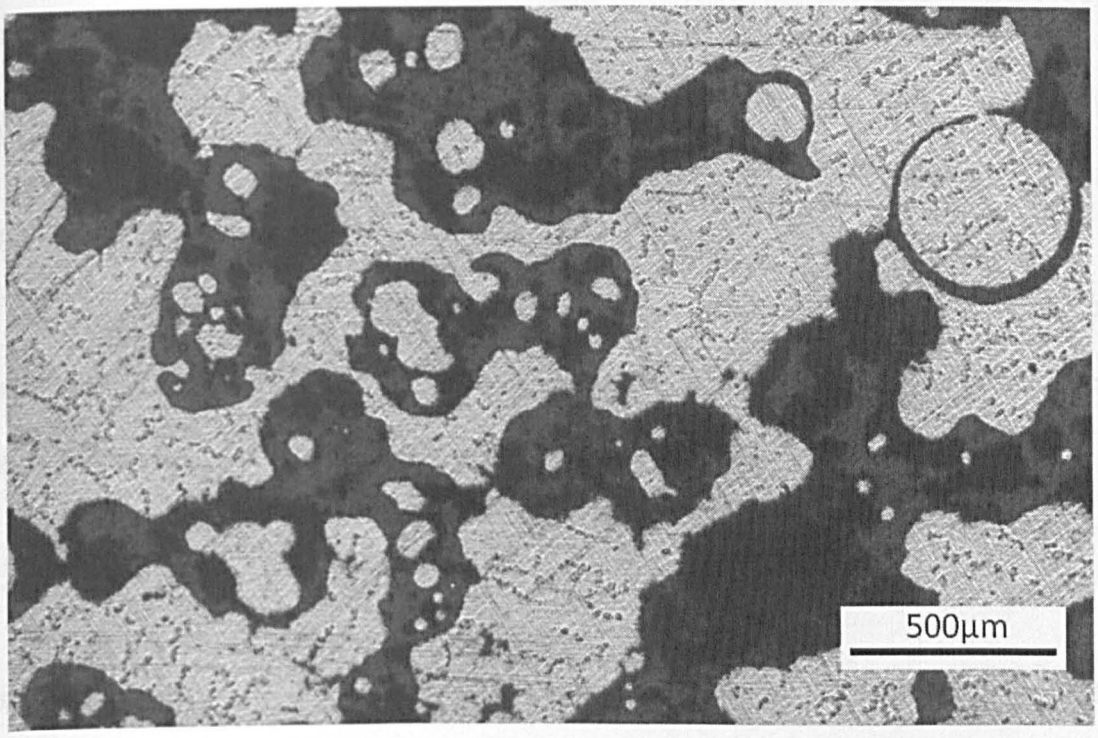

Fig. 4.8 The cross-sectional surface of a Co-Cr-Mo matrix syntactic foam sample fabricated by pressure casting.

Chapter 5 Conclusions and Future Work

5.1 Conclusions

5.1.1 Ti matrix syntactic foam

Ti matrix syntactic foam was manufactured using a powder metallurgy process. The performance of the Ti matrix syntactic foams with a wide range of Ti volume percentages, manufactured at different compaction pressures was evaluated.

The macrostructure of Ti matrix syntactic foam was affected by both the Ti volume percentage and the compaction pressure. The Ti matrix of the specimens with higher Ti volume percentages and manufactured with higher compaction pressures exhibited better integrity.

The densities and porosities of the Ti matrix syntactic foams with Ti volume percentages of 40%, 50%, 60%, 70% and 80%, fabricated with compaction pressures of 45, 70, 100, 150 and 200 MPa were measured. For a given Ti volume percentage, a higher compaction pressure resulted in a higher density and a lower porosity. For a given compaction pressure, increasing the Ti volume percentage slightly increased the density and decreased the porosity.

When the compaction pressure exceeded the compressive strength of the CMs, some CMs were crushed. The water absorption and volume measurement methods produced similar results in the volume percentage of crushed CMs. For a given Ti volume percentage of 40%, the volume percentages of crushed CMs in the Ti matrix syntactic foams fabricated with compaction pressures of 70, 100, 150 and 200 MPa were approximately 70%, 80%, 90% and 95%, respectively. Increasing the Ti volume percentage by every 10% resulted in decreases in the volume percentage of the crushed CMs of approximately 7%.

For a given Ti volume percentage of 40%, the compressive strengths of the Ti matrix syntactic foams fabricated with compaction pressures of 45, 70, 100, 150 and 200 MPa were 22, 25, 35, 45 and 59 MPa, and the flexural strengths were 12, 15, 18, 22 and 26 MPa, respectively. Increasing the Ti volume percentage by every 10% led to increases in both the compressive and flexural strengths by approximately 5 MPa.

The relationships between the elastic modulus and the volume percentage of Ti and compaction pressure were studied. For a given Ti volume percentage, increasing the compaction pressure below 100 MPa resulted in a higher elastic modulus. However, when the compaction pressure was increased to over 100 MPa, further increases of the compaction pressure decreased the elastic modulus. For a given compaction pressure lower than 100 MPa, increasing the Ti volume percentage resulted in an increase in the elastic modulus. For a given compaction pressure higher than 100 MPa, increasing the Ti

volume percentage resulted in a decrease in the elastic modulus. The Rockwell hardness of the Ti matrix syntactic foams increased linearly with the Ti volume percentage and the compaction pressure. The impact toughness of the Ti matrix syntactic foams increased significantly with increasing the Ti volume percentage.

The Ti matrix syntactic foam had excellent biological performance. The toxicity test showed that the Ti matrix syntactic foam had sufficient chemical inertness in the cell culture medium. The direct contact tests exhibited an excellent cell spreading on the Ti matrix syntactic foam surface. The examination of the calcifications of cells on the surface of Ti matrix syntactic foam by von Kossa stain method showed that the calcifications of osteoblasts were affected by the surface condition of the Ti matrix syntactic foam. The specimens fabricated with higher compaction pressures had much smoother surfaces, and thus less calcification of osteoblast.

5.1.2 Co-Cr-Mo alloy matrix syntactic foam

A feasibility study on the manufacturing of Co-Cr-Mo alloy matrix syntactic foam with the pressure and centrifugal casting processes was carried out. A high quality Co-Cr-Mo alloy matrix was obtained by both casting processes. However, several defects were detected in the Co-Cr-Mo alloy matrix syntactic foam, which were non-uniform distribution of CMs, porosity, partial filling of melt in the mould and deformed CMs. The non-uniform distribution of the CMs in the Co-Cr-Mo alloy matrix syntactic foam was the

major defect. The microstructure of the cross-sectional surface of the samples showed that most CMs were located at the parts next to the casting sprues. The samples fabricated by pressure casting had a better Co-Cr-Mo/CMs interface than those fabricated by centrifugal casting, because the pressure applied to the molten Co-Cr-Mo alloy in the pressure casting was higher than the centrifugal casting. However, a higher pressure resulted in more lost CMs during the casting. The weight percentages of the lost CMs in pressure and centrifugal casting were approximately 70% and 50%, respectively.

The porosity and partial filling defects were found in the samples fabricated by both casting processes. However, the partial filling defect appeared more frequently in the samples fabricated by centrifugal casting than in those by pressure casting. The deformation of CMs was evident, because the softening temperature of the CMs used in this study was lower than the melting point of the Co-Cr-Mo alloy.

5.2 Future Work

5.2.1 Ti matrix syntactic foam

The crushed CMs, which are caused by high compaction pressures, can increase the density and the elastic modulus of the Ti matrix syntactic foam. Increased density can lead to a decrease in the specific strength of the Ti matrix syntactic foam. Increased elastic modulus is not beneficial for reducing the stress shielding effect. In future studies, a stronger CM should be used to decrease or avoid the crushed CMs in the Ti matrix

syntactic foam. The elastic modulus of the Ti matrix syntactic foam would also be easier to control.

As shown in this thesis, the elastic modulus of the Ti matrix syntactic foam can be designed to be very close to human bone. However, the as-manufactured Ti matrix syntactic foam showed a brittle behaviour. For implant applications, brittle materials are not desirable as ductile materials. In future studies, improving the ductility of Ti matrix syntactic foam would be an interesting project.

5.2.2 Co-Cr-Mo alloy matrix syntactic foam

The Co-Cr-Mo alloy matrix syntactic foam manufactured in this thesis had many defects. Studies on the following measures can be carried out in the future to overcome the defects:

a. Improving the distribution of CMs in the syntactic foam by modifying the manufacturing process.
b. Using a CM with higher thermal resistance in the manufacturing to avoid being deformed.
c. Carrying out the manufacturing in a vacuum environment to avoid gas porosity.

References

Adams, C.I., Robinson, C.M., Court-Brown, C.M. & McQueen, M.M., (2001). "Prospective Randomized Controlled Trial of an Intramedullary Nail Versus Dynamic Screw and Plate for Intertrochnteric Fractures of the Femur". *Journal of Orthopaedic Trauma*, 15, pp. 394-400.

Akasaka, T., Yokoyama, A., Matsuoka, M., Hashimoto, T., Abe, S., Uo, M. & Watari, F., (2009). "Adhesion of Human Osteoblast-like cells (SaOS-2) to Carbon Nanotube Sheets". *Bio-Medical Materials and Engineering*, 19, pp. 147-153.

Ascenzi, A. & Bonucci, E., (1967). "The Tensile Properties of Single Osteons ". *The Anatomical Record*, 158, pp. 375-386.

Ascenzi, A. & Bonucci, E., (1968). "The Compressive Properties of Single Osteons". *The Anatomical Record*, 161, pp. 377-391.

Aydin, I., Briscoe, B. & Sanliturk, K.Y., (1996). "The Internal Form of Compacted Ceramic Components: A Comparison of Finite Element Modelling with Experiments". *Powder Technology*, 89, pp. 239-254.

Balch, D.k., O' Dwyer, J.G., Davis, G.R., Cady, C.M., III, G.T. Gray & Dunand, D.C., (2005). "Plasticity and Damage in Aluminum Syntactic Foams Deformed under Dynamic and Quasi-Static Conditions". *Materials Science and Engineering*: A, 391, pp. 408-417.

Banhart, J., Ashby, M.F. & Fleck, N.A., (1999). *Metal Foams and Porous Metal Structures*. Bremen: Verlag Metall Innovation Technologie MIT.

Banhart, J., Fleck, N. & Mortensen, A., (2003). "Cellular Metals Manufacture Properties Applications". Berlin: Verlag Metall Innovation Technologie MIT.

Boyan, B.D., Dean, D.D., Lohmann, C.H., Cochran, D.L., Sylvia, V.L. & Schwartz, Z. (2001). "The Titanium-bone Cell Interface *In Vitro*: The Role of the Surface in Promoting Osteointegration" In: Brunette, D.M., Tengnvall, P., Textor, M. & Thomsen, P. (eds.) *Titanium in Medicine: Material Science, Surface Science, Engineering, Biological Responses and Medical Applications*. London: Springer. pp. 561-585.

Briscoe, B.J. & Rough, S.L., (1998). "The Effects of Wall Friction in Powder Compaction". *Colloids and Surface A*, 137, pp. 103-116.

Brunette, D.M., (1988). "The Effects of Implant Surface Topography on the Behavior of Cells". *The International Journal of Oral & Maxillofacial Implants*, 3, pp. 231-246.

Buser, D. (2001). "Titanium for Dental Applications" In: Brunette, D.M., Tengnvall, P., Textor, M. & Thomsen, P. (eds.) *Titanium in Medicine: Material Science, Surface Science, Engineering, Biological Responses and Medical Applications*. Berlin: Springer. pp. 875-888.

Carter, D.R., Washington, S. & Hayes, W.C., (1977). "The Compressive Behavior of Bone as a Two-Phase Porous Structure". *The Journal of Bone and Joint Surgery*, 59, pp. 954-962.

Collis, J.J. & Embery, G., (1992). "Adsorption of Glycosaminoglycans to Commercially Pure Titanium". *Biomaterials*, 13, pp. 548-552.

Cooper, L.F., (2000). "A Role for Surface Topography in Creating and Maintaining Bone at Titanium Endosseous Implants". *Journal of Prosthetic Dentistry*, 84, pp. 522-534.

Coube, O. & Riebel, H., (2000). "Numerical Simulation of Metal Powder Die Compaction with Special Consideration of Cracking". *Powder Metallurgy*, 43, pp. 123-131.

Curtis, A. & Wilkinson, C., (1997). "Topographical Control of Cells". *Biomaterials*, 18, pp. 1573-1583.

Daoud, A., (2008). "Synthesis and Characterization of Novel ZnAl22 Syntactic Foam Composites via Casting". *Materials Science and Engineering*: A, 488, pp. 281-295.

Davies, J.E., (1998). "Mechanisms of Endosseous Integration". *International Journal of Prosthodontics*, 11, pp. 391-401.

Degasne, M.F., Basle, V., Demais, G., Hure, M., Lesourd, B. & Grolleau, L., (1999). "Effects of roughness, Fibronectin and Vitronectin of Attachment, Spreading, and Prolifeation of Human Osteoblast-Like Cells (SaOS-2) on Titanium Surfaces". *Calcified Tissue International*, 64, pp. 499-507.

Degischer, H.P. & Kriszt, B., (2002). *Handbook of Cellular Metals: Production, Processing, Applications*. German: WILEY-VCH.

Dizlek, M.E., Guden, M., Turkan, U. & Tasdemirci, A., (2009). "Processing and Compression Testing of Ti6Al4V Foams for Biomedical Applications". *Journal of Materials Science*, 44, pp. 1512-1519.

El-Ghannam, A., Ducheyne, P. & Shapiro, I.M., (1999). "Effect of Serum Proteins on Osteoblast Adhesion to Surface-Modified Bioactive Glass and Hydroxyapatite". *Journal of Orthopaedic Research*, 17, pp. 340-345.

El-Ghannam, A., (2004). "Advanced Bioceramic Composite for Bone Tissue Engineering: Design Principles and Structure-Bioactivity Relationship". *Journal of Biomedical Materials Research*, 69, pp. 490-501.

Elwing, H., Ivarsson, B. & Lundström, I., (1987). "Serum Complement Deposition on Platinum and Titanium Oxide Surfaces Measured by Ellipsometry at Liquid-Solid Interface". *Journal of Biomedical Materials Research*, 21, pp. 263-267.

Esposito, M. (2001). "Titanium for Dental applications" In: Brunette, D.M., Tengnvall, P., Textor, M. & Thomsen, P. (eds.) *Titanium in Medicine: Material Science, Surface Science, Engineering, Biological Responses and Medical Applications*. Berlin: Springer. pp. 827-873.

Evans, M., Spencer, M., Wang, Q., White, S.H. & Cunningham, J.L., (2006). "Design and Testing of External Fixator Bone Screws". *Journal of Biomedical Engineering*, 12, pp. 457-462.

Federation, Metal Powder Industries, (1998). *Powder Metallurgy Design Manual.* 3rd ed. Princeton: Metal Powder Industries Federation.

Fishman, Y.A., (2008). "Features of Shear Failure of Brittle Materials and Concrete Structures on Rock Foundations". *International Journal of Rock Mechanics and Mining Sciences*, 45, pp. 976-992.

FREESE, H. L., VOLAS, M. G. & WOOD, J. R. 2001. Metallurgy and Technological Properties of Titanium and Titanium Alloys. *In:* BRUNETTE, D. M., TENGVALL, P., TEXTOR, M. & THOMSEN, P. (eds.) *Titanium in Medicine: Material Science, Surface Science, Engineering, Biological Responses and Medical Applications.* Berlin: Springer.

Garcia, A.J., Ducheyne, P. & Boettiger, D., (1998). "Effect of Surface Reaction Stage on Fibronectin-mediated Adhesion of Osteoblast-like Cells to Bioactive Glass". *Journal of Biomedical Materials Research Part A*, 40, pp. 48-56.

German, R.M., (1985). *Liquid Phase Sintering.* New York: Plenum Press.

German, R.M., (1996). *Sintering theory and Practice.* New York: John Wiley & Sons, Inc.

Gibson, L.J. & Ashby, M.F., (1988). *Cellular Solids: Structure and Properties.* Oxford: Permagon Press.

Giesen, E.B.W., Ding, M., Dalstra, M. & Eijden, T.M.G.J. van, (2001). "Mechanical Properties of Cancellous Bone in the Human Mandibular Condyle are Anisotropic". *Journal of Biomechanics*, 34, pp. 799-803.

Gilbert, R.P., Liu, Y., Groby, J.P., Ogam, E., Wirgin, A. & Xu, Y., (2009). "Computing Porosity of Cancellous Bone Using Ultrasonic Waves, II: The Muscle, Cortical, Cancellous Bone System". *Mathematical and Computer Modelling*, 50, pp. 421-429.

Groessner-Schreiber, B. & Tuan, RS., (1992). "Enhanced Extracellular Matrix Production and Mineralization by Osteoblasts Cultured on Titanium Surfaces *in vitro*". *Journal of Cell Science*, 101, pp. 209-217.

Gunn, C., (2002). *Bones and Joints, A guide for Students.* 4th ed. Edinbergh: Churchill Livingstone.

Harrison, R.G., (2005). "The Cultivation of Tissues in Extraneous Media as a Method of Morpho-genetic Study". *The Anatomical Record*, 6, pp. 181-193.

Hartmann, M., CroBmann, I., Reindel, K. & Singer, R. F., (1999). "Microstructure and Mechanical Properties of Cellular Magnesium Matrix Composites". *Metal Foams and Porous Metal Structure*, pp. 331-336.

Havelin, I.I., Espehaug, B., Vallset, S.E., Engesaeter, L.B. & Langeland, N., (1993). "A survey of 17,444 total hip replacements". *Acta Orthopaedica Scandinavica*, 64, pp. 245-251.

Holgers, K.M. & Hakansson, B. (2001). "Titanium in Audiology" In: Brunette, D.M., Tengnvall, P., Textor, M. & Thomsen, P. (eds.) *Titanium in Medicine: Material Science, Surface Science, Engineering, Biological Responses and Medical Applications*. Berlin: Springer. pp. 909-928.

Huiskes, R., Weinans, H. & Rietbergen, B.V., (1992). "The Relationship Between Stress Shielding and Bone Resorption around Total Hip Stems and the Effects of Flexible Materials". *Clinical orthopaedics and Related Research*, 274, pp. 24-34.

Huiskes, R., (1993). "Stress Shielding and Bone Resorption in THA: Clinical Versus Computer-simulation Studies". *Acta Orthopaedica Belgica*, 59, pp. 118-129.

Hulbert, S.F., Young, F.A., Mathews, R.S., Klawitter, J.J., Talbert, C.D. & Stelling, F.H., (1970). "Potential of Ceramic Materials as Permanently Implantable Skeletal Prostheses". *Journal of Biomedical Materials Research*, 4, pp. 433-456.

Hyldahl, C., Pearson, S., Tepic, S. & Perren, S.M., (1991). "Induction and Prevention of Pin Loosening in External Fixation: an *In Vivo* Study on Sheep Tibiae". *Journal of Orthopaedic Trauma*, 5, pp. 485-492.

Inoue, T., Cox, J.E., Pilliar, R.M. & Melcher, A.H., (1987). "Effect of the Surface Geometry of Smooth and Porous-coated Titanium Alloy on the Orientation of Fibroblasts *In Vitro*". *Journal of Biomedical Materials Research*, 21, pp. 107-126.

Jacobs, J.J., Hallab, N.J., Urban, R.M. & Wimmer, M.A., (2006). "Wear Particles". *The Journal of Bone and Joint Surgery*, 88, pp. 99-102.

Joshi, M.G., Advani, S.G., Miller, F. & Santare, M.H., (2000). "Analysis of a Femoral Hip Prosthesis Designed to Reduce Stress Shielding". *Journal of Biomechanics*, 33, pp. 1655-1662.

Kandeil, A., Malherbe, M.C. de, Critchley, S. & Dokainish, M., (1977). "The Use of Hardness in the study of Compaction Behaviour and Die Loading". *Powder Technology*, 17, pp. 253-257.

Kane, K.R., DeHeer, D.H., Owens, S.R., Beebe, J.D. & Swanson, A.B., (1994). "Adsorption of Collagenase to Particulate Titanium: A Possible Mechanism for Collagenase Localization in Periprosthetic Tissue". *Journal of Applied Biomaterials*, 5, pp. 353-360.

Kassem, M., Rungby, J., Mosekilde, L. & Eriksen, E.F., (1992). "Ultrastructure of Human Osteoblasts and Associated Matrix in Culture". *Acta Pathologica Microbiologica et Immunologica Scandinavica (APMIS)*, 100, pp. 490-497.

Katti, K.S., (2004). "Biomaterials in Total Joint Replacement". *Colloids and Surface B: Biointerface*, 39, pp. 133-142.

Kiser, M., He, M.Y. & Zok, F.W., (1999). "The Mechanical Response of Ceramic Microballoon Reinforced Aluminum Matrix Composites Under Compressive Loading". *Acta Materialia*, 47, pp. 2685-2694.

Klein, C.P., Driessen, A.A., Groot, K.D. & Hooff, A.V.D., (1983). "Biodegradation Behavior of Various Calcium Phosphate Materials in Bone Tissue". *Journal of Biomedical Materials Research*, 17, pp. 769-784.

Klinger, A., Steinberg, D., Kohavi, D. & Sela, M. N., (1997). "Mechanism of Adsorption of Human Albumin to Titannium *In Vitro*". *Journal of Biomedical Materials Research*, 36, pp. 387-392.

Kuczynski, G.C. (1972). "Fundametals of Sintering Theory" In: Burke, J.J. & Weiss, V. (eds.) *Powder Metallurgy for High-Performance Applications*. New York: Syracuse University Press. pp. 101-117.

Kuno, H. & Kuri, I., (1983). "Study of the Pressure Distribution at the Bottom of a Pressed Powder Bed by Pressure-Detercting Sheets". *Powder Technology*, 34, pp. 87-91.

Lajtal, E.Z., (1974). "Brittle Fracture in Compression". *International Journal of Fracture*, 10, pp. 525-536.

Lausmaa, J. (2001). "Mechnica, Thermal, Chemical and Electrochemical Surface Treatment of Titanium" In: Brunette, D.M., Tengnvall, P., Textor, M. & Thomsen, P. (eds.) *Titanium in Medicine: Material Science, Surface Science, Engineering, Biological Responses, and Medical Applications*. Berlin: Springer. pp. 232-258.

Lenthe, G.H. van, Waal, D. & Huiskes, R., (1997). "Stress Shielding after Total Knee Replacement May Cause Bone Resorption in the Distal Femur". *Journal of Bone and Joint Surgery*, 79, pp. 117-122.

Lim, Y.J. & Oshida, Y., (2001). "Initial Contact Angle Measurements on Variously Treated Dental/Medical Titanium Materials". *Bio-Medical Materials and Engineering*, 11, pp. 325-341.

Long, M. & Rack, H.J., (1998). "Titanium Alloys in Total Joint Replacement- A Materials Science Perspective". *Biomaterials*, 19, pp. 1621-1639.

Lowery, G.L. & McDonough, R.F., (1998). "The Significance of Hardware Failure in Anterior Cervical Plate Fixation. Patients with 2- to 7- Year Follow-up". *Spine*, 23, pp. 186-187.

Macleod, H.M. & Marshall, K., (1977). "The Determination of Density Distributions in Ceramic Compacts Using Autoradiography". *Powder Technology*, 16, pp. 107-122.

Malchau, H., Herberts, P. & Ahnfelt, L., (1993). "Follow-Up of 92,675 Operations Performed 1978-1990". *Acta Orthopaedica Scandinavica*, 64, pp. 97-506.

Martin, R.B., (1972). "The Effects of Geometric Feedback in the Development of Osteoporosis". *Journal of Biomechanics*, 5, pp. 447-455.

Matsunaga, T., Kojo, T. & Tsujisawa, T., (2000). "Preferential Degradation of Osteoclasts by Titanium Tetrachloride". *Journal of Biomedical Materials Research*, 55, pp. 313-319.

McCarthy, C.K., Steinberg, G.G. & Agren, M., (1991). "Quantifying Bone Loss from the Proximal Femur after Total Hip Arthroplasty". *Journal of Bone and Joint Surgery*, 73-B, pp. 774-778.

McElhaney, J.H., Fogle, J.L., Melvin, J.W., Haynes, R.R., Roberts, V.L. & Alem, N.M., (1970). "Mechanical Properties of Cranial Bone". *Journal of Biomechanics*, 3, pp. 495-511.

McKellop, H.A., Rostlund, T., Ebramzadeh, E. & Sarmiento, A. (2001). "Wear of Titanium 6-4 Alloy in Laboratory Tests and in Retrieved Human Joint Replacements" In: Brunette, D.M., Tengnvall, P., Textor, M. & Thomsen, P. (eds.) *Titanium in Medicine: Material Science, Surface Science, Engineering, Biological Responses and Medical Applications*. Berlin: Springer. pp. 747-770.

Munting, E. & Verhelpen, M., (1995). "Fixation and Effect on Bone Strain Pattern of a Stemless Hip Prosthesis". *Journal of Biomechanics*, 28, pp. 949-961.

Myllymaa, K., Myllymaa, S., korhonen, H. & Lammi, M.J., (2009). "Improved Adherence and Spreading of Saos-2 Cells on Polypropylene Surfaces Achieved by Surface Texturing and Carbon Nitride Coating". *Journal of Materials Science: Materials in Medicine*, 20, pp. 2337-2347.

Nociti, F.H.J., Sallum, A.W., Sallum, E.A. & Bozzo, L., (1997). "Titanium implants in Rabbit Femur: A Histologic Evaluation". *Brazilian Dental Journal*, 8, pp. 105-111.

Ogino, M., Ohuchi, F. & Hench, L.L., (2004). "Compositional Dependence of the Formation of Calcium Phosphate Films on bioglass". *Journal of Biomedical Materials Research*, 14, pp. 55-64.

Oh, I.H., Nomura, N. & Hanada, S., (2002a). "Microstructures and Mechanical Properties of Porous Titanium Compacts Prepared by Powder Sintering". *Materials Transactions*, 43, pp. 443-446.

Oh, W.S., Shen, C., Alegre, B. & Anusavice, K.J., (2002b). "Wetting Characteristic of Ceramic to Water and Adhesive Resin". *The Journal of Prosthetic Denstistry*, 88, pp. 16-21.

Olin, C. (2001). "Titanium in Cardiac and Cardiovascular Applications" In: Brunette, D.M., Tengnvall, P., Textor, M. & Thomsen, P. (eds.) *Titanium in Medicine: Material Science, Surface Science, Engineering, Biological Responses and Medical Applications*. Berlin: Springer. pp. 889-908.

Oonishi, H., Hench, L.L., Wilson, J., Sugihara, F., Tsuji, E. & Matsuura, M., (2000). "Quantitative Comparison of Bone Growth Behavior in Granules of Bioglass, A-W Glass-ceramic, and hydroxyapatite". *Journal of Biomedical Materials Research Part A*, 51, pp. 37-46.

Orbulov, I.N., Dobranszky, J. & Nemeth, A., (2009). "Microstructural Characterisation of Syntactic Foams". *Journal of Materials Science*, 44, pp. 4013-4019.

Orvieto, R., Leichter, I., Rachmilewitz, E.A. & Margulies, J.Y., (1992). "Bone Density, Mineral Content, and Cortical Index in Patients with Thalassemia Major and the Correlation to Their Bone Fractures, Blood Transfusions, and Treatment with Desferrioxamine". *Calcified Tissue International*, 50, pp. 397-399.

Palmer, R.A., Gao, K., Doan, T.M., Green, L. & Cavallaro, G., (2007). "Pressure Infiltrated Syntactic Foams-Process Development and Mechanical Properties". *Materials Science and Engineering A*, 464, pp. 85-92.

Panagiotopoulos, E., Fortis, A.P., Millis, Z., Lambiris, E., Kostopoulos, V. & Vellios, L., (1994). "Pattern of Screw Loosening in Fractures Fixed with Conventional and Functional Plates". *Injury*, 25, pp. 515-517.

Park, J. & Lakes, R.S., (2007). *Biomaterials: An Introduction.* 3rd ed. New York: Springer.

Perren, S.M., Pohler, O.E.M. & Schneider, E. (2001). "Titanium as Implant Material for Osteosynthesis Applications" In: Brunette, D.M., Tengnvall, P., Textor, M. & Thomsen, P. (eds.) *Titanium in Medicine: Material Science, Surface Science, Engineering, Biological Responses and Medical Applications*. Berlin: Springer. pp. 783-825.

Postiglione, L. & Domenico, G.D., (2003). "Behavior of SaOS-2 Cells Cultured on Different Titanium Surfaces". *Journal of Dental Research*, 82, pp. 692-696.

Pugh, J.W., Rose, R.M. & Radin, E.L., (1973a). "Elastic and Viscoelastic Properties of Trabecular Bone: Dependence on Structure". *Journal of Biomechanics*, 6, pp. 475-485.

Pugh, J.W., Rose, R.M. & Radin, E.L., (1973b). "A Structure Model for the Mechanical Behavior of Trabecular Bone". *Journal of Biomechanics*, 6, pp. 657-670.

Puleo, D.A. & Nanci, A., (1999). "Understanding and Controlling the Bone-implant Interface". *Biomaterials*, 20, pp. 2311-2321.

Ramachandra, M. & Radhakrishna, K., (2005). "Synthesis-microstructure-mechanical Properties-wear and Corrosion Behaviour of an Al-Si(12%)-Flyash Metal Matrix Composite". *Journal of Materials Science*, 40, pp. 5989-5997.

Ratner, B.D. (2001). "A Perspective on Titanium Biocompatibility" In: Brunette, D.M., Tengnvall, P., Textor, M. & Thomsen, P. (eds.) *Titanium in Medcine: Material Science, Surface Science, Engineering Biological Responses and Medical Applications*. Berlin: Springer. pp. 2-12.

Rausch, G. & Banhart, J., (2002). *Handbook of Cellular Metals: Production, Processing, Applications*. German: Wiley-VCH.

Revankar, Gopal, (2003). *ASM Materials Information*. ASM International. Available at: http://products.asminternational.org/hbk/index.jsp. [Accessed 3rd October, 2010].

Ridzwan, M.I.Z., Shuib, Solehuddin, Hassan, A. Y., Shokri, A. A. & Ibrahim, M.N.M., (2006). "Optimization in Implant Topology to Reduce Stress Shielding Problem". *Journal of Applied Science*, 6, pp. 2768-2773.

Schepers, E., Clercq, M.D., Ducheyne, P. & Kempeneers, R., (1991). "Bioactive Glass Particulate Material as a Filler for Bone Lesions". *Journal of Oral Rehabilitation*, 18, pp. 439-452.

Schwartz, Z., Kieswetter, K., Dean, D.D. & Boyan, B.D., (1997). "Underlying Mechanisms at the Bone-surface Interface During Regeneration". *Journal of Periodontal Research*, 32, pp. 166-171.

Schwartz, Z., Lohmann, C.H., J.Oefinger, Bonewald, L.F., Dean, D.D. & Boyan, B.D., (1999). "Implant Surface Characteristics Modulate Differentiation Behavior of Cells in the Osteoblastic Lineage". *Advances in Dental Research*, 13, pp. 38-48.

SEER, 2005. Compact bone & spongy bone. [Online]. Available at: http://en.wikipedia.org/wiki/Bone. [Accessed 25 August 2010].

Serro, A.P., Fernandesa, A.C., Saramagoa, B., Lima, J. & Barbosa, M.A., (1997). "Apatite Deposition on Titanium Surfaces -The Role of Albumin Adsorption". *Biomaterials*, 18, pp. 963-968.

Shackelford, J.F. & Alexander, W., (2001). *Materials Science and Engineering Handbook.* 3rd ed. Boca, Raton, London, New York: CRC Press, pp. 81-82.

Skinner, P.W. & Powles, D., (1986). "Compression Screw Fixation for Displaced Subcapital Fracture of the Femur. Success or Failure?". *Journal of Bone and Joint Surgery- British Volume*, 68-B, pp. 78-82.

Soininvaara, T.A., Jurvelin, J.S., Miettinen, H.J. A., Suomalainen, O.T., Alhava, E.M. & Kroger, P.J., (2002). "Effect of Alendronate on Periprosthetic Bone Loss After Total Knee Arthroplasty: A one-Year, Randomized, Controlled Trial of 19 Patients". *Calcified Tissue International*, 71, pp. 472-477.

Stanford, C.M. & Keller, J.C., (1991). "The Concept of Osseointegration and Bone Matrix Expression". *Critical Reviews in Oral Biology & Medicine*, 2, pp. 83-101.

Steinemann, S.G. & Perren, S.M., (1984). Titanium Alloys as Metallic Biomaterials. In: Lutjering, G., Zwicker, U. & Bunk, W., Proceedings of the 5th International Conderence of Titanium. Mumich FRG, 10-14th Sep 1984, Germany: Deutsche Gesellschaft fur Metallkunde, pp. 1327-1334.

Steinemann, S.G., (1998). "Titanium - the Material of Choice?". *Periodontology 2000*, 17, pp. 7-21.

Stobener, K. & Rausch, G., (2009). "Aluminium Foam-Ploymer Composites: Processing and Characteristics". *Journal of Materials Science*, 44, pp. 1506-1511.

Sundgren, J.E., P. P. Bodo, Ivarsson, B. & Lundstrom, I., (1986). "Adsorption of Fibrinogen on Titanium and Gold Surfaces Studied by ESCA and Ellipsometry". *Journal of Colloid and Interface Science*, 113, pp. 530-543.

Surappa, M.K. & Rohatgi, P.K., (1981). "Preparation and Properties of Cast Aluminium-Ceramic Particle Composites". *Journal of Materials Science*, 16, pp. 983-993.

Swart, K.M., Keller, J.C., Wightman, J.P., Draughn, R.A., Stanford, C.M. & Michaels, C.M., (1992). "Short-term Plasma-cleaning treatments enhance *in vitro* Osteoblast Attachment to Tittanium". *Journal of Oral Implantology*, 18, pp. 130-137.

Tamura, R.N., Oda, D., Quaranta, V., Plopper, G., Lambert, R., Glaser, S. & Jones, J.C.R., (1997). "Coating of Titanium Alloy with Soluble Laminin -5 Promotes Cell Attachment and Hemidesmosome Assembly in Gingival Epithelial Cells: Potential Application to Dental Implants". *Journal of Periodontal Research*, 32, pp. 287-294.

Tao, X.F., Zhang, L.P. & Zhao, Y.Y., (2008). "Compressive Response of Al Matrix Syntactic Foam Manufactured by Liquid Sintering" In: Materials Science and Technology (MS&T) 2008. Pittsburgh, Pennsylvania, Pittsburgh, Pennsylvania: 2008 MS&T' 08, pp. 2587-2594.

Tao, X.F., Zhang, L.P. & Zhao, Y.Y., (2009). "Al matrix syntactic foam fabricated with biomodal ceramic microspheres". *Materials and Design*, 30, pp. 2732-2736.

Tao, X.F. & Zhao, Y.Y., (2009). "Compressive Behavior of Al Matrix Syntactic Foams Toughened with Al Particles". *Scripta Materialia*, 61, pp. 461-464.

Tengvall, P. (2001). "Proteins at Titanium Interfaces" In: Brunette, D.M., Tengnvall, P., Textor, M. & Thomsen, P. (eds.) *Titanium in Medicine: Material Science, Surface Science, Engineering, Biological Responses and Medical Applications*. London: Springer. pp. 457-483.

Thomas, I., (2007). "Mechanical Properties of Open-pore Titanium Foam". *Journal of Biomedical Materials Research Part A*, 81A, pp. 964-970.

Townsend, P.R., Rose, R.M. & Radin, E.L., (1975). "Buckling Studies of Single Human Trabeculae". *Journal of Biomechanics*, 8, pp. 199-201.

Wachter, N.J., Augat, P., Krischak, G.D., Mentzel, M., Kinzl, L. & Claes, L., (2001). "Prediction of Cortical Bone Porosity *In Vitro* by Microcomputed Tomography". *Calcified Tissue International*, 68, pp. 38-42.

Wang, X. & Ni, Q., (2003). "Determination of Cortical Bone Porosity and Pore Size Distribution using a low Field Pulsed NMR Approach". *Journal of Orthopaedic Research*, 21, pp. 312-319.

Welsch, G., Boyer, R. & Collings, E. W., (1994). *Materials Properties Handbook : Titanium Alloys.* Materials Park, OH: ASM International, pp. 125.

Wen, C.E., Mabuchi, M., Yamada, Y., Shimojima, K., Chino, Y. & Asahina, T., (2001). "Processing of Biocompatible Porous Ti and Mg". *Scripta Materialia*, 45, pp. 1147-1153.

Wen, C.E., Yamada, Y., Shimojima, K., Chino, Y., Asahina, T. & Mabuchi, M., (2002). "Processing and Mechanical Properties of Autogenous Titanium Implant Materials". *Journal of Materials Scinece: Materials in Medicine*, 13, pp. 397-401.

Wheeler, K.R., Karagianes, M.T. & Sump, K.R. (1983). "Porous Titanium Alloy for Prosthesis Attachment" In: Materials, American Society for Testing and (ed.) *Titanium Alloys in Surgical Implants, ASTM STP 796.* pp. 241.

Williams, D., (1976). *Biocompatibility of Implant Materials.* London: Sector Publising Limited.

Williams, D.F. (1973a). "The Mechanical and Physical Properties of Materials" In: Williams, D.F. & Roaf, R. (eds.) *Implants in Surgery.* London: W.B. Saunders Company Ltd. pp. 65-136.

Williams, D.F. (1973b). "The Selection of Implant Materials" In: Williams, D.F. & Roaf, R. (eds.) *Implants in Surgery.* London: W.B. Saunders Company Ltd. pp. 299-357.

Wimmer, C. & Gluch, H., (1998). "Aseptic Loosening after CD Instrumentation in the Treatment of Scoliosis: a Report about Eight Cases". *Journal of Spinal Disorders*, 11, pp. 440-443.

Windler, M. & Klabunde, R. (2001). "Titanium for Hip and Knee Prostheses" In: Brunette, D.M., Tengnvall, P., Textor, M. & Thomsen, P. (eds.) *Titanium in Medicine: Material Science, Surface Science, Engineering, Biological Responses and Medical Applications*. Berlin: Springer. pp. 704-737.

Wu, G.H., Dou, Z.y., Sun, D.L., Jiang, L.T., Ding, B.S. & He, B.F., (2007). "Compression Behaviors of Cenosphere-Pure Aluminum Syntactic Foams". *Scripta Materialia*, 56, pp. 221-224.

Yang, Y.Z., Tian, J.M., Tian, J.T., Chen, Z.Q., Deng, X.J. & Zhang, D.H., (2000). "Preparation of graded Porous Titanium Coating on Titanium Implant Materials by Plasma Spraying". *Journal of Biomedical Materials Research Part A*, 52, pp. 333-337.

Zahlan, N., Knight, D.T., Backhouse, A. & Leiper, G.A., (2001). "Modelling Powder Compaction and Pressure Cycling". *Powder Technology*, 114, pp. 112-117.

Zhang, L.P. & Zhao, Y.Y., (2007). "Mechanical Response of Al Matrix Syntactic Foams Produced by Pressure Infltration Casting". *Journal of Composite materials*, 41, pp. 2105-2117.

Zhao, Y.Y., Han, F. & Fung, T., (2004). "Optimisation of Compaction and Liquid-state Sintering in the Sintering and Dissolution Process for Manufacturing Al Foams". *Materials Science and Engineering*, A364, pp. 117-125.

Zhao, Y.Y. & Monaghan, L.E., (2008). A Novel Manufacturing Method for Titanium Foam for Biomedical Applications. In: 2008 World Congress on Powder Metallurgy & Particulate Materials. Washington, D.C., U.S., Washington, D.C., U.S.: MPIF, pp. 340-348.

Zhao, Y.Y., Tao, X.F. & Xue, X.B., (2008). Manufacture and Mechanical Properties of Metal Matrix Syntactic Foams. In: Materials Science and Technology (MS&T) 2008. Pittsburgh, Pennsylvania: 2008 MS&T'08, pp. 2607-2615.

Zhao, Y.Y. & Tao, X.F., (2009). Behaviour of Metal Matrix Syntactic Foams in Compression. In: Materials Science and Technolgy (MS&T) 2009. Pittsburgh, October 25-29, 2009, Pennsylvania: 2009 MS&T'09, pp. 1785-1794.